AN INTEGRATED APPROACH FOR PLANT MONITORING AND DIAGNOSIS USING MULTIRESOLUTION WAVELET ANALYSIS

A Dissertation

Presented for the

Doctor of Philosophy Degree

The University of Tennessee, Knoxville

Aucyone Augusto da Silva

December 1997

AN INTEGRATED APPROACH FOR PLANT MONITORING AND DIAGNOSIS USING MULTIRESOLUTION WAVELET ANALYSIS

A Dissertation

Presented for the

Doctor of Philosophy Degree

The University of Tennessee, Knoxville

Aucyone Augusto da Silva

December 1997

To my beloved wife whose dedication and sacrifice made this journey possible.

ACKNOWLEDGMENTS

I would like to thank my advisor, Dr. Belle R. Upadhyaya for his guidance and friendship during the period of this research. His insight and technical support made this work possible.

I would also like to thank Dr. R. E. Uhrig and Dr. L. F. Miller, of the Department of Nuclear Engineering, Dr. J. Wasserman of the Department of Mechanical and Aerospace Engineering and Engineering Science for giving part of their valuable time as members of my dissertation committee.

I would like to thank CNPq - Conselho Nacional de Pesquisas Tecnológicas, Brazil and CNEN - Comissao Nacional de Energía Nuclear, Brazil for providing the financial support for the realization of this research work.

I would like to express my gratitude to Dr. Rafael Perez who introduced me to the topic of wavelets.

I would also like to thank Dr. O. Glockler, from Ontario Hydro, Canada, for providing some helpful technical discussion during this research work.

I am most grateful to both the former and the present head of the Nuclear Engineering Department, Dr. T. W. Kerlin and Dr. H. L. Dodds, for their support during this research.

A special recognition is due to Stacy Harrison who read the manuscript in detail and made several suggestions to improve its presentation. Her helpful spirit made the difficult time easier for my family and me when we first arrived in the United States. Thank you Harrison family.

Thanks are due to my special friend, Marcia Kohls, who read this document and offered constructive comments. The period we spent together working on the wavelet topic is unforgettable. I have learned a lot from Marcia, and I am very proud of our friendship.

Finally, my sincere thanks to my old friend and companion, Paulo Sergio Brasko Ferreira, who has contributed to my research with his friendship, encouragement and suggestions.

ABSTRACT

The purpose of this dissertation is to develop a systematic approach for fault monitoring and diagnosis for nuclear power plant systems and rotating machinery using short-time Fourier transform (STFT) and wavelet transform techniques during stationary and transient operating conditions.

This research explored the significant improvements in the signal-to-noise ratio when the original signal was decomposed into different levels using the multiresolution analysis (MRA) technique. The MRA was combined with the standard digital signal processing techniques for diagnostics purposes. A data analysis system, that integrates several MATLAB signal processing tools, was developed and implemented with applications to a commercial pressurized water reactor and a rotating machinery system. A method for establishing optimal wavelet selection, using minimum entropy approach, was developed and applied to actual data.

The problems to be investigated in nuclear power plant systems were concerned with the detection and characterization of transients in the data. The stationary or time-dependent characteristics of fuel channel vibration and the estimation of the frequency characteristics of the transient signals were analyzed using the multiresolution analysis. The reactor data analysis revealed the dominant frequencies triggering the dips and spikes in the transmitter's output signals. The coherence, power spectrum and cross spectrum were estimated for the neutron detector and process signals.

The rotating machinery condition monitoring problem addressed the characterization of the start-up and shut-down signatures of a rotor rig under different operating conditions. The prominent spectral components of the signal were tracked in the time-frequency and time-scale domains during rotor speed variations. The combination of STFT and wavelet transform techniques provided a robust approach for detecting incipient changes in the process signal during steady-state operation. These changes might be indicative of possible anomalies in the plant equipment or in the process sensors.

Optimal wavelet functions were established for the problems of interest which were broadly classified as low frequency (0-20 Hz reactor signal) and medium frequency (20-500 Hz motor rig signals) information ranges. The result of this research was an on-line condition monitoring system that integrates multiresolution analysis (MRA) using wavelet transform and the short-time Fourier transform (STFT) method. The signal analysis methodologies were implemented using the MATLAB software tools.

LIST OF ACRONYMS

ANN:	Artificial Neural Networks
APSD:	Auto Power Spectral Density
CWT:	Continuous Wavelet Transform
DWT:	Discrete Wavelet Transform
FFT:	Fast Fourier Transform
FINCH:	Fully Instrumented Fuel Channels
FIR:	Finite Impulse Response Digital Filters
GUI:	Graphical User Interface
ID #:	Identification Number
IDWT:	Inverse Discrete Wavelet Transfrom
ICFD:	In-Core Flux Detector
MDAST:	MATLAB Data Analysis System Toolbox
MRA:	Multiresolution Analysis
MWe:	MegaWatt-electric
PWR:	Pressurized Water Reactor
QMF:	Quadrature Mirror Filter
RMS:	Root Mean Square
RPM:	Revolution per Minute
RRS:	Reactor Regulating System
SDS1:	Safety Display System 1
SDS2:	Safety Display System 2
STFT:	Short-Time Fourier Transform

TABLE OF CONTENTS

LIST OF TABLES

TABLE **PAGE**

LIST OF FIGURES

CHAPTER 1

Introduction

1.1 Background and Motivation

The demand for monitoring and fault diagnosis of process dynamics and sensors in industrial systems has increased the efforts to develop new data analysis techniques. The main goal of this technological improvement is to obtain more detailed information contained in the measured data than had been previously possible. Standard digital signals processing techniques, such as time series statistics, correlation analysis and fast Fourier transform (FFT) have been used to detect faults in plant components. The results showed that they were neither sensitive to small and short-term anomalies, nor in tracking nonstationary signals.

The early detection of anomalies in complex industrial systems is crucial for safety and economic operation. The challenge is to identify and characterize the causes of the anomalies during the incipient stage because the signals are sometimes weakened by noise background. New technologies are being developed for monitoring and fault diagnosis of plant systems. These technologies help to enhance decision making for maintenance and system reconfiguration.

Systems that operate in a stationary mode are usually analyzed with standard Fourier transform techniques. When a system is nonstationary or undergoes a transient, the Fourier technique does not provide proper information about the signals. The

analysis of nonstationary signals should be performed using the time-frequency (Short-time Fourier transform , STFT) and time-scale (wavelet transform) techniques. The integration of STFT and wavelet transform provides a more powerful tool for signal monitoring than the standard FFT analysis.

During the past decade wavelet transforms have been applied successfully to many problems in diverse fields of science and engineering. The integration and application of these methods in nuclear power plant condition monitoring is still in its infancy.

1.2 Statement of the Problem and Proposed Solution

The major effort of this research was to develop a method for monitoring and diagnosis of process or sensor anomalies using the discrete wavelet transform and short-time Fourier transform techniques and to apply this method to nuclear power plants and rotating machinery systems. The emphasis was on the analysis of transient and short-term behavior of nuclear power plant process signals and machinery signals.

The nuclear power plant data that were analyzed for research consisted of measurements of the flow and pressure sensor signals from a pressurized water reactor showing strong and irregular flow dips. The in-core and ex-core neutron flux detector signals, were also analyzed in order to monitor possible fuel assembly vibration during the full power reactor operation.

The nuclear power plant data analysis, using the wavelet and STFT techniques, pursued the detection and characterization of transients in the data. The estimation of the frequency contents of the flow and pressure signals before, during and after a transient was also considered. The definitions of the time dependency and stationary characteristics of the fuel channel vibration were also established. Functions such as coherence, phase, cross spectrum, and power spectrum were evaluated.

The rotating machinery monitoring and diagnosis was concerned with the investigation of a rotor assembly behavior during steady-state and transient operating conditions. The nonstationary analysis was performed using the discrete wavelet transform and STFT techniques to characterize the star-up and shut-down signatures of the rotor rig under different operating conditions (normal, imbalance and misalignment). The prominent spectral components of the signals were tracked in the time-frequency domain during the motor speed variation. The stationary analysis integrated the multiresolution analysis (MRA) and STFT techniques.

The multiresolution analysis (MRA) theory was used to perform most of the data analysis in this dissertation. This technique promises to bring new insight into signal analysis. It also offers significant improvements in the signal-to-noise ratio. The nonstationary data analysis was investigated using the discrete wavelet mapping (2-D and 3-D DWT) technique to characterize the time-frequency signatures.

A multichannel data analysis system, which combines the features of MRA and the robustness of FFT techniques, was developed to obtain the spectral **and** cross-spectral densities and coherence of several signals from the experimental systems.

This dissertation research performed a systematic investigation of different types of wavelet functions and identifies the optimal wavelet to apply for each proposed problem. Figure 1.1 shows the basic blocks indicating the technological development that was performed in the dissertation research activities.

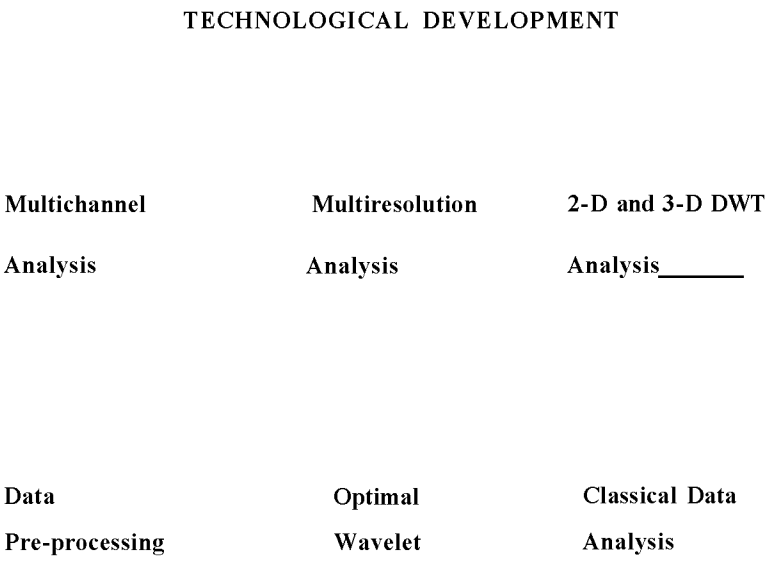

Figure 1.1. Technological Development

1.3 Review of Previous Work

The frequency-domain analysis has been applied successfully in many engineering problems since Baptiste Jean-Joseph Fourier introduced the Fourier analysis in 1860. The Fourier transform uses, as its orthonormal basis functions, infinite sinusoidal waves. The interpretation of the derived signatures requires that the signal be stationary. The average calculation over time and local-time information is not available.

The Fourier analysis and its applications are extensively discussed in the literature. The Fourier technique has been used as a standard method for the analysis of signals from nuclear power plants and from process plant machinery [1, 2, 3].

The traditional Fourier spectral analysis is not appropriate for characterizing nonstationary signals. To overcome this problem, Gabor [4] introduced the short-time Fourier transform (STFT) for time-frequency analysis. Although the time-frequency distribution method is very useful, it has a resolution limitation. The literature on the applications of this technique, in several engineering problems, is very extensive. See, for example, references [5-9].

The wavelet transform introduces the time-scale analysis and it overcomes the limitations of the time-frequency techniques. The wavelet transform provides new insight into digital signal processing. It overcomes the limitations of the Fourier transform. Although the wavelet transform technique is relatively new, there are quite a few articles

and books published on the wavelet theory and its applications. See, for example, references [10-22, 28].

Nonstationary analysis in a nuclear power plant using the instantaneous auto-regressive (AR) model technique [23-24] and adaptive AR technique [3] for rotating machinery have been reported. This method was shown to be highly efficient in detecting changes in the statistical properties of the signals.

Reference [25] describes an application of the multiresolution analysis (MRA) in nuclear power plant signal analysis. In this reference, signals from a steam generator, measured during power transients, were decomposed. After decomposing the signals into nine wavelet levels their variances were computed. The results revealed a significant difference in the lower bands in the transient case.

References [26, 27] describe a signal estimation method using wavelet and Artificial Neural Networks (ANN). The time series signal components from the wavelet decomposition were used as inputs to an ANN, with the corresponding power spectral densities. Once the network was trained, another part of the signal not used before was estimated. The estimation of the main signal through the estimation of the sub-band signal components is quite accurate. This technique is very important in the context of monitoring and fault detection, and further research is necessary in this area [40-42].

In reference [54], the author shows the application of the wavelet transform to detect the singularity of dynamic systems after the signal is de-noised. The threshold method developed in this reference was applied to the dynamics of the Korea multipurpose research reactor.

In the machinery condition monitoring area there are several applications of modern signal processing techniques, such as the short-time Fourier transform , Wigner-Ville distribution and wavelet transform. Results obtained by using the wavelet technique for motor monitoring, under transient condition, have recently shown that this technique promises to be a powerful tool to detect frequency components indicative of the location of faults [30, 44, 64, 69, 72, 78].

1.4 Contributions of the Dissertation

There are several areas of research in nonstationary and stationary signal analysis. The development of an integrated signal processing approach and applications to machinery surveillance and diagnosis of instrumentation behavior in a nuclear power plant are the focus of this research.

The following are the contributions of this dissertation:

- Development and implementation of an integrated system approach for fault monitoring and diagnosis in nuclear power plants, using short-time Fourier

transform (STFT) and discrete wavelet transform techniques during transient conditions.

Development of a data analysis method with application to nuclear power plants, to detect and characterize transients in the data and estimate their frequency contents.

Implementation of a combined multiresolution analysis (MRA) and fast-Fourier transform (FFT) technique (multichannel analysis), to be applied in the analysis of stationary data from nuclear power plant.

Implementation of an integrated approach for fault monitoring and diagnosis in machinery condition using discrete wavelet transform technique during transient condition.

Implementation of a combined STFT and MRA technique with applications to analysis of stationary and nonstationary data from a rotating machinery to detect incipient changes in the measured signatures.

Demonstration of the effectiveness of diagnosing machinery condition using the combined STFT and MRA technique.

Development of a method for the selection of optimal wavelet functions.

Development and implementation of a MATLAB data analysis system toolbox.

Development of guidelines for selection and use of the wavelet functions.

1.5 Organization of the Dissertation

Chapter 2 of this dissertation presents a review of the time-frequency and time-scale theories. Chapter 3 presents the basic ideas about the discrete wavelet transform, multiresolution analysis and filter banks theory. Chapter 4 describes the implementation of the programs developed. Chapter 5 details the machinery experiment and the data analysis method. Chapter 6 describes the reactor experiments and data analysis method. Conclusions, recommendations and possible future work are outlined in Chapter 7. A complete list of references is provided. Appendix A contains additional results of reactor data analysis. A computer code for the selection of optimal wavelet functions is given in Appendix B.

CHAPTER 2

Theory of Time-Frequency and Time-Scale Analysis

2.1 Introduction

The Fourier transform is one of the classical tools used for random signal analysis. It decomposes the signal into constituent frequency components. Although the Fourier method is capable of isolating a peak frequency, given a pure frequency signal, some problems may be encountered when a signal contains two frequencies at close intervals. Two peaks are obtained but without any information of time-localization. In other words, a stationary signal is very well represented by the Fourier transform, but the time-related information in nonstationary signals is not recovered.

The time-frequency representation, known as the short-time Fourier transform (STFT), was introduced in 1946 by Gabor [4]. It was shown to overcome the problems of nonstationary signal analysis, but it has fixed frequency localization.

The wavelet transform offers a different compromise: the frequency localization is proportional to the frequency level, and as a consequence, the time localization gets finer at higher frequencies. According to Daubechies [11], the wavelet transform is a tool that cuts up data into different frequency components, and then studies each component with a resolution matched to its scale. The use of the wavelet transform has increased rapidly since it was rediscovered by two French researchers, Yves Meyer and Jean Morlet

[18]. The application of this new method has gained special attention in the signal processing field and several research activities have been actively pursued.

The wavelet transform overcomes the resolution limitations of the Fourier and STFT techniques. It was immediately accepted as a powerful tool for different engineering applications. Image processing, acoustics, fractal analysis, seismic analysis, sub-band coding and short-time Fourier transform, data compression, biomedical signal processing, condition monitoring, mathematics and statistics are several areas in which the wavelet transform has been successfully utilized. Several works have been published. Some relevant examples may be found in the following references [7, 10, 15, 17, 18, 19-22, 38-46, 51-56, 62-64, 68, 87, 92, 93].

Although the applications of wavelet analysis in nuclear engineering and machinery diagnosis are just beginning, a significant number of publications may be found on this subject [6, 8, 19, 20, 25-27, 30, 40, 44, 54, 64, 65, 69, 72, 78, 79, 85-88, 100, 105, 106].

A basic knowledge of the theories of short-time Fourier transform and wavelet transform is necessary for a thorough understanding of the above references. The following sections describe some basic concepts related to the theory used in this dissertation.

2.2 Short-Time Fourier Transform

The short-time Fourier transform (STFT) introduced by Gabor in 1946 [4] is useful in representing the time localization of frequency components of signals. The STFT spectrum is obtained by windowing the signal through a fixed dimension window (Figure 2.1). The signal may be considered approximately stationary in this window. The window dimension fixes both time and frequency resolutions. To define the STFT, let us consider a signal x (t') with the assumption that it is stationary when it is windowed through a fixed dimension window g (t'), centered at time location **T**. The Fourier transform of the windowed signal yields the STFT.

$$STFT(x,f) = \int_{-\infty}^{\infty} x(f)\, g(f-T)\, e^{\sim 2\pi f f'} df \qquad (2.1)$$

This equation maps the signal into a two-dimensional function in the time-frequency (t, f) plane. The analysis depends on the chosen window g (t'). Once the window g (f) is chosen, the STFT resolution is fixed over the entire time-frequency plane (Figure 2.2).

The STFT represents a compromise between time and frequency-based views of a signal. It provides some information about both. However, we can only obtain this information with limited precision. Precision is determined by the size of the window.

Figure 2.1. Short Time Fourier Transform Windowing Process

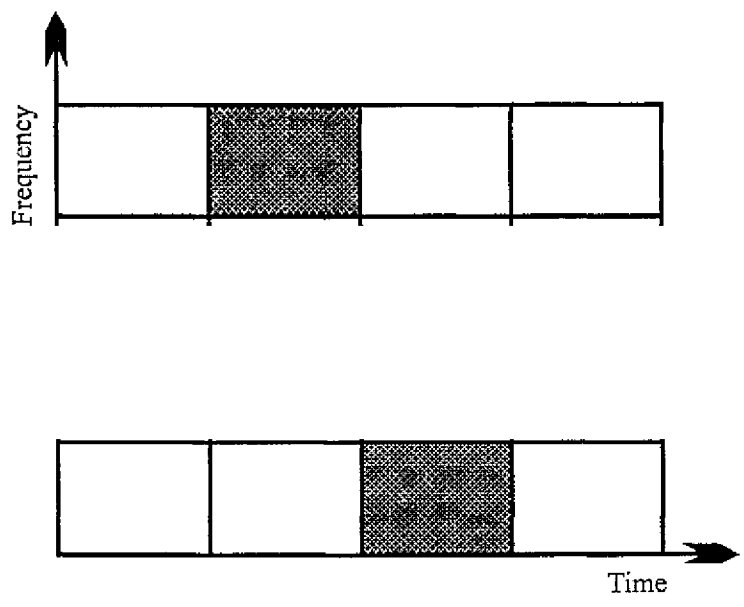

Figure 2.2. Bandwidth of STFT is Uniform in the Frequency Domain

The STFT is limited by the uncertainty principle which does not allow achieving a fine resolution in time and frequency simultaneously. As the time resolution is improved, by changing the window length, the frequency resolution is worsened. The Heisenberg inequality, which bounds the product of the bandwidth Af and the time, Δt is given by

$$\mathbf{A / * A / >} \quad — \tag{2.2}$$

Once the window g (t') has been chosen for the STFT, the time frequency resolution is fixed over the entire time-frequency plane. Usually, the STFT is represented by a plot called the STFT spectrogram, which depicts a signal's energy distribution in the time-frequency domain [29].

2.3 Continuous Wavelet Transform (CWT)

The class of functions that represent the wavelet transform are those that are square-integrable on the real line [14]. This class is denoted as $L^2(\mathbf{R})$. Thus, the notation $f(x) \in L^2$ means

$$\int_{-\infty}^{\infty} |\mathbf{f(x)}|^2 \, \mathbf{dx} < \infty \tag{2.3}$$

The sets of functions that are generated in the wavelet analysis are obtained by dilating (scaling) and translating (time-shifting) a single prototype function $\psi(x)$, which is called a basic wavelet. This function is oscillatory in type and is usually centered at the origin "dying out" rapidly as $x \to \infty$. Figure 2.3 shows two examples of wavelet prototype functions, the Morlet and Mexican Hat wavelets. These wavelet functions are defined by:

$$\psi(x) \sim e^{-\frac{x^2}{2}} \cos(5x) \qquad \text{Morlet} \qquad (2.4)$$

$$\psi(x) = (-\wedge = {}_{7r} ha\text{-}x) e^{\ast} \qquad \text{Mexican Hat} \qquad (2.5)$$

Both functions have [-5, 5] as the effective support.

The continuous wavelet transform (CWT) is rigorously discussed in references [11,14]. The wavelet function $\psi(x) \in L^2(R)$ has two characteristic parameters, called dilation a and translation b, which vary continuously.

A set of wavelet basis functions, $\psi_{ab}(x)$, may be generated by translating and dilating the basic wavelet $\psi(x)$ as:

$$\psi_{a,b}(x) = \frac{1}{\sqrt{|a|}} \psi\left(\frac{x-b}{a}\right) \text{ with } a, b \in U \; a \wedge O \qquad (2.6)$$

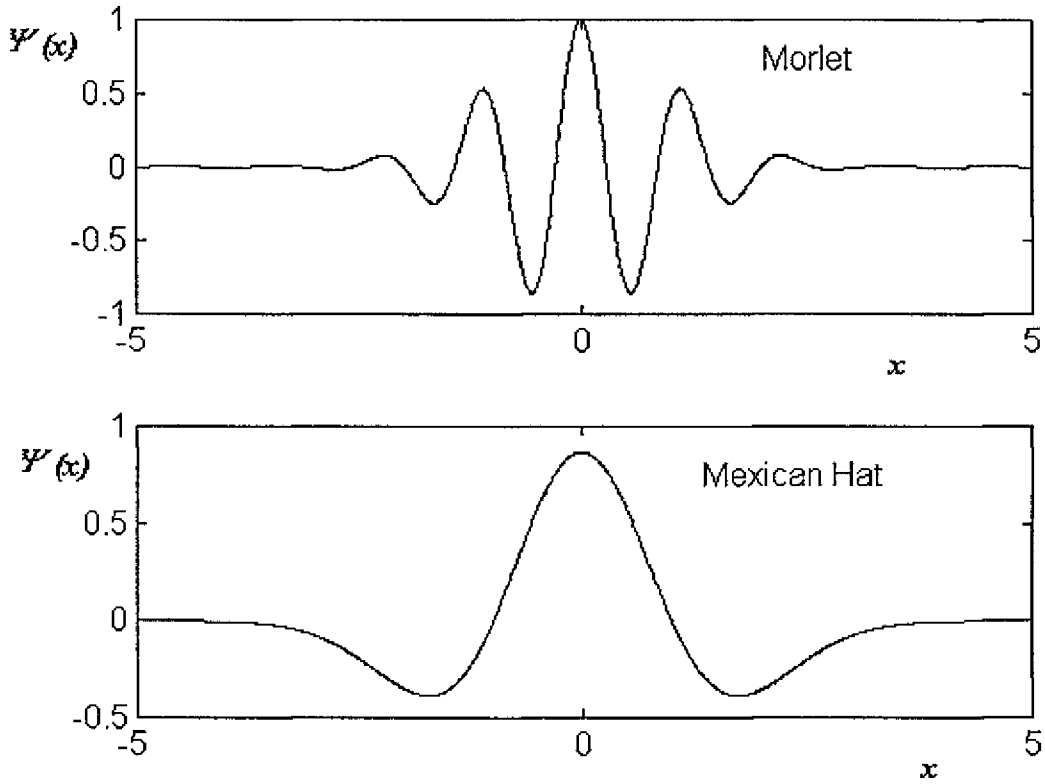

Figure 2.3. Examples of Wavelet Basis Functions, (a) Morlet Wavelet (b) Mexican Hat Wavelet

Figure 2.4 shows an example where the Mexican Hat wavelet scale "a" and position "b" parameters change. In Equation 2.6 the translation parameter "b" controls the position of the wavelet in time. By changing the value of "b" the wavelet is translated. The "narrow" wavelet can access high frequency information, while the more dilated

wavelet can access low frequency information. This means that the parameter "a" varies for different frequencies. For better accuracy, the time interval should be relatively small to obtain high-frequency information, and relatively wide for low-frequency information. These facts show that the wavelet has a zoom-in and zoom-out capability, that is, the wavelet is flexible to provide a time-frequency window that contracts at high frequencies. The Figure 2.5 shows that for the wavelet basis function , the higher the time resolution (smaller scale parameter "a") is, the worse the frequency resolution.

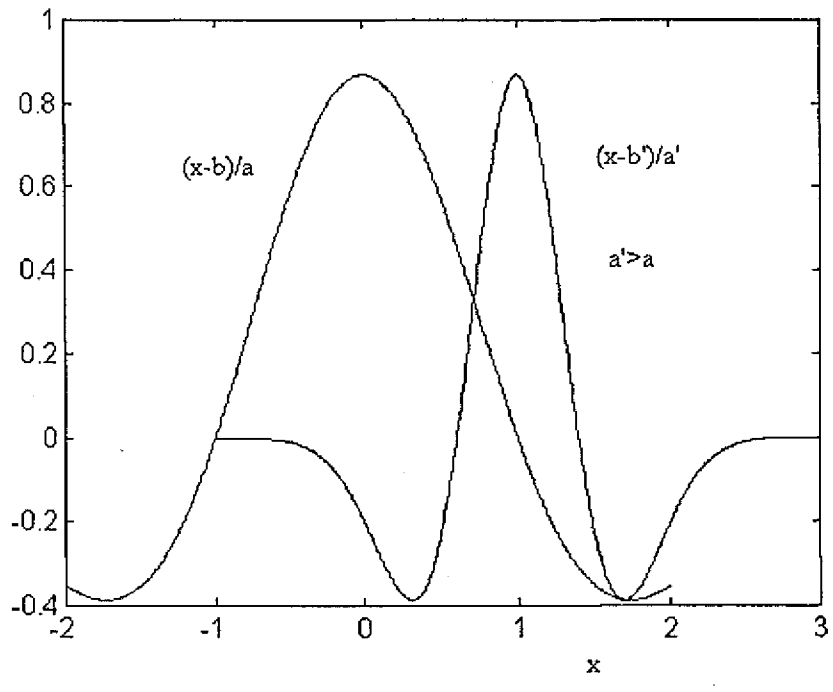

Figure 2.4. Varying the Scale "a" and Position "b" Parameters of a Mexican Hat Wavelet

Time

Figure 2.5. Bandwidth of Wavelet Transform

The continuous wavelet transform of a function / e $L^2(R)$ is defined as:

$$W_{a,b}(f) = \{f, y_{a,b}\} = \int f(x)\psi_{a,b}(x)dx \quad (2.7)$$

The wavelet coefficients are given as the inner product of the function being transformed with each basis function. The wavelet $y/(x)$ satisfies the admissibility condition [14]

(2.8)

where yr is the Fourier transform $y/$. The fmiteness of C_x restricts the class of $L^2(R)$ function $y/$ that can be used as the basic wavelet in the definition of the integral wavelet transform. The function $y/$ must also be a window function in $l^2(R)$, so that

$$\int_{-\infty}^{\infty} |y/(x)|\,dx < \infty \tag{2.9}$$

From Equation (2.8) the following relation is defined.

$$\hat{y}(0) = 0 \Rightarrow \int_{-\infty}^{\infty} y/(x)\,dx = 0 \tag{2.10}$$

This equation shows that the basis function $y/$ is compact support.

The previous equations lead to the definition of the inverse wavelet transform as:

$$/(x) = \frac{1}{C_x} \int_{a} \int_{b} W_f(a,b)\, \frac{1}{\sqrt{a}}\, y/\left(\frac{x-b}{a}\right) \frac{da\,db}{a^2} \tag{2.11}$$

The applications of the continuous wavelet transform (CWT) may be found in different areas, as described in references [6, 15, 22]. The CWT is often represented graphically and plotted as two-dimensional images, with color or gray-scale value

corresponding to the modulus and phase of W_{ab}. This representation is called a scalogram.

2.4 Wavelet Prototype Functions

The family of wavelet prototypes is very extensive and the wavelets are selected according to the problem to be investigated. Therefore a prior knowledge of the wavelet basis function is important in obtaining the right information during the analysis of a problem.

Alfred Haar first mentioned the term wavelet in 1909. The Haar wavelet family is of the simplest wavelets known.' The prototype Haar wavelet yr and the respective scaling function $<f)$ (the scaling function is an auxiliary function used to compute the $y/)$ are shown in Figure 2.6. These functions can be represented by the Daubechies wavelet of order 1 (dbl) and they are defined as:

$$y/(x) \quad 1 \quad \text{if} \quad 0<x<\frac{1}{2}$$

$$y/(x) \quad -1 \quad \text{if} \quad \frac{1}{2} < x < 1 \qquad (2.12)$$

$$j(x) \quad 1 \quad \text{if } x \text{ e } [0,1]$$

$$<t>(x) \quad 0 \quad \text{if JC} \wedge [0,1]$$

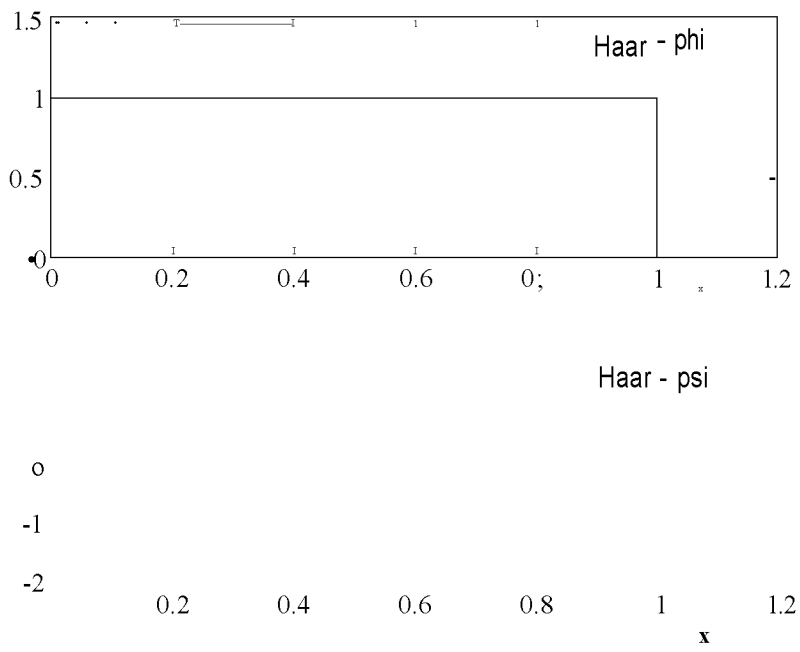

Figure 2.6. Haar Wavelet

Daubechies invented one of the most elegant families of wavelets. They are called compact supported orthonormal wavelets, which make discrete wavelet analysis practical [48]. The Daubechies wavelets have no explicit analytical expression but they can be defined by functional equations and their coefficients may be computed recursively using a very simple algorithm [12, 16]. This is discussed in the next chapter. The orthonormal wavelets have some special properties and are state in Table 2.1.

The scaling function ***(j)(x)*** and the corresponding wavelet ***ys(x)*** are defined by [12]:

Table 2.1. Wavelet Basis Function Properties [48,16]

Daubechies Wavelets **(dbN)**

1) General Properties

- phi exists and the analysis is orthogonal
- psi and phi are compactly supported
- psi has a given number of vanish moments

2) Possible analysis

- continuous transform
- discrete transform

3) Main nice properties

- Support
- Vanishing moments
- FIR filters

4) Main difficulties

- Poor regularity (smoothness)

5) Specific properties

- asymmetry

$$\langle t\rangle(x) \quad = \sum_{k=0}^{N-1} ?_j C_k \langle fi(^{2x}\text{-}^{k}) \qquad (2.13)$$

$$v(x) \quad = \sum_{*=0}^{N-1} Y(-l) \qquad c_k \langle f\rangle(^{2x\ +\ k}\ -\ ^{N\ +\ V}$$

Where N is an even number of wavelet coefficients $\mathbf{ç_k}$, $\mathbf{k} = 0$ to $N - 1$. The number **A:** is an integer, positive, zero or negative. These equations must satisfy the following orthogonality conditions in order to obtain the wavelet coefficient Q_k [12]:

1. Conservation of area: The scaling function is unique and retains the unit area during iteration. This condition is ensured by

2. Accuracy: Strang [12, 16] showed the condition that wavelet coefficients must satisfy in order to achieve the best possible accuracy to represent the signal being analyzed. This condition is given by the following equation:

$$\sum_{A=0}$$

The variable m has the following values: $m = 0,1,2\ldots, N/2 - 1$.

3. Orthogonality: In order to generate a an orthogonal wavelet basis system in $L^2(R)$, the following condition must be satisfied:

$$\sum_k c_k C_{k+2m} = Q \qquad m \neq 0 \tag{2.16}$$

The Daubechies wavelets follow the above requirements, and they are shown in Figures 2.7-2.9.

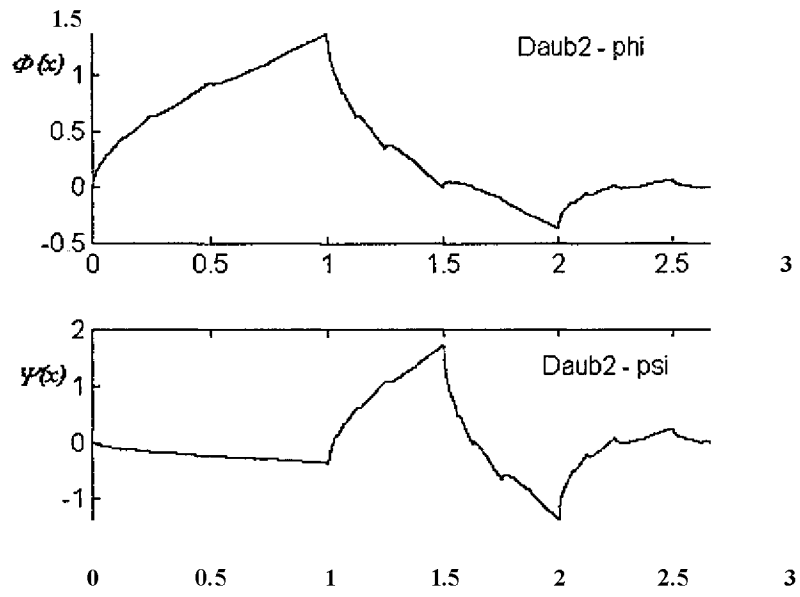

Figure 2.7. Daubechies Wavelet Basis Function **(db2)**

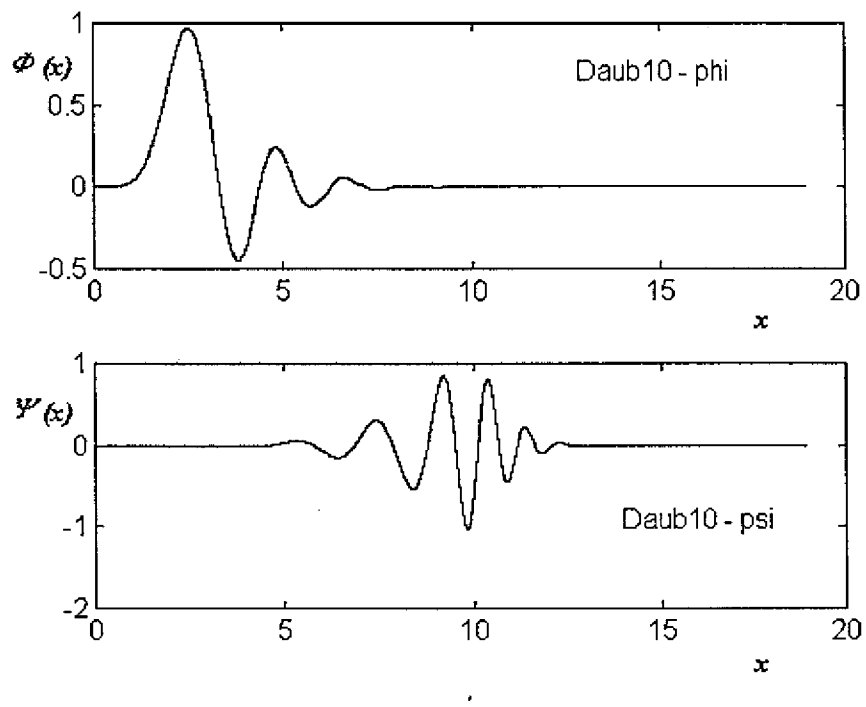

Figure 2.8. Daubechies Wavelet Basis Function (db10)

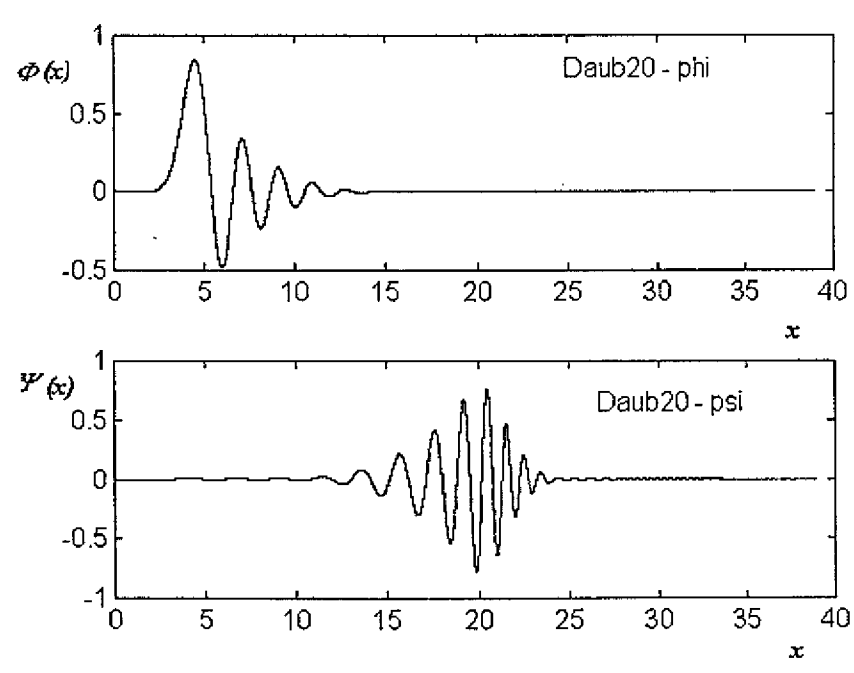

Figure 2.9. Daubechies Wavelet Basis Function (db20)

The MATLAB Wavelet Toolbox [48] includes several families of wavelets, such as Biorthogonal, Coiflets, Symlets, Morlet, Mexican Hat and Meyer wavelets.

A class of orthonormal wavelet basis, named wavelet packets, was introduced by Coifman and Meyer [16]. The family of wavelet packets, also known as wavelet packet atoms, is a collection of modulated waveforms, which correspond roughly to a covering of the time-frequency domain. The wavelet packet basis provides a specific way of coding a signal, preserving its global energy and providing a reconstruction of its features.

Mallat's algorithm computes the wavelet packet coefficients [48]. For a given signal, one can select the optimal wavelet basis to represent the signal. The minimum Shannon entropy of the expansion determines the choice of the basis function. This method is discussed in Chapter 4.

The family of wavelets introduced by Newland [12] is known as harmonic wavelets. Harmonic wavelets are orthogonal wavelets that may be expressed by

$$W_{m,n}() = \{\exp(in2nx)-\exp(im2nx)\}/i27v(n-m)x, \quad / = \mathbf{V} - Ï . \tag{2.17}$$

The level ***m,n*** denotes a wavelet in the frequency band ***m(2n)\on(2n).*** The variables **m** and ***n*** are real and positive. The condition ***n > m*** is necessary to form a complete set of wavelets. The adjacent wavelet levels must have Fourier transforms

whose frequency bands touch each other [12]. Figure 2.10 depicts the harmonic wavelet prototype function for $m = 1$, $n = 2$.

There are advantages of using complex harmonic wavelets. First, because they are complex, they can detect a harmonic frequency component, whatever its phase. Secondly, the complex harmonic wavelet has an efficient algorithm for wavelet computation. An extensive discussion of the harmonic wavelet properties is found in references [12,19,20].

The criteria for selecting the prototype wavelet function to be used in the wavelet transform signal analysis is discussed in Chapter 4.

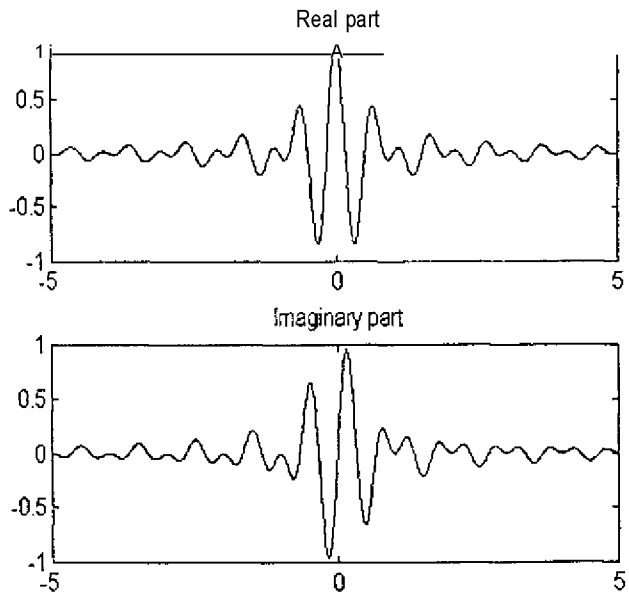

Figure 2.10. Harmonic Wavelet Prototype

CHAPTER 3

Discrete Wavelet Transform (DWT), Multiresolution Analysis (MRA) and Filter Banks

3.1 Introduction

The basic theories of discrete wavelet transform, multiresolution analysis and filter banks are discussed in this chapter. There are several references which elaborate on the mathematical rigors and details of these topics. The basic formulation of various algorithms is discussed.

3.2 Discrete Wavelet Transform

The computation of the wavelet coefficients using the continuous wavelet transform requires a considerable effort. The purpose of using the discrete wavelet transform (DWT) is to reduce the computational burden. The scales and positions are chosen based on powers of two, so called dyadic scales and positions, which make the analysis much more efficient and accurate.

The discrete representation of an orthonormal compactly supported wavelet basis of $L^2(R)$ is formed by dilation and translation of a single function $\psi(x)$, called the wavelet function. Assuming that the dilation parameter a and translation parameter b take only discrete values

$$a = a^{j}_{0}$$
$$b = kb_{0}a^{j}_{0} \tag{3.1}$$

where $k, j \in Z$, $a_0 > 1$, and $b_0 > 0$. Substituting these parameters in the Equation (2.6) the wavelet function may be rewritten as:

$$\psi_{j,k}(x) = a_0^{-j/2}\, \psi(a_0^{-j}x - kb_0) \tag{3-2}$$

The discrete wavelet transform (DWT), obtained substituting the Equation (3.2) into Equation (2.5), is defined as:

$$DWT(f) = \langle f, \psi_{j,k} \rangle = \int f(x)\, a_0^{-j/2}\, \psi(a_0^{-j}x - kb_0)\, dx \tag{3.3}$$

The inverse discrete wavelet transform reconstructs the function $f(x)$ as:

$$f(x) = T \sum_{j=-\infty}^{\infty} \sum_{k=-\infty}^{\infty} \langle f, \psi_{j,k} \rangle \psi_{j,k} \tag{3-4}$$

where $\psi_{j,k}$ are dual functions of $\psi_{j,k}$ [14].

An efficient algorithm can be constructed to evaluate the integral wavelet transform defined in Equation 3.3 and for reconstructing ***f(x)*** from Equation 3.3, only using discrete samples. In this case, the frequency axis is partitioned into bands by using power of two for the scale parameter ***a***. Considering only samples at the dyadic values (here the parametersb_0 and $\mathbf{a}_0$, in Equation 3.1, assume the following values b_0 = 1 and $\mathbf{a}_0$ = 2) ***b = k2^j*** on the time-axis, when ***a = 2^j,*** the Equation 3.3 becomes

$$DWT = < f, w_{j,k}(x) > = \int_{-\infty} f(x)\{2^{j/2}\psi(2^{-j}x - k)\}dx \qquad (3.5)$$

The function ψ_{jk}, defined by Equation 3.2, constitutes an orthonormal basis for $L^2(R)$ and is given by

$$\psi_{j,k}(x) = 2^{-j/2}\psi(2^{-j}x - k); \quad j,k \in Z.$$

The wavelet prototype functions defined by Equation (3.5), as explained in Section 2.4, were created by Daubechies [11]. Mallat [31] introduced an efficient algorithm to perform the DWT known as the Multiresolution Analysis (MRA). It is well known in the signal processing area as ***the two-channel sub-band coder.*** The MRA was formulated based on the study of orthonormal compactly supported wavelet functions. The concept of MRA provides a natural framework for the understanding of wavelet functions. These ideas are presented in detail in the following section.

3.3 Multiresolution Analysis (MRA) Properties and Filter Banks

The multiresolution analysis of $L^2(R)$ consists of successive approximations of the space Vj of $L^2(R)$, $j \in Z$, where Z is a set of integers, with the following properties [11,14,37]:

1. Nested: $Vj \subset V_{j+1}$,

2. Scaling: $v(x) \in V_j \iff v(2x) \in V_{j+1}$,

The function $v(2x)$ covers the same time period of time with twice as many points as $v(x)$. Thus, $v(x)$ is a coarser (less detailed) representation than $v(2x)$. $V(2x)$ is a finer (more detailed) representation than $v(x)$, with higher resolution than $v(x)$. Vj corresponds to a different scale/ resolution, as j takes different values.

3. Shift invariance: $V(JC) \in V_0 \iff v(x+1) \in V_0$

4. Closure or Completeness: $\bigcup_{y=-\infty}^{\infty} Vj$ is dense in $L^2(R)$

Any signal in $L^2(R)$ can be approximated by signals in the union of space Vj.

5. Emptiness: $\bigcap_{j=-\infty}^{\infty} Vj = \{0\}$

Emptiness means that $|/_{v}-(JC)| \to 0$ as $j \to -oo$.

6. There exists a scaling function $\mathbf{0}(;t) \in V_{o}$ such that

$$0_{M}(x) = 2^{\wedge/} 0(2^{-j}x-k);j,k\in Z \tag{3.6}$$

forms an orthonormal basis of V_{o}, i.e.,

$$\mathbf{K} * \mathbf{f} * \wedge \wedge = <\mathbf{V}*' \tag{3-7}$$

where J is the well known Kronecker symbol.

For the scaling function $<p_{\xi}(x)$ e V_{o} c F_{p} there is a sequence $\{/^{\wedge}\}$ so that the $0(x)$ satisfies the condition

$$(j>(x)^{\wedge}2Y,h_{k}<j)(2x-k) \tag{3.8}$$
$$k \quad .$$

This equation is known as *the refinement equation, dilation equation, or hvo-scale difference equation.*

Furthermore, let us define W_{j} as a complementary space of V_{j} in V_{j+1}, such that

$$V(JC) \in W, \iff V(2JC) \text{ e } FF_{,+1} \tag{3.9}$$

and

$$v(x) e^{*} F_{0} \iff v(x+1) e JF_{0}$$

We then conclude

$$\overset{00}{0}_{j=-<} \; Wj = V\{K\}. \tag{3.10}$$

Equation (3.10) states that the set of basis functions formed by translated of $<f>(x)$ and dilated translated of $y/(x)$ span all $L^{2}(R)$.

Since the $y/(x)$ is a wavelet [14] and it is also an element of $V_{@}$, a sequence $\{g_{k}\}$ exists such that

$$_{k}(x) = 2Y_{A}g_{ft} \; ¿(2^{*} - ^{*}) \tag{3.11}$$

Based on the previous discussions, we conclude that the multiscale representation of a signal $f(x)$ may be achieved in different scales of the frequency domain by means of an orthogonal family of functions $\$(x)$, in the form of weighted sums of shifted and

dilated versions of that signal. The following steps will show how to compute the function in Vj.

The projection of the signal $f(x) \in V_0$ on V_1 defined by $Pf(x)$ is given by

$$\text{iV}/'(*)=\text{E}^{\text{c}}\text{MM}*> \qquad (3\text{-}12)$$

The coefficients c_{jk} are obtained by the inner product between the function $f(x)$ on the basis $<f>_{jk}$

$$Cj,_k = \int f(x) f_{j,k}(x)\,dx \qquad (3.13)$$

The projection of the function $/(x)$ on the subspace Wj is defined by

The coefficients d_{jk} are obtained by the inner product of $f(x)$ and $y/_{jk}$ defined by

$$dj,_k=\int f(^{x})v'j*(^{x})^{dx} \qquad (3\text{-}15>$$

Because Vj = © $W_{\llcorner \omega}$ the original function $/(x)\ e\ V_{o}$ can be rewritten as

$$f(x)=Y_{k}c_{hk}<Pjx)+Y^{r}L^{a}j*yj*(^{*})> \qquad {}^{1\ >}\ J\ o \tag{3-i6}$$

The coefficients c_{jk} and d_{jk} are inner products between $f(x)$ and $<f>_{jk}$(JC), and $f(x)$ and $^{\wedge}/_{j,t}(\mathbf{x})$, respectively, and they are given by [5]

The multiresolution representation is linked to Finite Impulse Response (FIR) filters. The scaling function $<j>$ and the wavelet $y/$ are obtained using the filter theory and consequently also the coefficients defined in Equations (3.17) and (3.18). As an illustrative example [5], let us obtained the scaling function $<f>$ and then the mother wavelet $y/$, since they are closely related to each other.

Using Equation (3.8) and applying the Fourier transform to both sides yields

(consider the variable x as time and $x = ^{\wedge})$

$$\langle f\rangle(t)e^{-i\omega t}dt = 1/K \int \langle f\rangle(t-k\Delta t \tag{3.19}$$

By replacing the integration variables, Equation (3.19) becomes

$$O(\omega) = \mathrm{JTfyWf}; \tag{3.20}$$

where $Q?(\omega)$ is the Fourier transform of $\langle j\rangle(t)$. $H(a)$ is the discrete Fourier transform of h_k which is periodic in frequency. As $\langle\$\rangle(0) * 0$, $H(0) = 1$. This means that $H(\omega)$ is a lowpass filter. Decomposing Equation (3.20), and considering $0(0,) = 1$, the following expression is obtained

$$*=i \quad 2$$

The above equation shows that the scaling function $\langle t\rangle(t)$ is computed by the lowpass filter $H(a\rangle)$. The mother wavelet $y/(t)$ is computed by defining the function $G(\omega)$ so that

$$H(a)G(a\rangle) + H(\langle Q + 7c)G'(a\rangle + 7u) = 0 \tag{3.22}$$

The pair ***H(co)*** and ***G(co)aie*** known as ***quadrature mirror filters*** for MRA. One solution of the Equation (3.22) is

$$G(co) = -e^{-jo}H(o\} + n:) \tag{3.23}$$

Substituting ***H(0) = l*** and ***H(x) = 0*** into (3.23) yields ***G(0)*** = 0 and ***G(n)*** = 1, respectively. This means that ***G(a>)*** is a highpass filter.

The inverse Fourier transform of ***G(a>)*** yields

$$g_n=(-\)^k h_n, \quad \text{ft} = 0,1,2,\ldots \tag{3.24}$$

Using the above equations and Equation (3.11), the following expression is obtained

$$V(a>) = \frac{1}{2} G(^)ff[H(^_{k=2}\frac{-}{2}) \tag{3.25}$$

where ***^(co)*** is the Fourier transform of ***y/(t).***

The approximation coefficient $c_{j,k}$ in Equation (3.17) can be computed recursively by a lowpass filter H. Figure 3.1 illustrates the operation defined in Equation (3.17), where the block following the lowpass filter denotes downsampling by two (^ 2) In Equation (3.18), g_k corresponds to a highpass filter, and the detail coefficient d_{jk} are series of wavelet coefficients which may be obtained by the filter banks, as shown in Figure 3.2.

Equations (3.17) and (3.18) show that, given the high-resolution coefficients, we may obtain the low-resolution coefficients. Conversely, we can obtain the high-resolution coefficients based on the low-resolution coefficients:

$$c_{J,k} = V2(IX_{-21}.c_{,-M} + 2>*_{-21}.rf;-_M) \qquad (3\text{-}26)$$

Therefore, through this relationship we may recover the original signal by using a filter, which represents the inverse discrete wavelet transform, as shown in Figure 3.3.

The process described in Figures 3.2 and 3.3 was implemented by Mallat [31]. This process is an important connection between wavelet theory and multiresolution filter banks. The implementation of the theoretical concepts presented in this chapter is discussed in Chapter 4.

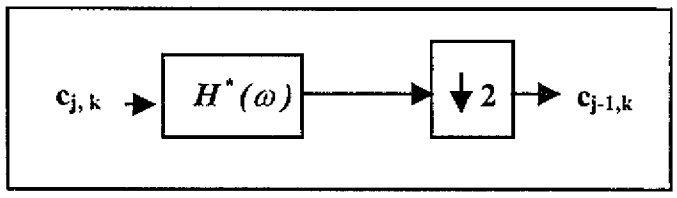

Figure 3.1. Computation of the Low-Resolution Coefficients Cj_i,k **Using the Lowpass Filter** *H*(a)[5]*

C0-2&

M

H((ù)* -	+ 2
G*(Cù) -	| 2

d(j-\JK)

G*(0))[4f2 *d(j-ljc)*

Figure 3.2. Discrete Wavelet Transform via Digital Filter Banks [5]

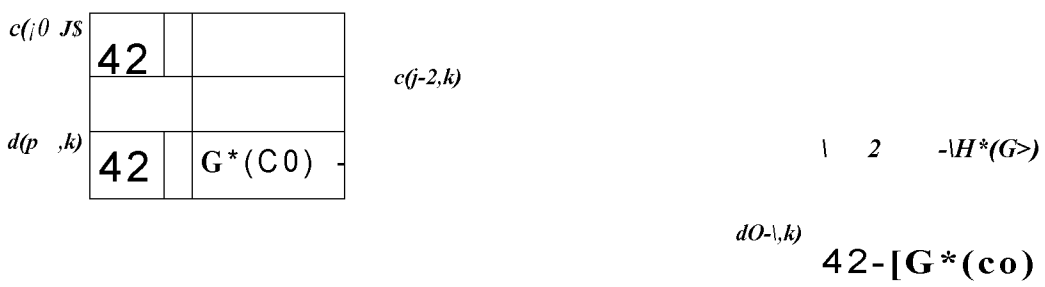

Figure 3.3. Inverse Discrete Wavelet Transform via Digital Filter [5]

CHAPTER 4

System Implementation

4.1 Introduction

The previous theoretical discussion suggests the construction of a system able to perform all tasks necessary to obtain information that characterizes the behavior of the monitored system during its operation. To accomplish the proposed tasks, an integrated system was developed to perform the analysis of wide-band signals.

4.2 MATLAB Data Analysis System Toolbox

The data analysis system implemented in this dissertation was designed to provide an integration among several powerful MATLAB toolboxes and the programs developed for the applications concerned with the research work. A general idea about the implementation of the developed system and its applications is shown schematically in Figure 4.1. The fast Fourier, short-time Fourier, and the wavelet transform techniques were applied to experimental measurements from equipment monitoring and process sensors. The computational results were processed using the statistical and graphical toolboxes. An illustration of the general components utilized to build the proposed system is shown in Figure 4.2. The MATLAB data analysis system toolbox (MDAST) is very flexible and allows one to add or remove any desired tool.

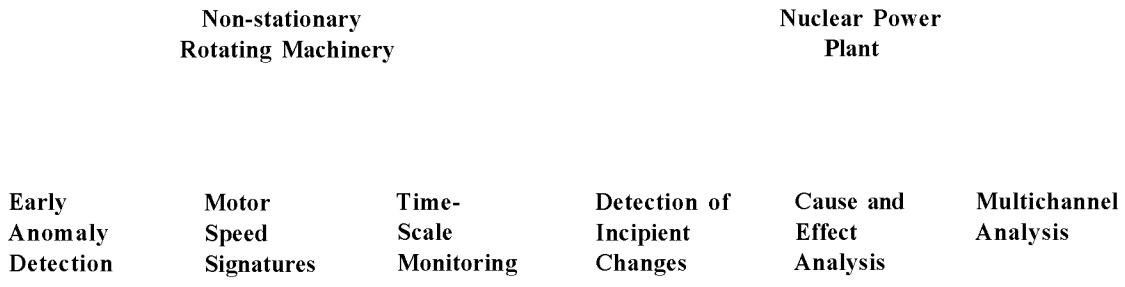

Figure 4.1. Implementation and Applications of the MATLAB Data Analysis System Toolbox (MDAST)

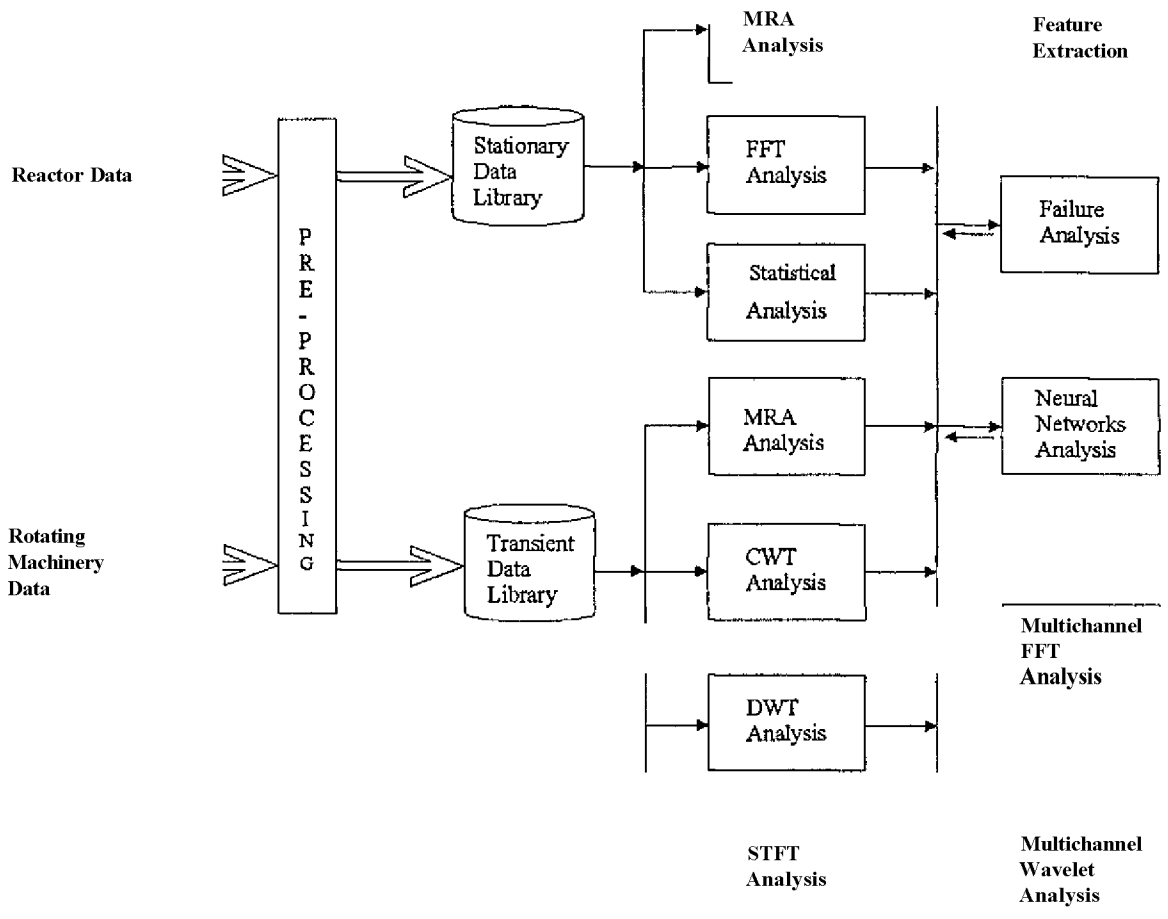

Figure 4.2 MATLAB Data Analysis System Toolbox

The major feature of the MDAST is its ability to analyze stationary and non-stationary signals by combining some advanced signal processing methods and to integrate them to the standard signal processing techniques. The following sections provide details of various components of the implemented signal processing system.

4.2.1 Pre-Processor

The pre-processor showed in Figure 4.2 consists of a program, which performs the normalization of data and removes the DC-level component from the signal.

4.2.2 Short-Time Fourier Transform

The time-dependent Fourier transform is provided by the MATLAB Signal Processing Toolbox by using the command line ***specgram,*** as shown in Program 1 (Appendix B). The function ***specgram*** computes the windowed discrete-time Fourier transform of the signal by sliding a selected window as described by Figure 2.2. A Harming window was selected to perform the rotating machinery analysis. The coefficients of a Harming window are defined as

$$w(k) = 0.5(1-\cos(2n\text{-}\hat{}\text{—})), \quad k = \backslash,\ldots,n \qquad (4.1)$$
$$n + \backslash$$

where n is an integer.

The analysis of the reactor data using STFT is performed using Program 2 listed in Appendix B. A Gaussian window is used when the discrete-time Fourier transform of the signals is computed. The coefficients of a Gaussian window are defined as

$$w(k) = \left(-\hat{}_{r}\right)\hat{}\,-\quad {}^{z*L}_{* = 1,..,\kappa} \qquad (4.2)$$

Further discussion of the implementation of STFT using the Gaussian window may be found in reference [6].

4.2.3 MATLAB Wavelet Toolbox

The wavelet toolbox is a collection of functions built in on the MATLAB platform that can be used to perform signal analysis using different wavelet basis functions [48]. Although the wavelet toolbox has a very efficient graphics user interface (GUI), it was decided to use the command line as an easy option to integrate all features of the developed system.

Essentially, the wavelet toolbox contains several command line functions that allow one to examine the characteristics of the individual wavelets, compute some statistical functions, compute the continuous wavelet transform (CWT), discrete wavelet transforms (DWT), and the synthesis of the one-dimensional signal. There are also some useful functions for signal denoising and compression (according to reference [48], "the

notion behind compression is based on the concept that a regular signal component can be accurately approximated using a small number of approximation coefficients and some of the detail coefficients").

The scheme used to implement the DWT was developed by Mallat [31]. This scheme applies the classical filter known as the ***two-channel sub-band coder*** using conjugate ***Quadrature Mirror Filters*** (QMF). The command line functions used to perform the DWT are described in Program 3 (Appendix B).

In the multiresolution analysis, the input signal is stripped off by convolving the original signal with two complementary filters: a highpass filter ***(HiF_D)*** to obtain signal details and a lowpass filter ***(LoF_D)*** to obtain the approximations, followed by dyadic decimation (The command line function ***dyaddown,*** in the MATLAB wavelet toolbox, is used to perform the dyadic decimation and it keeps the even index elements). The approximations are high-scale, low-frequency components of the signal. The details are the low-scale, high-frequency components. This procedure is illustrated in Figure 4.3. The number of stages of the DWT for a given signal of length N is $\log_2 N$. The signals at each decomposition level can be reconstructed using the reconstruction steps described in Figure 4.4 (inverse discrete wavelet transform). Figure 4.5 shows the results of an analyzed signal by the MRA algorithm using the GUI features of MATLAB Wavelet Toolbox [48]. In this figure a signal s is decomposed to eight sub-band levels. The reconstructed approximation signals and detail signals, at each level, are plotted. Program 3 (Appendix B) gives the command line functions to perform the MRA.

Decomposition step

Low-pass filter *downsample* *approx. coefif.*

L,F_D * 2

cA,

level y + 1

level j *H.F D* i 2 cD_{j+1}

Highpass filter *downsample* *detail coefif.*

Initialization cA_0 = *signal*

Figure 4.3. One-Dimension DWT decomposition Step Scheme [48]

Reconstruction step

approx. coefif. *upsample* *Low-pass filter*

cA, 42 *L.F D* >

level j U wkeep cA_{7+1}

cD, 42 *H,F_D*

level y + 1

detail coefif. *upsample* *Highpass filter*

where: **wkeep** takes the central part ofU with a convenient length.

Figure 4.4. One-Dimension IDWT Decomposition Step Scheme [48]

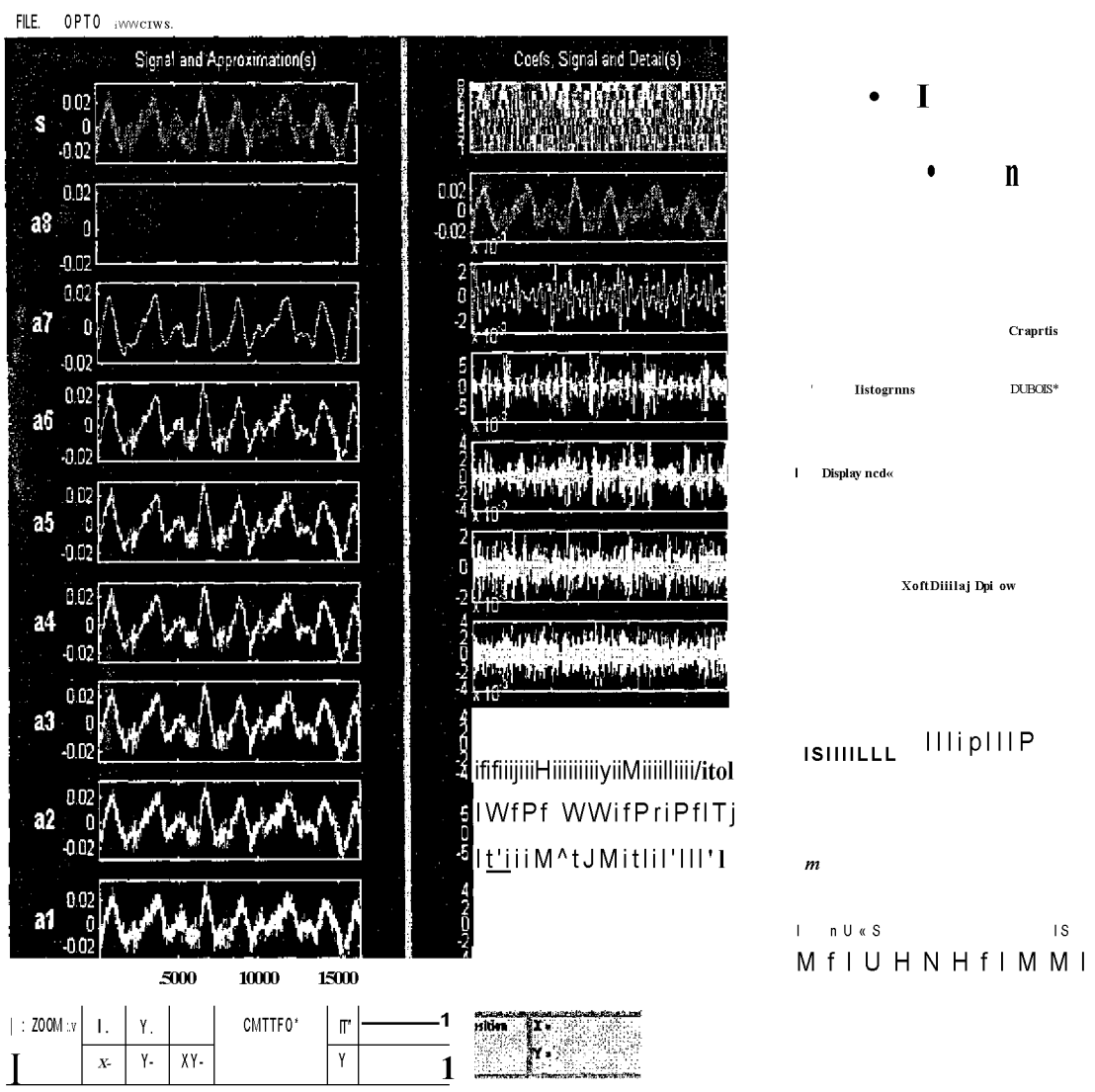

Figure 4.5. MRA Results from Using MATLAB Wavelet Toolbox. The original Signal (s) is Decomposed into Approximations (a) and Details (d) Signals [48]

4.2.4 Optimal Wavelet Selection

The selection of the wavelet basis function to be used to compute the wavelet transform coefficients is crucial in order to assure the best match with the signal during the computational steps. The selection of the basis function is related to the best reconstruction of the signal and the best identification of features in the analyzed signal. The challenge is to find out which wavelet basis is most suitable for application under study. Usually the selection procedure is based on the experience developed in a specific research field.

This research work deals with vibration signal measurements from rotating machinery and nuclear power plant systems at different operating conditions. Signals from tachometers, proximity probes, accelerometers, in-core and ex-core neutron detectors, flow and pressure sensors are candidates for analysis using wavelet transform techniques. This variety of signals requires that a method be used to select the wavelet prototype. The optimal wavelet basis selection method implemented in this work is based on the minimum entropy energy [67, 83].

By definition, the entropy energy E must be an additive cost function. This function is defined by the equation:

$$E(0) = 0 \quad \text{and} \quad E(s) = £ \tag{4-3}$$

The variable 5 is the signal and s_i are the coefficients of s in an orthonormal wavelet basis. The entropy E must be an additive cost function such that $E(0) = 0$ and $E(s) = \sum E(s_i)$. The entropy of the decomposition signal is computed using Shannon's entropy defined by

$$E(s) = -\sum s_i^2 \log(s_i^2), \tag{4.4}$$

with the convention **01og(0) = 0.**

The minimum entropy is obtained using E_{min} = *min^E^,* where the indices i = **1,..** are the different wavelet basis family used.

Program 4 (Appendix B) computes the entropy energy E of a decomposition signal using the MATLAB Wavelet Packet command line function ***wentropy.*** In the signal decomposition process, the optimal wavelet basis is defined as the one, which results in minimum, entropy energy at a specific decomposition level. The minimum entropy value obtained for each wavelet prototype used is recorded. Finally, when all wavelet families are analyzed, the results are plotted. Some results are shown in the next Chapters 5 and 6.

4.2.5 Discrete Wavelet Transform Algorithm Using the Harmonic Wavelet

The harmonic wavelet algorithm basically computes the wavelet coefficients that are defined by

$$\text{"».»,* = (» - ™)} \int_{J}^{\ll} \text{f/(*) Wm,»}\left(\frac{x}{n-m}\right) d\,x \tag{4.5}$$

$$a_{,,,,,,k} = (m\text{-}n) \int f(x) w_{mn}\left(x - \frac{}{,}\right) dx_{n-m} \tag{4.6}$$

where $f(x)$ is a real function, $a_{m,n,k}$ is the complex conjugate of $a_{m\,n\,k}$.

The harmonic expansion formula of $/(x)$ for $mliz < \omega < n2\%$ is given by the equation:

$$f(x) = tt_0 + Y_J \sum_{Itn\ \pounds o}^{n-m-l} (m,n,k\ W_{m,n}\left(\frac{x}{n-m}\right) + \text{" '"•'>'" "}>\text{"-"}\left(\frac{x}{n-m}\right) \tag{4.7}$$

In this case there are $m\text{-}n$ wavelets in the frequency band $mlii < \omega < n2n$ each spaced $1 / (« - m)$ apart in the x-domain, so that the position index has to run from $k = 0tok = n\text{-}m\text{-}l$. The summation over m, n covers pair of numbers, starting with

m = \, in the sequence 1,n; $n,p;p,q;q,r$etc.where \<n< p <q <r, and continuing to **oo** . The variable w is the complex conjugate of w .

There are two advantages in using harmonic wavelets. First, because they are complex, they can detect a harmonic frequency component, whatever its phase. Second, it is a very efficient algorithm for the wavelet computation. The algorithm used to compute the a_{mnk} coefficients can be devised utilizing two applications of the FFT. According to Newland [12], the Mallat's algorithm for wavelet derived from dilation equations is a sequential algorithm in the sense that successive wavelet levels are computed in sequence (from the highest level and working downwards). In contrast, the FFT algorithm for harmonic wavelets is a parallel algorithm. This fact gives a significant advantage in real time applications.

An extensive discussion of harmonic wavelet properties and the harmonic wavelet transform algorithm may be found in references [12,19, 20, 88]. Program 5 (Appendix B) contains the command line functions to compute the harmonic wavelet coefficients.

The harmonic wavelet transform analysis gives the maps (2-D plot of the square values of the wavelet coefficients) in the time-scale domain. The maps provide clear information about the evolution of the monitored signal during the transients. This

dissertation uses wavelet map concepts for machinery vibration analysis and for nuclear power plant experiments.

4.2.6 Discrete Dilation Wavelet Transform Algorithm

The dilation wavelet (Daubechies wavelet) can be obtained recursively using the general iteration equation defined by the resulting expression [12, 88].

$$t,(x) = cJ_{M}(2x) + c^{\wedge}{}_{M}(2x- 1) + cJ_{H}(2x -2) + cJ_{H}(2x - 3) \quad (4.8)$$

where c's are numerical (real) constants either positive or negative.

An example of the numerical solution of Equation (4.8) is given by the Daubechies 4 wavelet defined as:

$$0j(x) = c_{0}\langle\rangle (2x) + c_{x}\langle f\rangle(2x - 1) + c_{2}0(2x - 2) + c_{3}0(2x - 3) \quad (4.9)$$

After successive iterations Equation (4.8) should result in a stable value. The dilation wavelet $w(x)$ defined using the stable $\langle p(x)$ is given by:

$$w(x) = -c^{\wedge}\text{ÇL}x) + c_{2}\langle f\rangle(2x - 1) - c^{\wedge}(2x - 2) + c_{q}\langle j\rangle(2x - 3) \quad (4.10)$$

The numerical values of the coefficients of this equation are determined using the orthogonal properties. The number of coefficients N can be extended, but a value of $N = 20$ is used in practical calculations (Daubechies 20).

The discrete dilation wavelet transform algorithm is essentially based on Mallat's pyramid algorithm, so that numerical iteration defined by Equation (4.8) becomes basically a process of matrix multiplication. The above process may be expressed by two matrices L_n and H_n with n rows and $2n$ columns. The array of coefficients that define the matrices are composed of the coefficients that appear in the equations that define $\langle j \rangle$ and w. The coefficients $c_0, c_1, c_2, \ldots, c_{N-1}$ are specifically chosen to achieve the orthogonality and accuracy. There are details shown in reference [12] that follow the relations applied to the matrices L_n and H_n of the same order.

$$\frac{1}{2}LL' = I; \quad LH' = 0$$

$$HL' = 0; \quad \frac{1}{2}HH' = I \tag{4.11}$$

In addition there is a perfect reconstruction condition

$$\frac{1}{2}(HH' + LL') = I \tag{4.12}$$

This algorithm is discussed in reference [12] and the command line to perform these steps is given in Program 5 in the Appendix B.

4.2.7 Mean-Square Wavelet Maps

The mean-square wavelet maps are the contour plots, which contain in the y-direction the wavelet level information and in x-direction the time information. The map plane has a grid that covers all wavelet levels and positions. The height of the surface is proportional to the squared wavelet coefficient amplitudes. The construction of the wavelet maps is based on Parseval's theorem. The results for the dilation wavelet expansion formula is given by [12]

$$\frac{1}{N}\sum_{n=0}^{N-1} f_n^2 = \sum_{j=1}^{j_0-1}\frac{1}{2^{j-1}}\sum_{k=0}^{2^{j-1}} a_{j,k}^2 + a_{N/2}^2 \qquad (4.13)$$

where f_n is a real function and $N = 2^{j_0}$. The variable N is the signal sample value.

The results for the harmonic wavelet expansion formula is given by

$$\frac{1}{N}\sum_{n=0}^{N-1} f_n^2 = \sum_{j=1}^{j_0-1}\sum_{k=0}^{2^{j-1}} a_{j,k}^2 + a_{N/2}^2 \qquad (4.14)$$

In this case there are only $j = 0$ to $n_0 - 2$ wavelets.

According to Newland [12], "at level / there are 2^{j} wavelets in the unit interval. For a train of wavelets, all the same scale, the wavelets are spaced $-^{j}$ apart so that their fundamental frequency is 2^{j} cycles/unit interval. Therefore, wavelet level is a measure of frequency with the fundamental frequency doubling as we move upwards from one level to the next. Since the signals analyzed have independent variable x as time, the map can be interpreted as a plot of frequency (increasing in octaves) versus time ".

The harmonic wavelet analysis gives, in the time-scale domain, the map, which provides a clear information about the evolution of the monitored signal during the transients. References [12, 20] give an extensive discussion of the mathematical basis and applications of the mean-square wavelet maps. This dissertation used the maps to represent the plots from the wavelet vibration analysis of rotating machinery and nuclear power plant experiments. The 3-D plots utilizing the squared wavelet coefficients are also used during the signal analysis. This type of representation is called wavelet power spectrum density. Program 6 (Appendix B) provides all command line functions to obtain the 2-D maps and 3-D plots using the algorithms described in this section.

4.2.8 Multichannel Wavelet Analysis

The multichannel data analysis of the signals was performed combining the wavelet multiresolution analysis and the fast Fourier transform algorithms. The signal is decomposed into details and approximations signals that contain, at each level, different

frequency band information. The multichannel analysis computes, using the wavelet coefficients at a sub-band level, the auto-power spectral density, cross-power spectral density, coherence and phase. The advantages of using this method rely on the fact that one can eliminate the undesired frequencies. Thus, the signal analysis is performed in a "clean" way. Program 7 performs the wavelet and FFT multichannel integration (Appendix B). The results of applications of this method are presented in Chapters 5 and 6.

4.2.9 Statistical Analysis

MRA and statistical analysis are combined to obtain the mean and RMS values at each sub-band level of the decomposed signal. The purpose of this analysis is to verify if there is any non-stationary trend in the measurement data. Program 8 (Appendix B) gives the command line functions to perform the statistical analysis.

CHAPTER 5

Rotating Machinery Experiment and Data Analysis Method

5.1 Introduction

The need for monitoring and diagnosis of process dynamics and sensors, in industrial systems, has increased the efforts towards developing new data analysis techniques. The main goal of this technological improvement is to extract more detailed information contained in the measured data. Standard digital signal processing techniques such as time series statistics, correlation analysis and the fast Fourier transform have been used to detect faults in plant components. The results showed that they were not sensitive to small and short-term anomalies.

This chapter provides a general but precise idea about the potential use of a novel method for monitoring and diagnosis of rotating machinery. This method combines two powerful signal processing tools: the fast Fourier transform and the wavelet transform.

5.2 Rotating Machinery Experiment

Early detection of anomalies in rotating equipment such as motors, pumps, turbines, compressors, etc., is crucial for the safety and economic operation of an industrial system. The challenge is to identify and characterize the causes of anomalies in the incipient stage, since the background noise sometimes may weaken the signals.

Stationary signals are often analyzed using the standard Fourier transform techniques. When a system is non-stationary or undergoes a transient, the Fourier technique does not provide proper information about the characteristic changes in the signals. The analysis of non-stationary signals should be performed using time-frequency (STFT) and time-scale (wavelet transform) techniques. Integrating STFT and the wavelet transform provides a more powerful tool for signal monitoring than the standard FFT analysis alone.

The wavelet transform techniques for fault monitoring and diagnosis of machinery have been increasingly used during recent years, since these techniques allow us to perform the analysis of a system during transients. The application of traditional techniques is limited to stationary processes. The combination of STFT and discrete wavelet transform techniques is a new approach that can be used for a localized analysis of the signals in the time-frequency or the time-scale domain and it provides a powerful tool for condition monitoring and fault diagnosis [8, 44 64, 65 and 72]. The purpose of this task is to implement a combined STFT and Discrete wavelet transform technique to analyze transient and stationary data from rotating machinery, as well as to demonstrate the effectiveness of diagnosing machinery condition during changing speeds.

5.2.1 Description of the Experiment

The experiment described in this chapter, performs the condition monitoring of machinery to predict some anomalies that may occur under varying load conditions

(normal, imbalance and misalignment) in the rotor rig. The STFT and wavelet transform techniques were used to perform data analysis, and they characterized, the start-up and shut-down signatures of the rotor rig under different operating conditions. The prominent spectral components of the signals were tracked in time-scale and time-frequency domains during motor speed variations. Conclusions were made indicating the advantages of using this new signal analysis method.

The experimental set-up is well described in reference [3]. The machinery system is comprised of a motor loaded with a rotor rig as shown in the Figure 5.1. Four bearings were used in the test rig. The rotor rig was operated at normal condition at constant speed of 3,600 RPM before shut-down. The rig was then allowed to coastdown to a stop. The rig was then restarted and the motor speed was increased steadily to approximately 7,200 RPM. The test run was repeated for different anomalies (imbalance and misalignment) imposed on the rotor rig. The data acquisition was performed using the Data Translation DT2801-7A *AID* converter and GLOBAL LAB, the Data Translation's acquisition software.

The shaft speed was measured by a tachometer (keyphaser which measures the rotational frequency of the shaft by tracking a notch on the shaft) and the shaft motion was measured with a displacement transducer. The signals measured in the transient condition have a length of acquisition of 400 seconds, and a sampling frequency of 500 Hz.

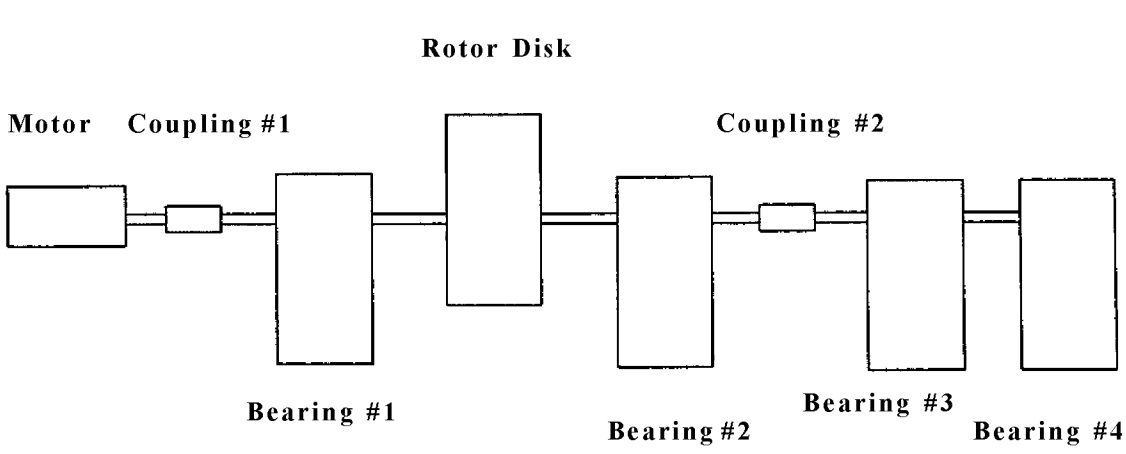

Figure 5.1. Rotor Rig Scheme [3]

The measurements in stationary condition have a length of 40 seconds, and a sampling frequency of 2,000 Hz. The data were filtered by highpass and lowpass analog filter. The highpass filter was set at 1 Hz in order to maximize the *AID* converter resolution while the lowpass was set at a frequency of Lowpass=0.45x sampling_frequency. This was done in order to avoid the Nyquist aliasing effect [3]. The amplification of the speed transducer output was set to 1.0 volt per volt while the displacement transducer gain was set to 100 volts per volt using amplifiers built-in the *AID* converter.

The following tasks were included as part of the data analysis of the rotor rig measurements.

- Early anomaly detection, using STFT and wavelet techniques, under varying load conditions.

- The characterization of the motor signature, at start-up and shut-down, for different operating conditions.

- Tracking of the predominant spectral components of the sensor signals, in the time-scale and time-frequency domains, during motor speed variations.

- Comparison of the different signal analysis techniques.

5.2.2 Data Analysis Method and Results

The motor data analysis was performed using the MATLAB data analysis system toolbox described in Chapter 4. Two different sets of data were used and were classified as stationary and non-stationary. The data are described in the Table 5.1. The stationary motor rig data were analyzed using the following steps.

- Format and convert the data to ASCII type.
- Remove the DC level and normalize the data using the electronic gain.
- Perform the data analysis using the standard Fourier transform to obtain the auto-power spectral density (APSD).
- Define the optimal wavelet basis function to be used for MRA.
- Perform the data analysis using the MRA.
- Perform the Short-time Fourier transform (STFT) of the original data.
- Perform the combined MRA and STFT analysis.
- Perform the multichannel data analysis of selected sensors.

The analysis of non-stationary data was done following the steps described bellow:

- Format and convert the data to ASCII type.
- Remove the DC level and normalize the data using the electronic gain.
- Perform the data analysis using the standard Fourier transform to obtain the auto- power spectral density (APSD).
- Determine the optimal wavelet basis function to be used for MRA.
- Perform the STFT of the raw data.
- Perform the Discrete wavelet transform (DWT).

TABLE 5.1. Stationary and Non-Stationary Data Parameters

Sensor ID	Condition	Event	Data Length (sec)	Sampling Frequency (Hz)	Sensor Type
1	Normal	Steady-State	40	2000	Speed and Displacement
2	Normal	Transient	400	500	Speed
3	Normal	Transient	400	500	Displacement
4	Imbalance	Steady-state	40	2000	Speed and Displacement
5	Imbalance	Transient	400	500	Speed
6	Imbalance	Transient	400	500	Displacement
7	Misaligned	Steady-state	40	2000	Speed and Displacement
8	Misaligned	Transient	400	500	Speed
9	Misaligned	Transient	400	500	Displacement

5.2.3 Results of Stationary Data Analysis

5.2.3.1 Normal Case

Figures 5.2 and 5.3 show the time-amplitude plots of tachometer and horizontal proximity probe sensors from steady-state file ID #1. Figures 5.4 and 5.5 show the power spectral densities. The IX running speed of the motor (60Hz) is shown in Figure 5.4 together with prominent harmonics. A 160 Hz peak can be detected, and according to previous analysis [3], it is related to the structural resonance. Figure 5.5 shows the 60 Hz speed motor frequency, which means that imbalance and/or misalignment exists in the rotor rig even in the normal case [3]. The FFTs were calculated using 1024 point per block and a total of 2^{16} data points. The time-frequency power spectra (3-D) of the original tachometer and proximity probe sensor signals are obtained using the STFT technique. They are shown in Figures 5.6 and 5.7 for each sensor. A Harming window was used to perform the STFT analysis.

The wavelet multiresolution analysis (MRA) was performed using an optimal wavelet (Daubechies wavelet, Daub20). Five decomposition levels were initially selected for the analysis. The detailed reconstructed signals, at each sub-band level, were obtained for each sensor and they are shown in Figures 5.8 and 5.9. Table 5.2 shows the frequency range for each MRA level. The motor speed (60 Hz) at the 5^{th} level can be enhanced with this local analysis. The MRA results are combined with the STFT analysis, and 3-D plots and can be obtained for a specific sub-band level (5^{th} level). Figures 5.10 and 5.11 portray each of the sensors examined.

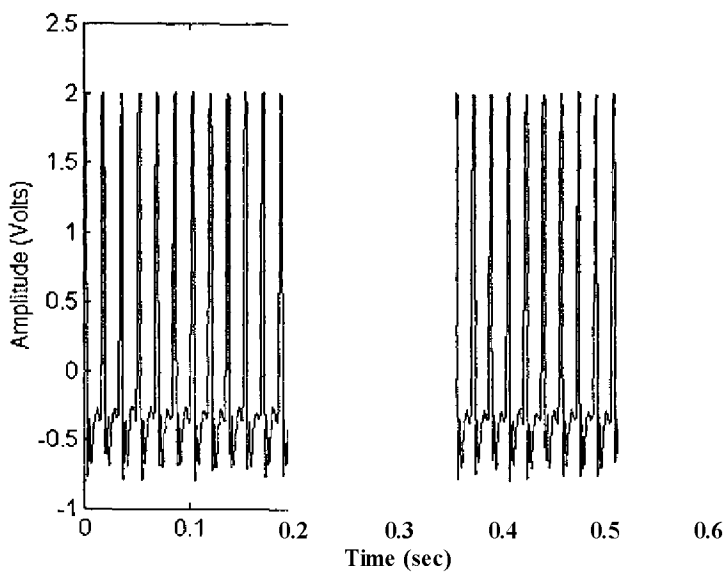

Figure 5.2. Time-Amplitude Plot of Tachometer Signal at Normal and Steady-State Condition

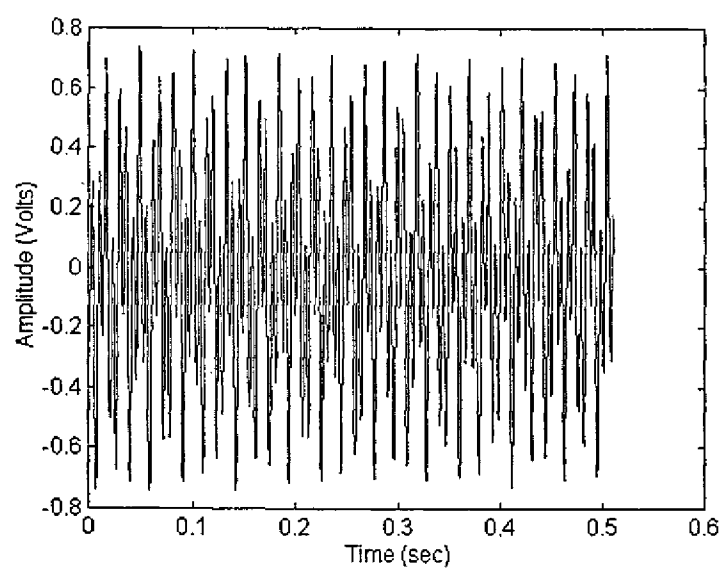

Figure 5.3. Time-Amplitude Plot Signal of Proximity Probe at Normal and Steady-State Condition

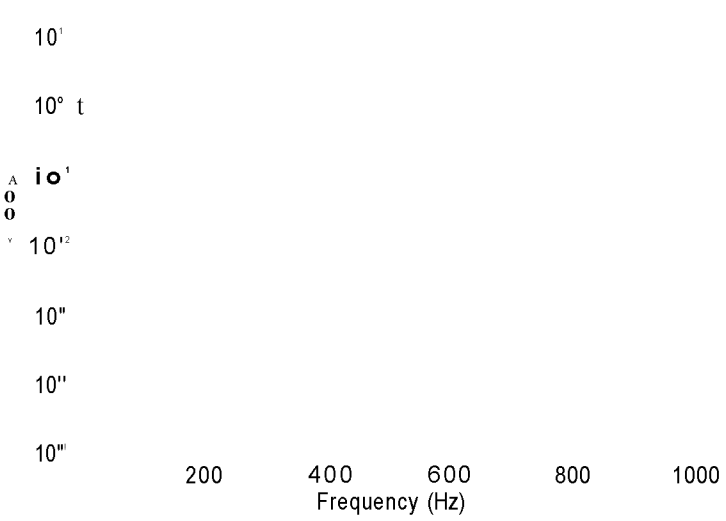

Figure 5.4. FFT Power Spectral Density Estimation of Signal at Normal and Steady-State Condition

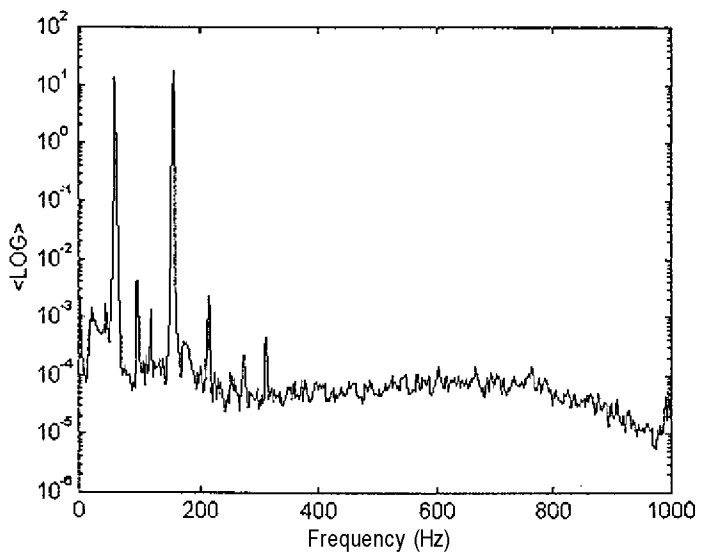

Figure 5.5. FFT Power Spectral Density Estimation of Proximity Probe Signal at Normal and Steady-State Condition

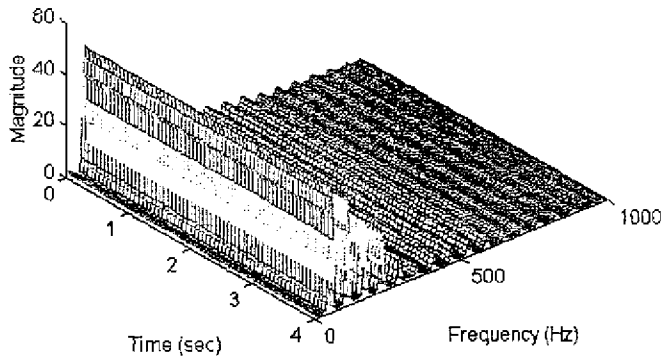

Figure 5.6. STFT Time-Frequency Power Spectral Density Estimation of Tachometer Signal at Normal and Steady-State Condition

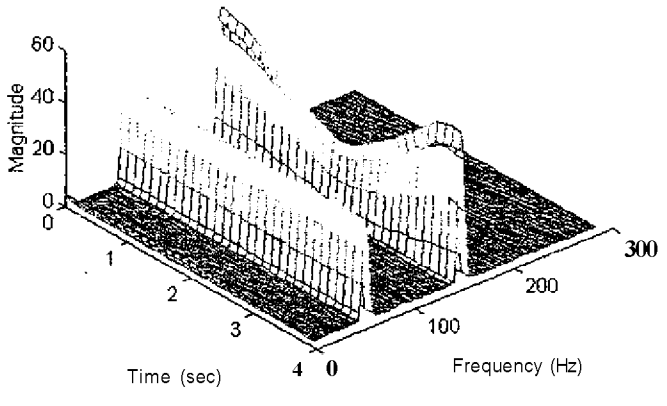

Figure 5.7. STFT Time-Frequency Power Spectral Density Estimation of Proximity Probe Signal at Normal and Steady-State Condition

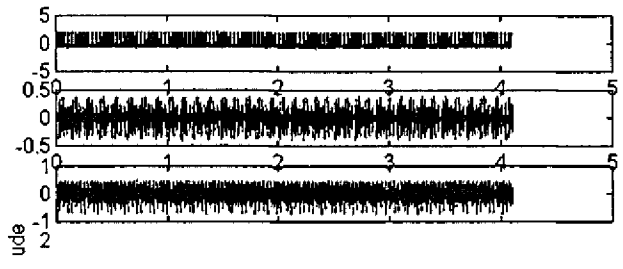

Figure 5.8. Multiresolution Analysis Results Showing the Detail Reconstructed Tachometer Signals at Normal and Steady-State Condition (original signal at the top and 5th level at the bottom)

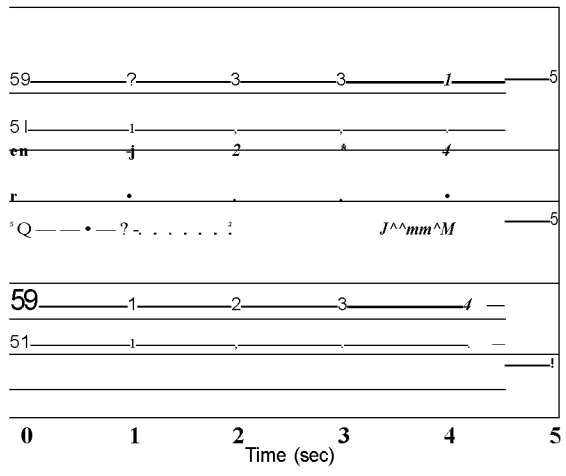

Figure 5.9. Multiresolution Analysis Results Showing the Detail Reconstructed Signals of Proximity Probe Signal at Normal and Steady-State Condition (original signal at the top and 5th level at the bottom)

Table 5.2. Frequency Bands for MRA of Tachometer and the Proximity Probe Stationary Analysis (sampling rate = 2000 Hz)

MRA Level	Approximation Levels Frequency Range (Hz)	Detail Levels Frequency Range (Hz)
1	0-500	500 - 1000
2	0-250	250 - 500
3	0-125	125 -250
4	0 - 62.5	62.5 - 125
5	0 - 32.25	32.25 - 62.5

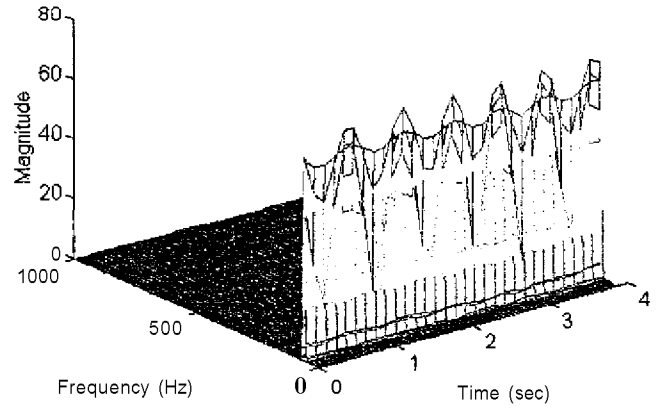

Figure 5.10. STFT & MRA Time-Frequency Power Spectral Density Estimation of Tachometer Signal at Normal and Steady-State Condition (original signal at the top and 5th level at the bottom)

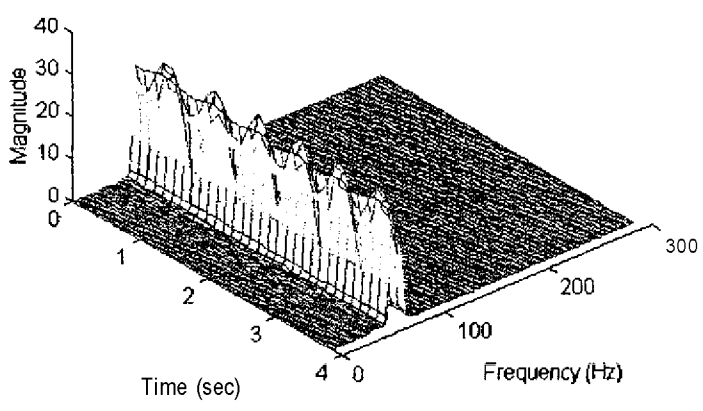

Figure 5.11. STFT & MRA Time-Frequency Power Spectral Density Estimation of Proximity Probe Signal at Normal and Steady-State Condition (original signal at the top and 5th level at the bottom)

The multiresolution analysis results, shown in Figures 5.8 and 5.9 for the tachometer and proximity probe sensors, provide the necessary information to track the behavior of the system at different frequency ranges. The running speed (fundamental frequency) was isolated from any undesired frequency, and an enhanced analysis was performed. The STFT was then combined with MRA, and a localized analysis of the signal was performed.

5.2.3.2 Imbalance Case

Mass imbalance is one of the most common causes of vibration and it is very easy to diagnose. Imbalance is a condition where the center of mass does not coincide with the center of rotation, due to the unequal distribution of the rotor mass about the center of rotation. The imbalance creates a vibration frequency exactly equal to the rotational speed, with amplitude proportional to the amount of imbalance [3, 104].

Figures 5.12 and 5.13 show the time amplitude signal for the tachometer and the proximity probe. Their respective auto power spectra are shown in Figures 5.14 and 5.15. As it was expected some frequency components increased their amplitudes when compared with a normal case. This increasing effect can be found in the STFT analysis, as shows in Figures 5.16 and 5.17. Figures 5.18 and 5.19 portray MRA analysis results. The combined STFT and MRA analysis, shown in Figures 5.20 and 5.21, provides localized information on the IX running speed of the rotor rig. Thorough details are given in the above figures when compared with the STFT analysis of the original signal (Figures 5.16 and 5.17).

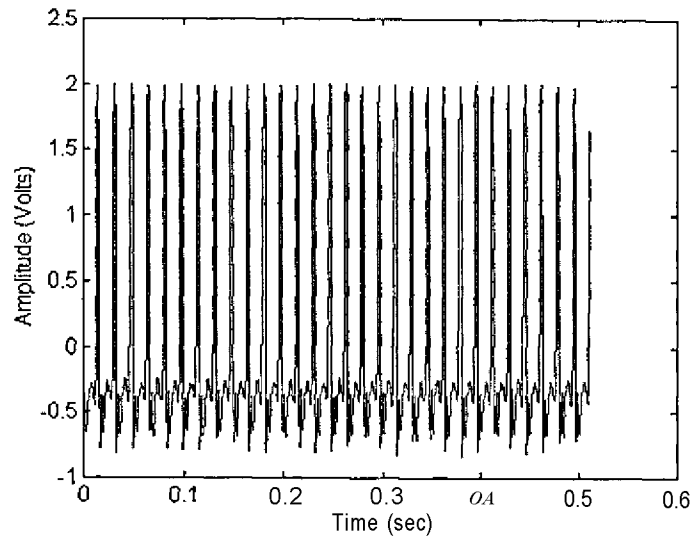

Figure 5.12. Time-Amplitude Plot of Tachometer Signal at Imbalance and Steady State Condition

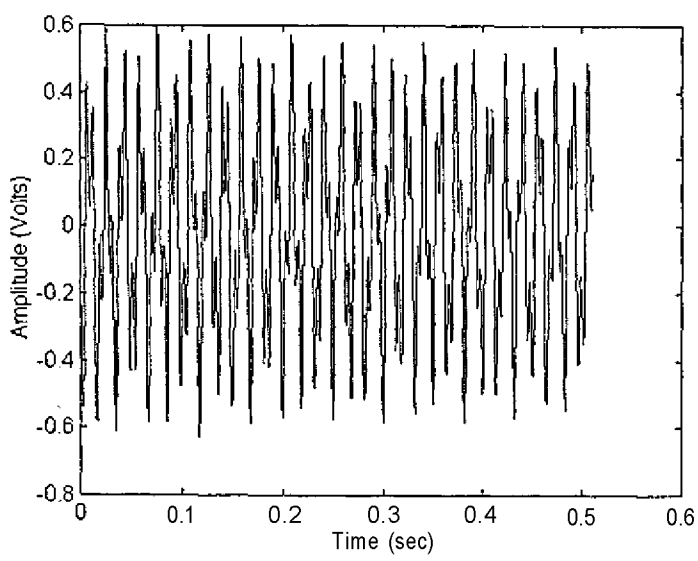

Figure 5.13. Time-Amplitude Plot Signal of Proximity Probe at Imbalance and Steady-State Condition

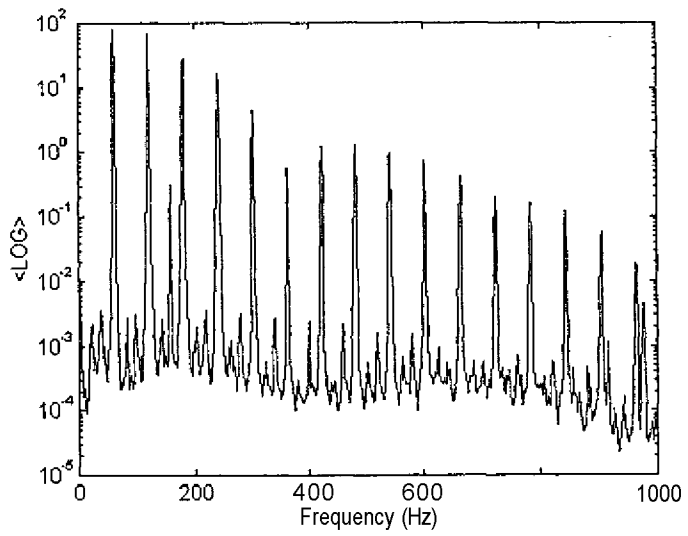

Figure 5.14. FFT Power Spectral Density Estimation of Tachometer Signal at Imbalance and Steady-State Condition

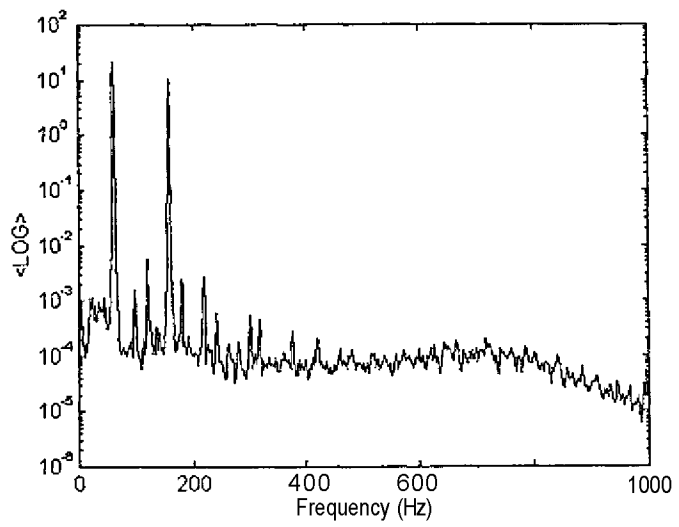

Figure 5.15. FFT Power Spectral Density Estimation of Proximity Probe Signal at Imbalance and Steady-State Condition

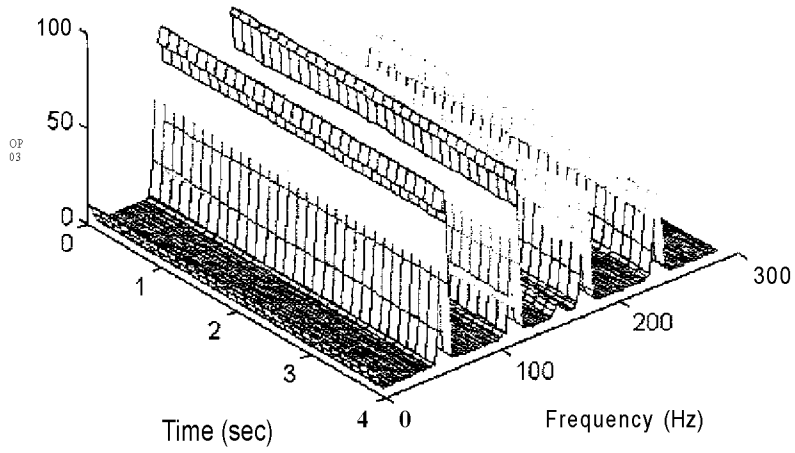

(a)

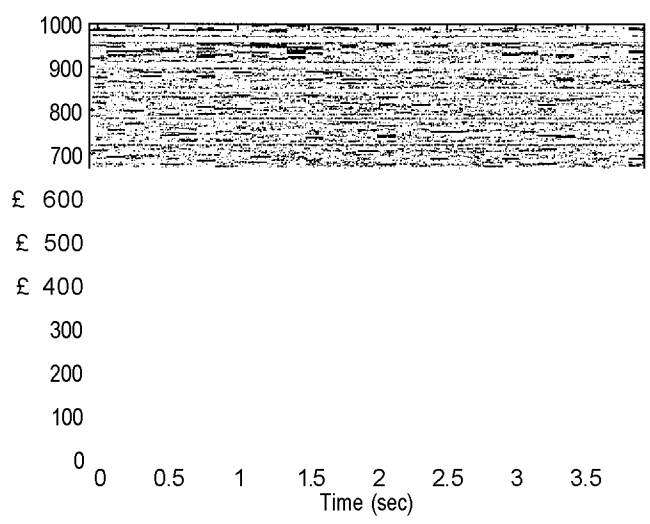

(b)

Figure 5.16 STFT Time-Frequency Power Spectral Density Estimation of Tachometer Signal at Imbalance and Steady-State Condition, (a) 3-D Plot, (b) 2-D Plot

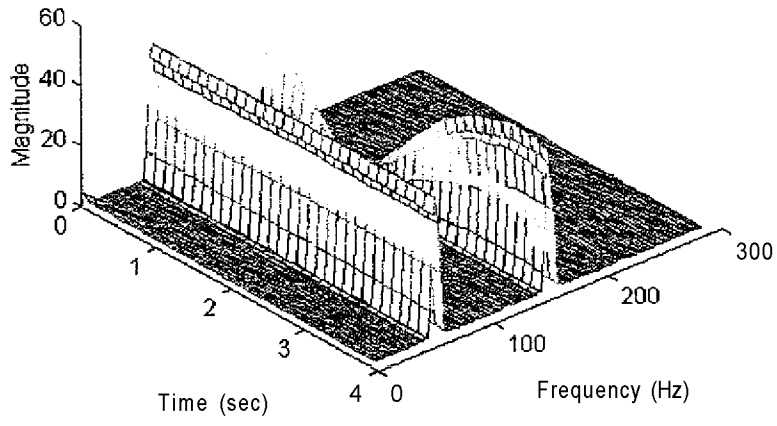

(a)

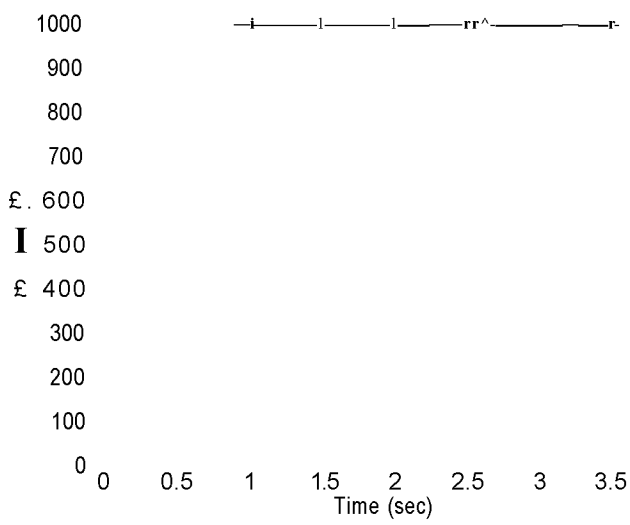

(b)

Figure 5.17. STFT Time-Frequency Power Spectral Density Estimation of Proximity Probe Signal at Imbalance and Steady-State Condition, (a) 3-D Plot, (b) 2-D Plot

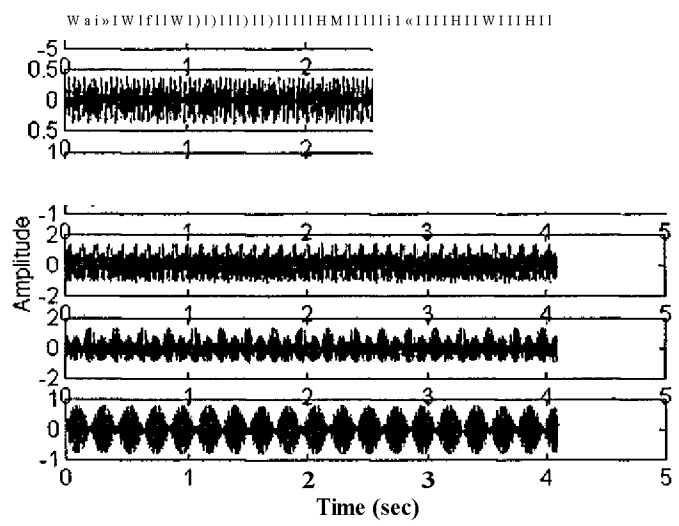

Figure 5.18. Multiresolution Analysis Results Showing the Detail Reconstructed Signals of Tachometer Signal at Imbalance and Steady-State Condition (original signal at the top and 5th level at the bottom)

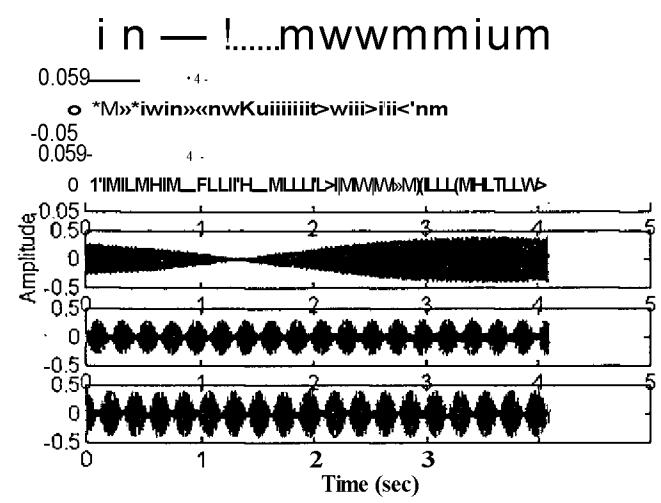

Figure 5.19. Multiresolution Analysis Results Showing the Detail Reconstructed Signals of Proximity Probe Signal at Imbalance and Steady-State Condition (original signal at the top and 5th level at the bottom)

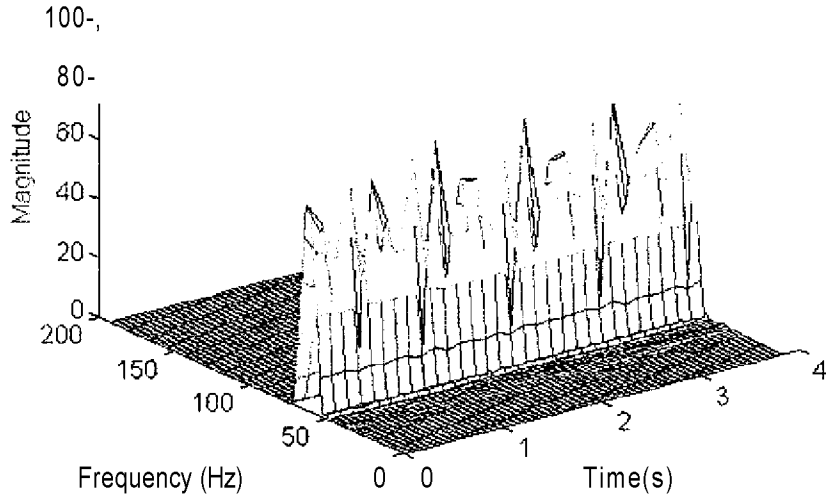

Figure 5.20. STFT & MRA Time-Frequency Power Spectral Density Estimation of Tachometer Probe Signal at Imbalance and Steady-State Condition.

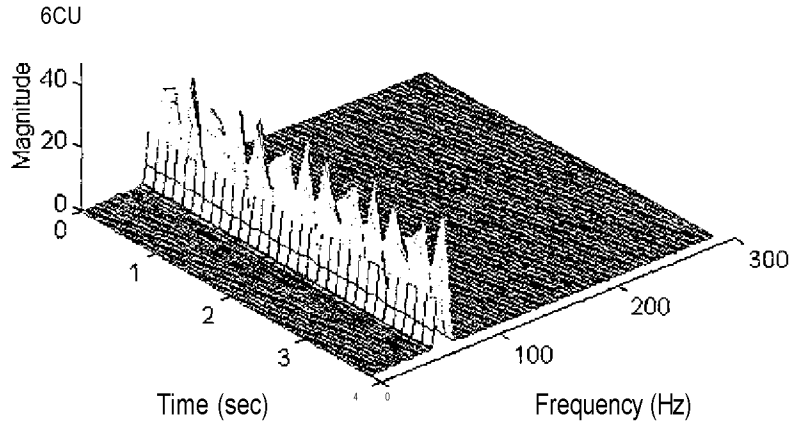

Figure 5.21. STFT & MRA Time-Frequency Power Spectral Density Estimation Proximity Probe Signal at Imbalance and Steady-State Condition

5.2.3.3. Misalignment Case

Coupling misalignment is a condition in which the shafts of the drive machine and driven machine are not on the same centerline. There are different types of misalignment such as parallel, angular, vertical and horizontal. The parallel misalignment is the most common type, and it results in a large 2X running speed spectral component in a radial direction. The angular misalignment results in a large IX running speed spectral component in the radial and axial directions [3,104].

Misalignment shows up in the frequency domain as a series of harmonics of the running speed. The time-amplitude plots of the measured signals are shown in Figures 5.22 and 5.23. The STFT power spectrum of the tachometer is shown in Figure 5.24. It reveals that its amplitude power spectrum has significantly increased when compared with the normal case shown in Figures 5.6 and 5.7. Figure 5.25 shows the results for the proximity probe, while revealing increased amplitude in the IX running speed and the 160 Hz component of the structural resonance. The results obtained using the MRA are portrayed in Figures 5.26 and 5.27 and the combined STFT and MRA analysis results are displayed in Figures 5.28-5.31.

5.2.4 Non-stationary Data Analysis Results

The non-stationary analysis was performed using the STFT and DWT techniques, in order to track the predominant spectral components of the sensor signals, in the time-scale and time-frequency domain, during motor speed variations. The STFT technique used a Harming window to compute the Fourier coefficients.

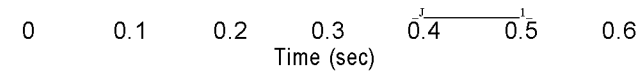

Figure 5.22. Time-Amplitude Plot of Tachometer Signal at Misalignment and Steady-State Condition

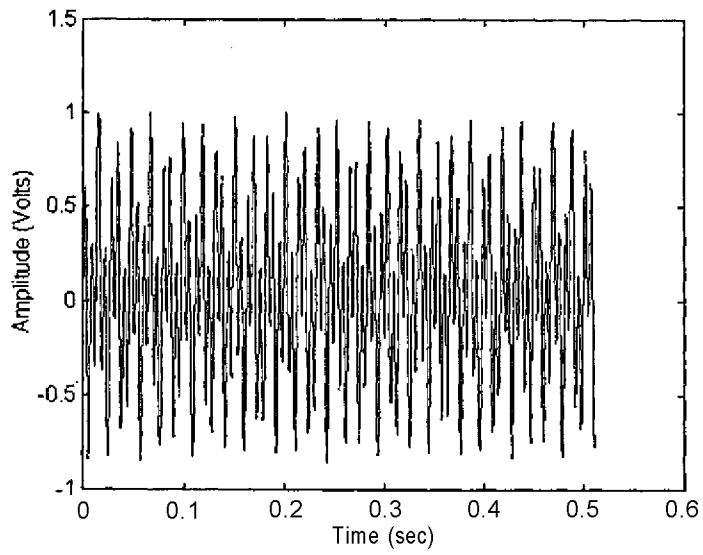

Figure 5.23. Time-Amplitude Plot Signal of Proximity Probe at Misalignment and Steady-State Condition

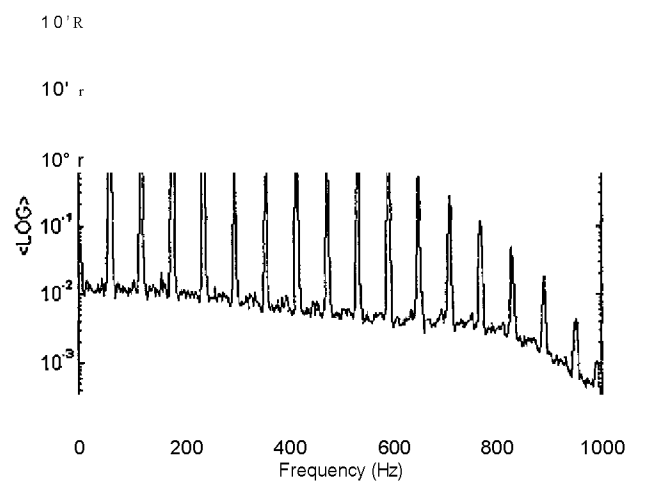

Figure 5.24. FFT Power Spectral Density Estimation of Tachometer Signal at Misalignment and Steady-State Condition

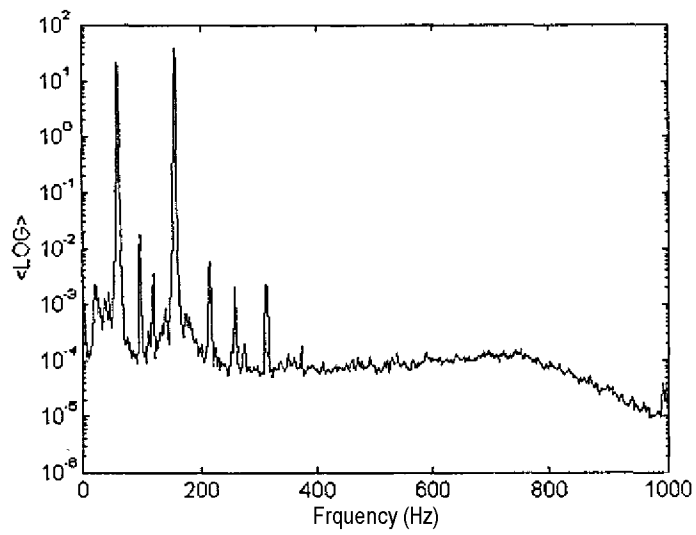

Figure 5.25. FFT Power Spectral Density Estimation of Proximity Probe Signal at Misalignment and Steady-State Condition

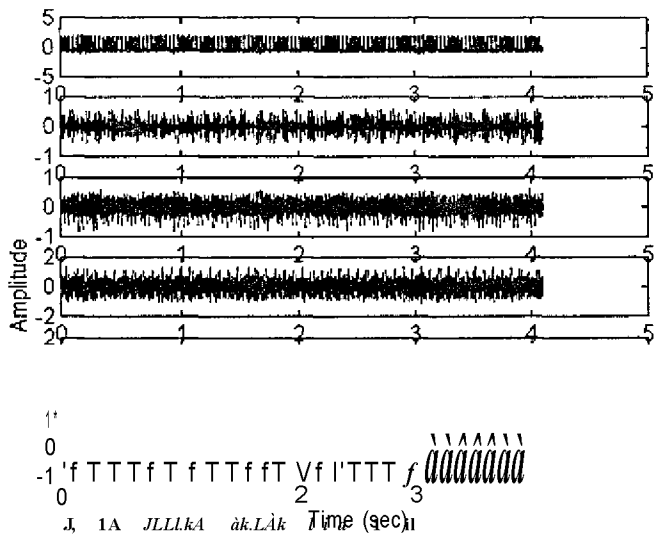

Figure 5.26. Multiresolution Analysis Results Showing the Detail Reconstructed Signals of Tachometer Signal at Misalignment and Steady-State Condition (original signal at the top and 5th level at the bottom)

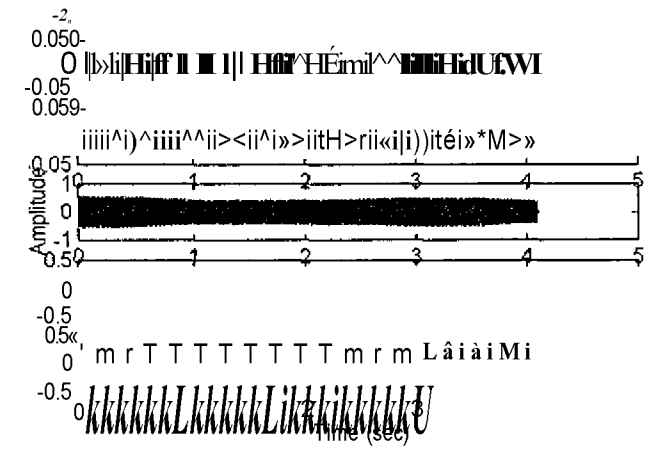

Figure 5.27. Multiresolution Analysis Results Showing the Detail Reconstructed Signals of Proximity Probe Signal at Misalignment and Steady-State Condition (original signal at the top and 5th level at the bottom)

Time (sec) 4 0 Frequency (Hz)

(a)

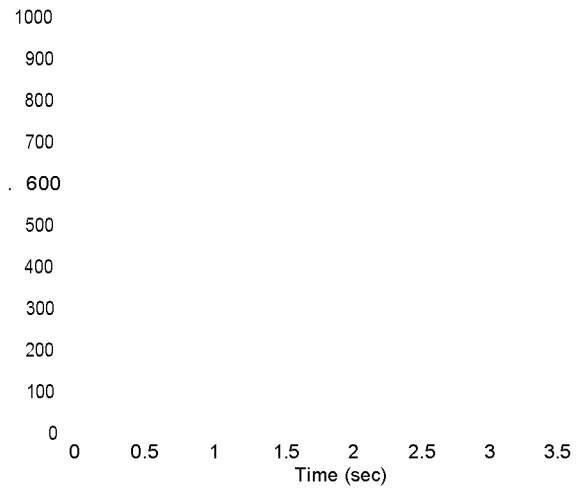

Figure 5.28. STFT Time-Frequency Power Spectral Density Estimation of Tachometer Signal at Misalignment and Steady-State Condition, (a) 3-D Plot (b) 2-D Plot

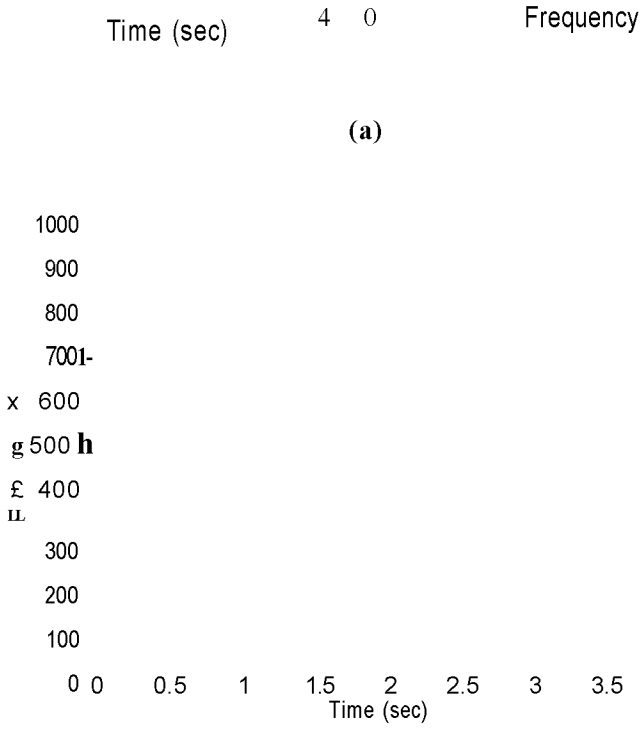

Figure 5.29. STFT Time-Frequency Power Spectral Density Estimation of Proximity Probe Signal at Misalignment and Steady-State Condition, (a) 3-D Plot, (b) 2-D Plot

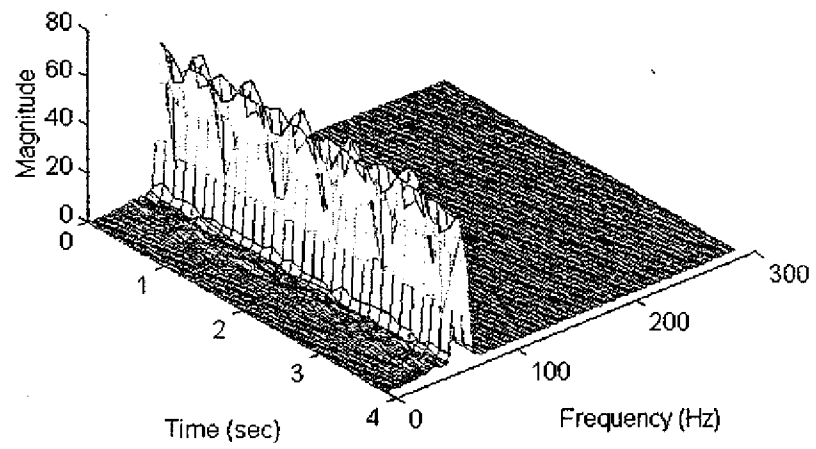

Figure 5.30. STFT & MRA Time-Frequency Power Spectral Density Estimation of Tachometer Signal at Misalignment and Steady-State Condition

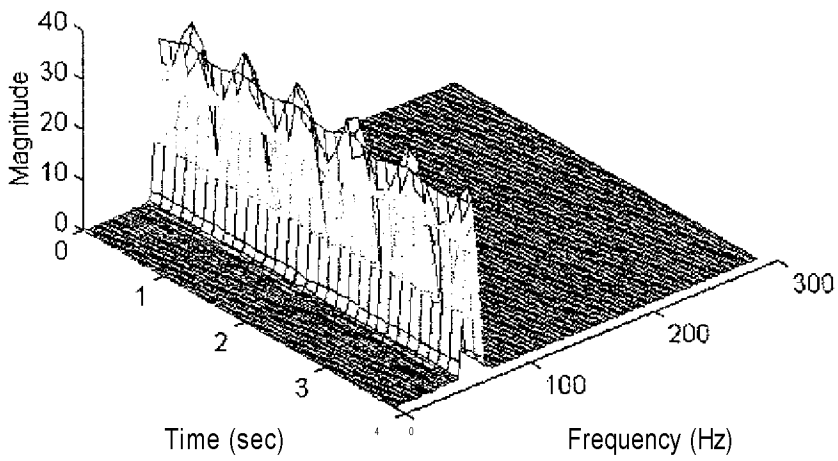

Figure 5.31. STFT & MRA Time-Frequency Power Spectral Density Estimation of Proximity Probe Signal at Misalignment and Steady-State Condition

For the discrete wavelet transform (DWT) computation the harmonic basis wavelet was selected because its algorithm is fast and the features of the wavelet basis function match with the characteristics of the measurement signals. During the DWT analysis each decomposition level is associated with its frequency center, as shown in Table 5.3. The DWT coefficients are squared and their 2-D plots were obtained.

The time-amplitude plots of the signal measurements at transient condition (normal, imbalance and misaligment) are shown in Figures 5.32-5.37. These signals were used for STFT and DWT transient analysis.

TABLE **5.3.** Frequency Bands for **DWT** Tachometer and Horizontal Proximity Probe Sensor Non-Stationary Analysis (sampling rate = **500** Hz)

Wavelet Level	Frequency Center (Hz)
11	3.90
12	7.81
13	15.62
14	31.25
15	62.50
16	125.00
17	250.00

0 50 100 150 200 250 300
Time (sec)

Figure 5.32. Time-Amplitude Plot Signal of Tachometer at Normal and Transient Condition

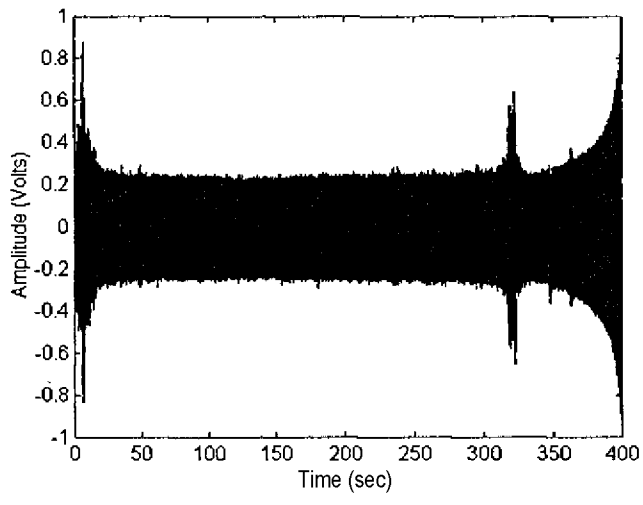

Figure 5.33. Time-Amplitude Plot Signal of Proximity Probe at Normal and Transient Condition

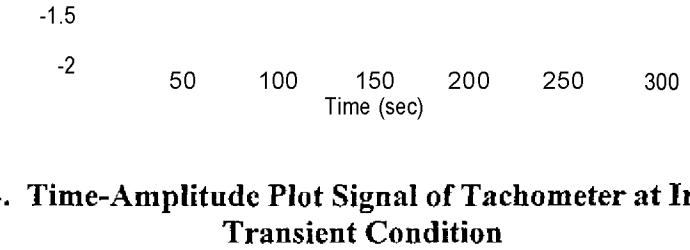

Figure 5.34. Time-Amplitude Plot Signal of Tachometer at Imbalance and Transient Condition

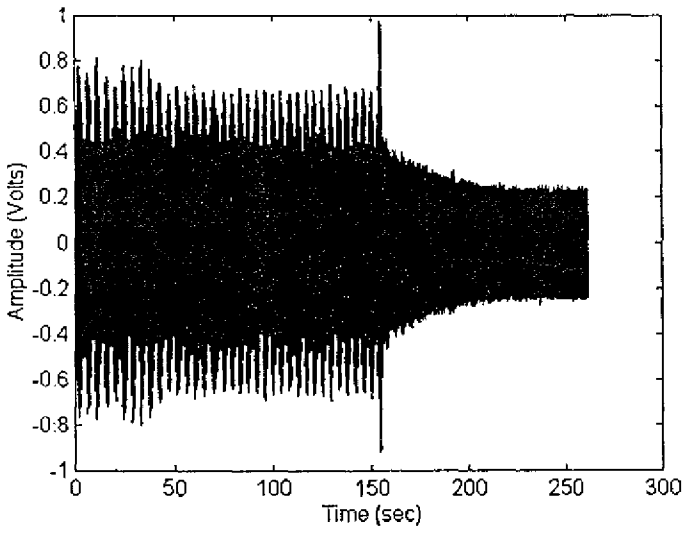

Figure 5.35. Time-Amplitude Plot Signal of Proximity Probe at Imbalance and Transient Condition

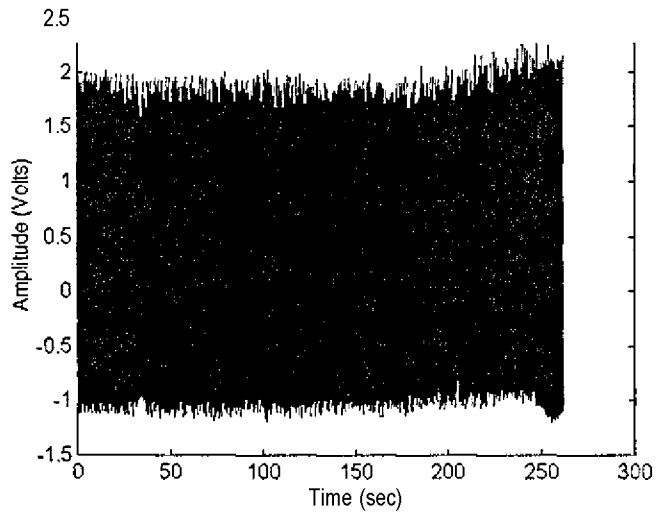

Figure 5.36. Time-Amplitude Plot Signal of Tachometer at Misalignment and Transient Condition

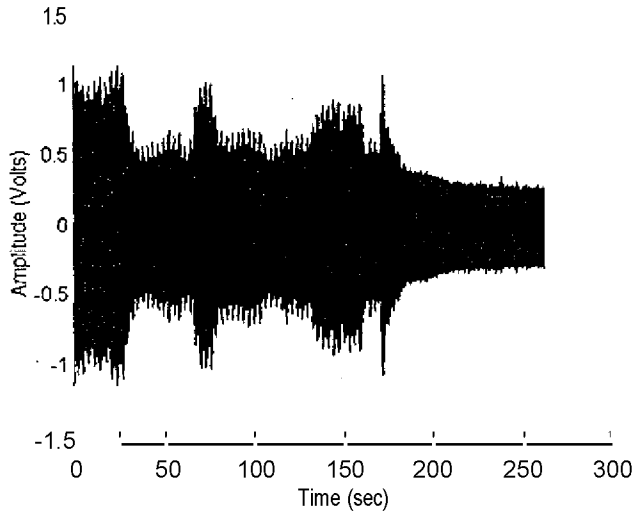

Figure 5.37. Time-Amplitude Plot Signal of Proximity Probe at Misalignment and Transient Condition

5.2.4.1 Normal and Transient Conditions

In the normal and transient conditions, the STFT analysis results were obtained and displayed in Figures 5.38 and 5.39 (2-D and 3-D plots). The tachometer signal analysis reveals the IX running speed at 60 HZ and the respective 2X, 3X and 4X running speed harmonics. The running speed was decreased during coastdown and its lower frequency value can be found at 140 seconds. The proximity probe signal analysis results shown in Figure 5.39(b) reveals an important characteristic of the 160 Hz resonance structure spectral component, that is, the magnitude of the power spectrum changes as the running speed changes.

The DWT analysis produces the wavelet power spectrum. The analysis results for tachometer and proximity probe signals are shown in Figures 5.40 and 5.41 respectively. The power spectra, in the 2-D map representation, precisely reveal the time-scale behavior of each signal when the transients were performed on the system.

5.2.4.2 Imbalance and Transient Condition

The results of STFT transient analysis at imbalance condition are shown in Figures 5.42 (tachometer) and 5.43 (proximity probe). Figures 5.44 and 5.45 show the map plots obtained using the harmonic wavelet transform. Figures 5.42 and 5.43 reveal that the amplitude of the IX spectral component increases during the transient, as expected for the imbalance condition. Both spectra show the 160 Hz structural resonance component and its decreasing amplitude during the coastdown.

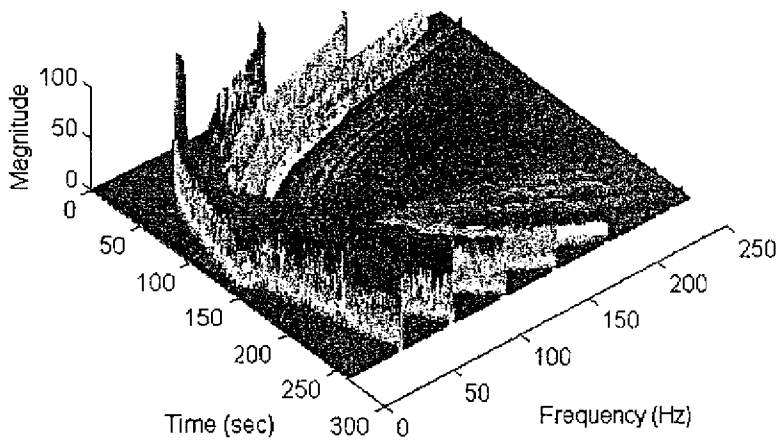

(a)

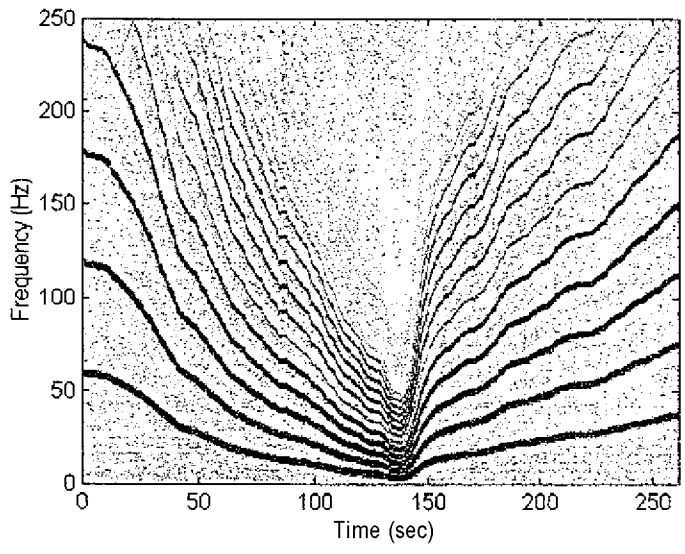

(b)

Figure 5.38. STFT Time-Frequency Power Spectral Density Estimation of Tachometer Signal at Normal and Transient Condition, (a) 3-D Plot, (b) 2-D Plot

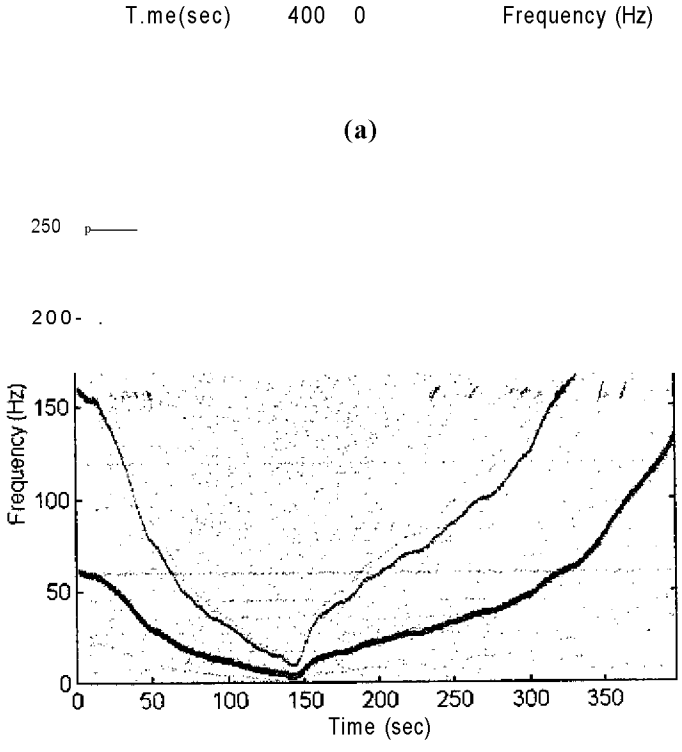

Figure 5.39. STFT Time-Frequency Power Spectral Density Estimation of Proximity Probe Signal at Normal and Transient Condition, (a) 3-D Plot, (b) 2-D Plot

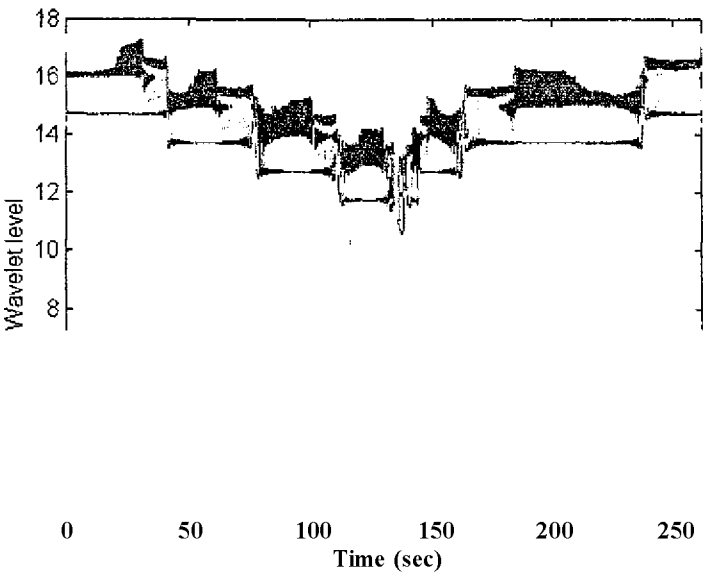

Figure 5.40. DWT Time-Scale Power Spectral Density Estimation of Tachometer Signal at Normal and Transient Condition

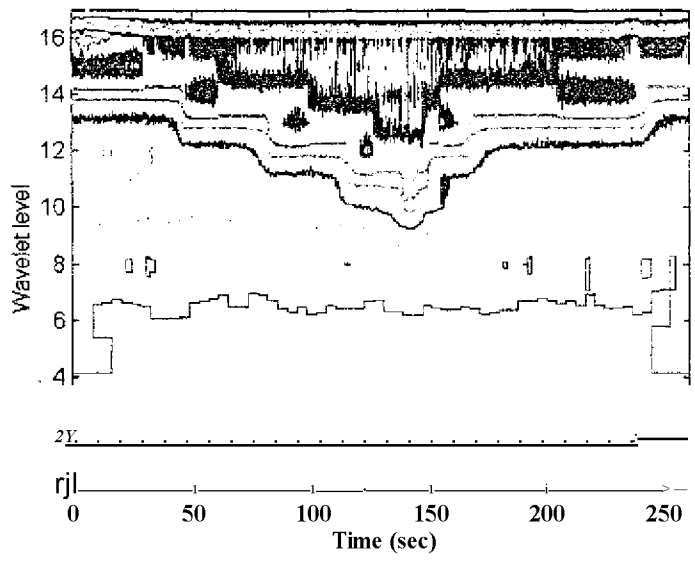

Figure 5.41. DWT Time-Scale Power Spectral Density Estimation of Proximity Probe Signal at Normal and Transient Condition

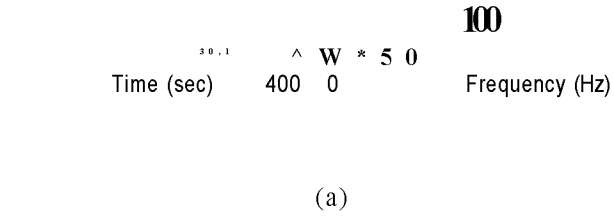

(a)

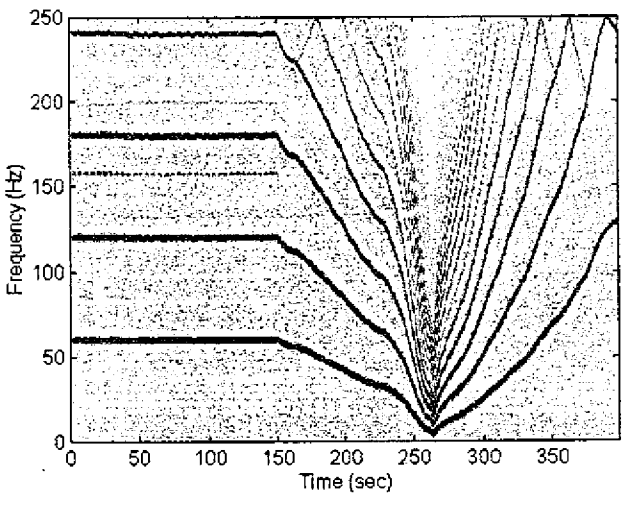

(b)

Figure 5.42. STFT Time-Frequency Power Spectral Density Estimation of Tachometer Signal at Imbalance and Transient Condition, (a) 3-D Plot, (b) 2-D Plot

50

Time (sec) 400 0 Frequency (Hz)

(a)

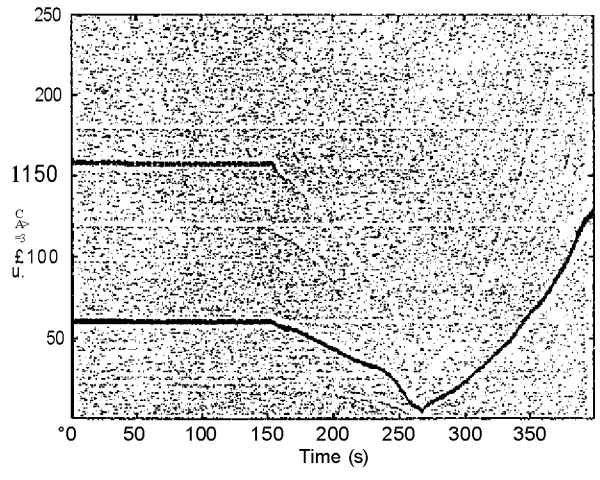

(b)

Figure 5.43. STFT Time-Frequency Power Spectral Density Estimation of Proximity Probe Signal at Imbalance and Transient Condition, (a) 3-D Plot, (b) 2-D Plot

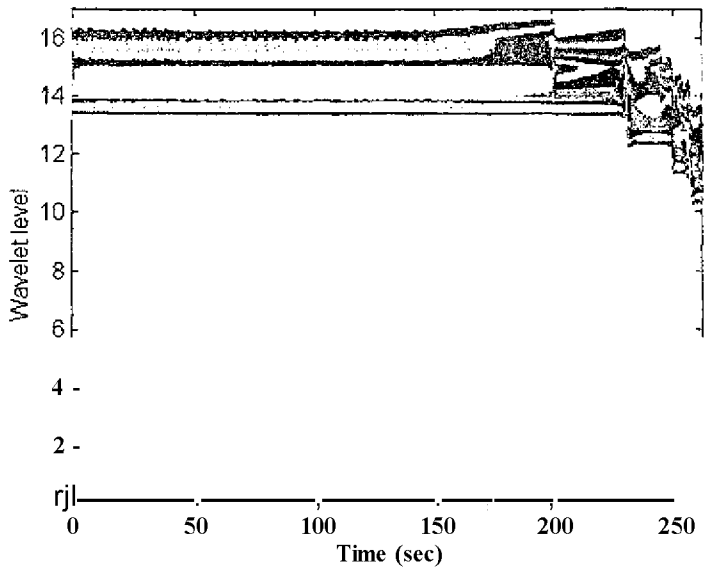

Figure 5.44. DWT Time-Scale Power Spectral Density Estimation of Tachometer Signal at Imbalance and Transient Condition

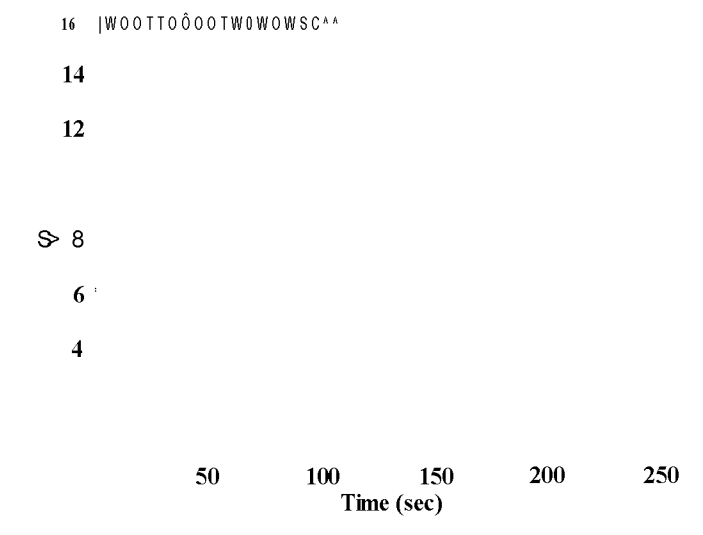

Figure 5.45. DWT Time-Scale Power Spectral Density Estimation of Horizontal Proximity Probe Signal at Imbalance and Transient Condition

The discrete wavelet transform analysis gives precise information about the time-scale behavior of the system during the transients. The exact information about the time interval, where the transient occurs, can be obtained using the 2-D plots.

5.2.4.3 Misalignment and Transient Condition

The transient behavior of the system in misalignment condition can be monitored using STFT and the DWT analysis. Figures 5.46 and 5.47 show the STFT results obtained when the IX running speed is changed.

The tachometer signal analysis reveals the increase in the magnitude of the power spectral density, and it also shows some frequency components in between the harmonics of the running speed. During coastdown, the lowest value of the IX running speed frequency is achieved at 310 seconds (Figure 5.46).

The proximity,probe signal analysis reveals that the structural resonance spectral component changes during the steady-state interval (Figure 5.47). The previous results obtained using STFT analysis can also be seen using DWT analysis. These results are shown in Figure 5.48 and 5.49.

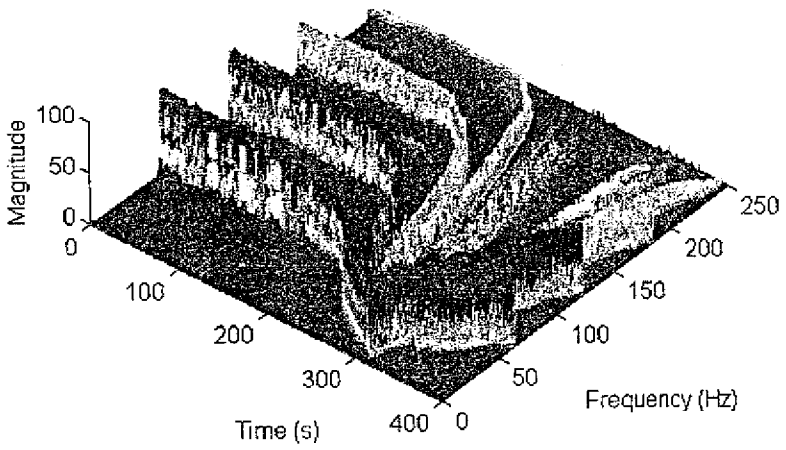

(a)

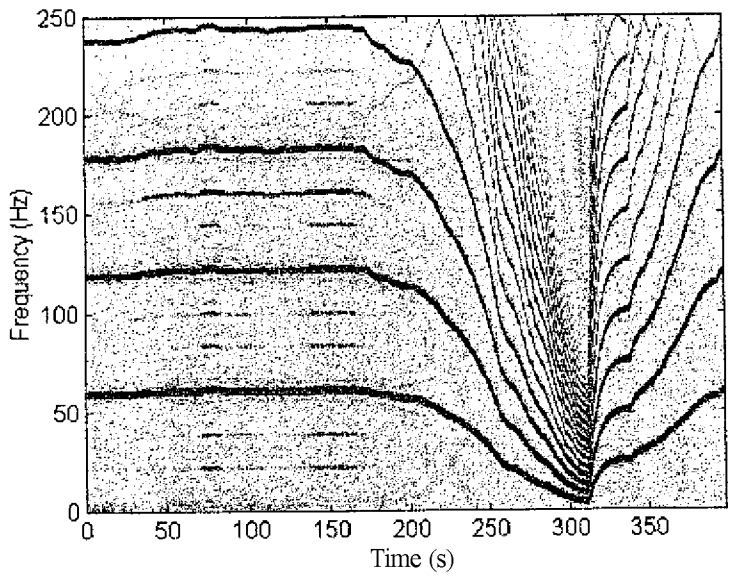

(b)

Figure 5.46. STFT Time-Frequency Power Spectral Density Estimation of Tachometer Signal at Misalignment and Transient Condition, (a) 3-D Plot (b) 2-D Plot.

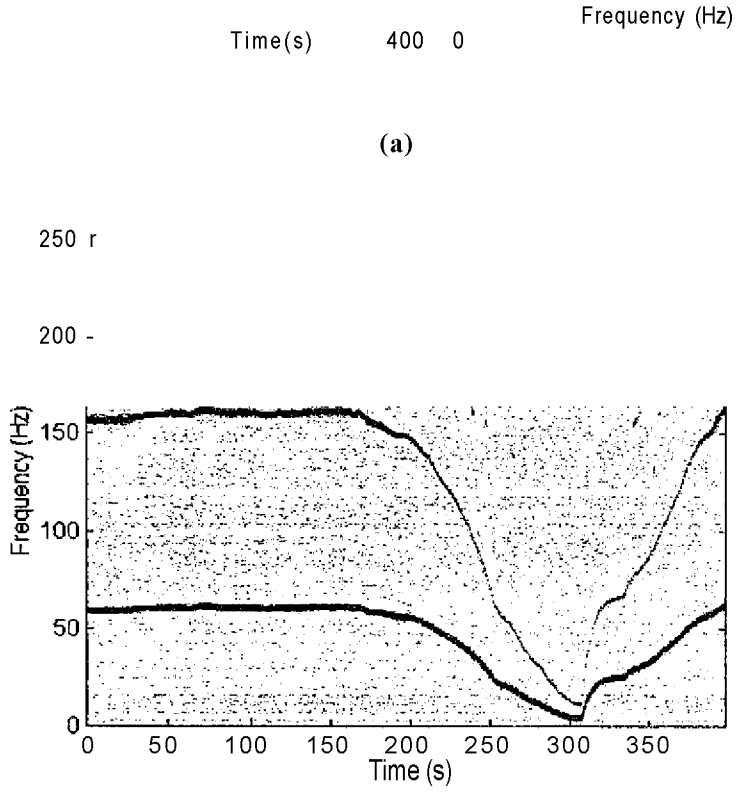

Figure 5.47. STFT Time-Frequency Power Spectral Density Estimation of Proximity Probe Signal at Misalignment and Transient Condition, (a) 3-D Plot, (b) 2-D Plot

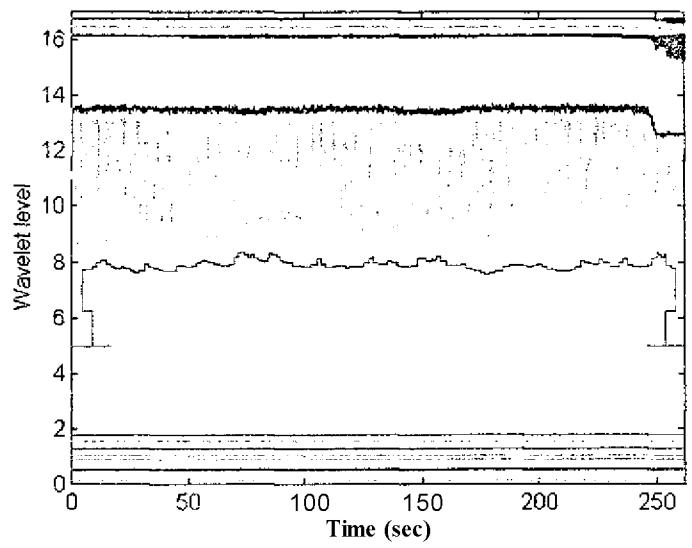

Figure 5.48. DWT Time-Scale Power Spectral Density Estimation of Tachometer Signal at Misalignment and Transient Condition

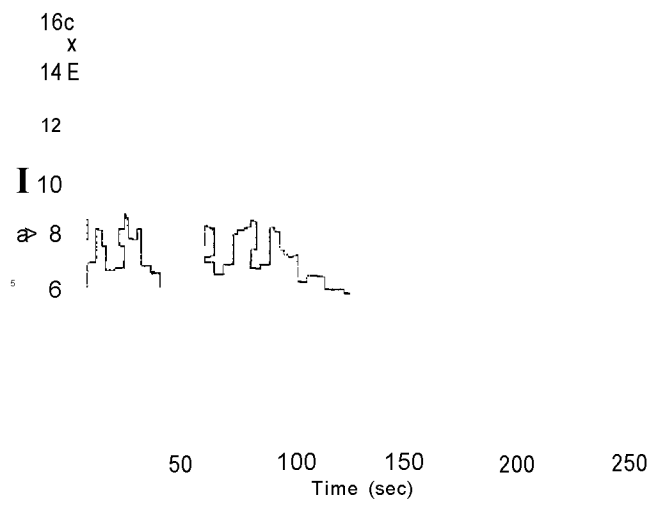

Figure 5.49. DWT Time-Scale Power Spectral Density Estimation of Proximity Probe Signal at Misalignment and Transient Condition

5.3 Conclusions

A method for processing equipment data for fault monitoring and isolation of rotating machinery systems during stationary and transient operation was developed. Steady-state and transient data were acquired from a rotor rig under different operating conditions (normal, misalignment and imbalance). Several signal measurements from the tachometer and proximity probe were available from the test runs.

The signals from a rotor rig test were conditioned and processed using the wavelet and short-time Fourier transforms. The frequencies obtained through the data analysis, for stationary and transient condition, were tracked visually using 2-D and 3-D plots. Different procedures for the data analysis may be implemented using these developed tools. The procedure selected depends on the type of experiment being performed. This research investigated the best method to be employed for vibration analysis using wavelet and short-time Fourier transforms.

The continuous wavelet analysis gives a large amount of detail (some redundant). The discrete analysis seems to be the most appropriate method, because it is fast and does not require many computations. The multiresolution analysis (MRA) was one of the best tools to be used for monitoring the vibration signals, because it provided a localized information in different frequency bands. The integration of STFT and MRA results in a unique diagnosis tool. The harmonic wavelet analysis, in the time-scale domain, gave the maps which provided a clear information about the evolution of the monitored signal

during the transients. By combining the information provided by the two techniques we obtained a better understanding of machinery behavior during transient conditions. The STFT clearly showed the time-frequency evolution of the system under analysis and the harmonic wavelet maps (2-D plot) complement the results by showing in detail the occurrences of the abrupt changes during motor speed variations. The harmonic wavelet transform was able to detect the time instants at which changes in the motor speed were made. On the other hand the STFT was able to track the non-stationary data to identify the time-dependent changes in the frequency components.

The signal processing techniques mentioned before characterized the start-up and shut-down signatures of the rotor rig under different operating conditions. The prominent spectral components of the signals were tracked in the time-frequency and time-scale domains during the rotor speed variation. The analysis indicated the appearance and disappearance of certain frequencies during the coastdown experiment such as the 160 Hz structural resonance component.

The results of combining STFT and wavelet analysis showed the advantages of this method in detecting incipient changes in process signals during steady-state operations. These changes might be indicative of possible anomalies in plant equipment or in process sensors.

CHAPTER 6

Analysis of Neutron Detector and Process Sensor Signals from a Pressurized Water Reactor

6.1 Introduction

During the past decade wavelet transforms have been applied successfully to many problems in such diverse fields as science and engineering. The integration and application of these methods to nuclear power plants is still in its infancy.

The nuclear power plant data, analyzed in this dissertation, are measurements from flow and pressure sensor signals from a pressurized water reactor (PWR) showing strong and irregular flow dips. The in-core flux detector signals, monitored during the full power reactor operation, are also analyzed.

The nuclear power plant data analysis, using the wavelet and STFT techniques, pursues the detection and characterization of transients in the data. The definition of time dependency and stationary characteristics of fuel channel vibration, the estimation of the frequency contents of the transient signals, and the identification of signal changes are presented in this chapter. The coherence, power spectrum and cross spectrum are estimated from the measurements and are combined with the multiresolution analysis.

6.2 Description of the Data

The time series data being used in this research are divided in two sets: Set #1 includes data from fuel assembly vibration measurements. This set uses in-core and ex-core neutron detectors. Set #2 contains several measurements from pressure and flow sensors [36, 49, 50]. The data were acquired from a commercial 515 MWe PWR plant.

6.2.1 Data Set #1 - Fuel Assembly Vibrations

The measurements listed in Table 6.1 are vertical in-core flux detectors (ICFDs - self-powered in-core flux detectors with platinum-clad inconel emitter) and ion chamber signals from the PWR, at full power operation. Data were acquired at a 25 Hz sampling rate. Sixteen channels were recorded containing in-core flux detector with platinum-clad inconel emitter and the ion-chambers with three output signals (log, log rate, linear) in the reactor's shut-down system No.2 (SDS2 - Channel E).

Detecting and monitoring fuel channel vibrations by noise analysis of the ICFDs is an important issue in nuclear power plants, because of potential fuel damages caused by flow-induced vibration. The data analysis method utilized a new technique capable of defining the time dependency and stationary condition of fuel assembly vibration.

Table 6.1. Fuel Assembly Vibration Data

No.	ID Name	Signal Type	Conversion factor/(DC)	Gain
1	01 IE VFD2-3E	In-core n.	3.46 V (DC)	40
2	02 2E VFD2-5E	In-core n.	3.48 V (DC)	40
3	03 6E VFD10-1E	In-core n.	3.27 V (DC)	40
4	04 7E VFD10-2E	In-core n.	3.42 V (DC)	40
5	05 8E VFD11-1E	In-core n.	3.45 V (DC)	40
6	06 9E VFD12-2E	In-core n.	3.42 V (DC)	40
7	07 12E VFD17-2E	In-core n.	3.26 V (DC)	40
8	08 13E VFD18-1E	In-core n.	3.48 V (DC)	40
9	09 15E VFD22-2E	In-core n.	3.36 V (DC)	40
10	10 16E VFD25-6E	In-core n.	3.34 V (DC)	40
11	11 17E VFD26-1E	In-core n.	3.44 V (DC)	40
12	12 18E VFD23-6E	In-core n.	3.45 V (DC)	40
13	13 15F VFD23-2F	In-core n.	3.51 V (DC)	40
14	14 IC-ELOG	Ex-core n.	3.92 V (DC)	200
15	15 IC-E LOGRATE	Ex-core n.	2.52 V (DC)	40
16	16 IC-E LINEAR	Ex-core n.	2.99 V (DC)	40

6.2.2 Data Set # 2 - Flow and Pressure Measurements

The data, described in Table 6.2, contain measurements of the flow and pressure transmitter signals, showing strong and irregular flow dips, from a nuclear power plant. These data were acquired at a 50 Hz sampling rate. Sixteen channels were recorded including orifice-based and venturi-based flow signals, absolute pressure signals in the flow transmitters high-legs, and axial and transverse signals of the flow transmitters impulse lines (both high-legs and low-legs). The orifice-based flow signal is used in the reactor's shut-down system No.1 (SDS1 - channel F). The ventury-based flow signal is used in the reactor regulating system (RRS) measured in "fully instrumented fuel channels" (FINCH) [49,50]. Each file has a 2-byte integer representing an ADC voltage range of ± 5 volts.

6.3 Data Analysis Method

6.3.1 Introduction

Reactor noise analysis has been one of the most important tools for monitoring and extracting information about the reactor system dynamics. Usually, FFT analysis is the standard technique used to obtain the parameters that represent the system's behavior, and assumes a stationary condition. For non-stationary measurements it is necessary to find another form of analysis in order to obtain the correct information. The wavelet techniques have been introduced recently for monitoring the reactor system dynamics. This dissertation presents the results of application to a commercial PWR power plant.

Table **6.2.** Pressure and Flow Data

No.	ID Name	Signal Type	Conversion factor/(DC)	Gain
1	01 F3FDPLGF	Flow		8
2	02 FINCH FLOW DP	Flow	-	80
3	03 F3FHISIDEP	Flow	-	4
4	04 F3F LOSIDE P	Flow		4
5	05 FINCH HISIDEP	Flow		8
6	06 FINCH LOSIDEP	Flow	-	8
7	07 RIH PRESS	Pressure		80
8	08 ROH PRESS	Pressure	-	80
9	09 AXF3FHILEG	Flow	-	80
10	10 TRF3FHILEG	Flow		40
11	11 AXF3FLOLEG	Flow	-	40
12	12 TRF3FLOLEG	Flow		20
13	13 AX FINCH HILEG	Flow	-	400
14	14 TR FINCH HILEG	Flow	-	200
15	15 AX FINCH LOLEG	Flow		400
16	16 TR FINCH LOLEG	Flow		200

The reactor data need to be converted to an ASCII format to be used with the developed data analysis system. This pre-processing step removes the DC component from each signal and normalizes the data using the electronic gain. The general strategy implemented consists of initially performing the analysis of each sensor signal using the STFT and the discrete wavelet transform, to obtain the power spectrum information of each sensor in the time-frequency and time-scale domains.

The next step is to process the data using the multiresolution analysis (MRA) to obtain details about the imbedded anomalies in the signals (abrupt changes or trends). The sub-band frequency information, given by the MRA, is expected to provide new insight into the behavior of reactor signals. At this stage, several wavelet basis functions are tested to define the one which gives the best analytical results (optimal wavelet selection).

The analysis of data from a nuclear power plant is performed using the MRA, STFT and the multichannel wavelet analysis techniques. The MATLAB system analysis developed for these applications was shown in Figure 4.2. The following sub-tasks are defined for this research work:

- The detection and characterization of transients in the data using the wavelet technique.
- The detection of sensor anomalies using the wavelet multi-Resolution Analysis.
- Comparison between wavelet analysis technique and other approaches.

The wavelet transform may be used directly to perform a time-scale analysis of the reactor data. Another approach is to decompose the signal into sub-band components and then use the STFT to perform the frequency analysis. The latter approach helps in identifying frequency bands that are most significant in showing time-varying signal behavior.

6.3.2 Neutron Detector Signal Analysis for Monitoring Fuel Assembly Vibration

The analysis of fuel assembly vibration data in set #1 is performed using the neutron detector signals and the steps described below. During data analysis, either the time dependency or the stationary characteristics of the fuel channel vibration is identified.

Normalize the data using the gain information given in Table 6.1.

Perform the data analysis using the standard fast Fourier transform (FFT) to obtain the auto-power spectral density (APSD).

Define the optimal wavelet function to be used.

Perform the data analysis using multiresolution wavelet technique (MRA).

Obtain the APSD, coherence and phase at different MRA levels.

Perform statistical analysis (mean and RMS values) for each MRA level in order to verify any trend in the data.

Perform the MRA and STFT analyses.

Perform the discrete wavelet transform (DWT), and obtain 2-D and 3-D plots.

6.3.3 Reactor Coolant Flow and Pressure Data Analysis

Data in set #2 contain measurements of the flow and pressure sensor signals from a different PWR unit. Following are the specific steps in data analysis

- Estimation of the frequency contents of the flow and pressure signals before, during and after the transients (spikes and/or dips), using time-frequency and time-scale approaches.
- Estimation of the APSD, coherence and phase of some flow/pressure signals using MRA in order to reveal the dominating frequencies triggering the dips in the flow transmitter's output.

In order to accomplish these tasks, the following analysis steps were defined.

- Normalize the data using the gain information given in Table 6.2.
- Perform the data analysis using the standard fast Fourier transform (FFT) to obtain the auto-power spectral density (APSD).
- Define the optimal wavelet function to be used.
- Perform the data analysis using MRA.
- Perform the MRA and STFT analyses.

- Perform the DWT data analysis for the transient frequency identification (obtain 2-D and 3-D plots).
- Perform multichannel data analysis (selected channels).

6.4 Results

6.4.1 Fuel Assembly Vibration Monitoring

From Table 6.1, two in-core neutron detector signals were selected and analyzed for fuel assembly vibration according to the steps described in Section 6.3.2. Figures 6.1 and 6.2 show the time series plots of two in-core channel measurements. Figures 6.3 and 6.4 show the auto-power spectra obtained using the FFT algorithm.

Preliminary background information about this data set reveals that there are two peaks in the auto-power spectra and coherence functions at 1.9 Hz and 2.4 Hz, which seem to be caused by mechanical vibration. The source of vibration has not yet been identified. The first and second mode frequencies of the detector tube vibrations in the flux noise spectra were also identified. According to the previous analysis [36], the most interesting effect of the vibrating fuel channels is that the vertical ICFDs, lined up along the same set of (horizontal) fuel channels, exhibit a small peak around 4.5-6 Hz in the auto power spectrum, and a bigger peak in their coherence functions (Figure 6.5), even if the ICFDs are far from each other. The phase is either zero, or close to 180 depending on whether the two ICFDs are on the same side, or different sides of the vibrating fuel channel(s) (Figure 6.6).

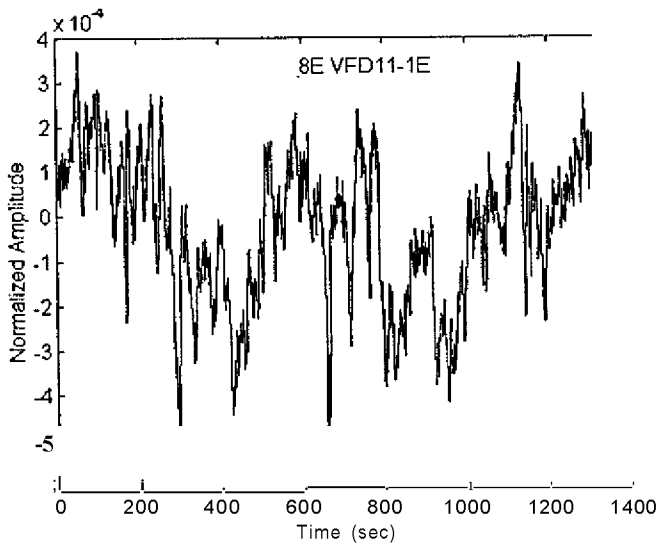

Figure 6.1. Time-Amplitude Plot from Sensor ID #5.

Figure 6.2. Time-Amplitude from Sensor ID #8

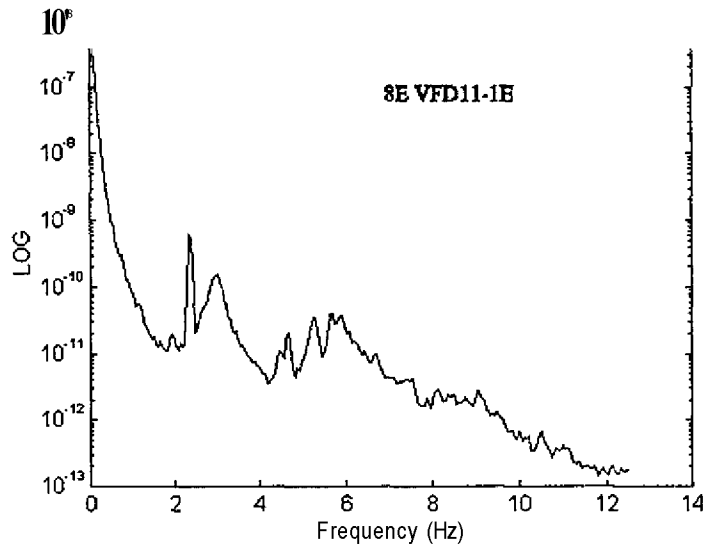

Figure 6.3. Auto Power Spectrum from the Sensor ID #5

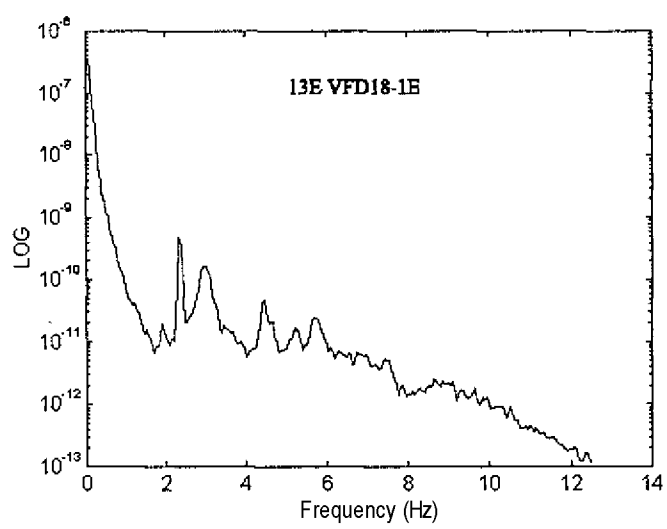

Figure 6.4. Auto Power Spectrum from the Sensor ID #8

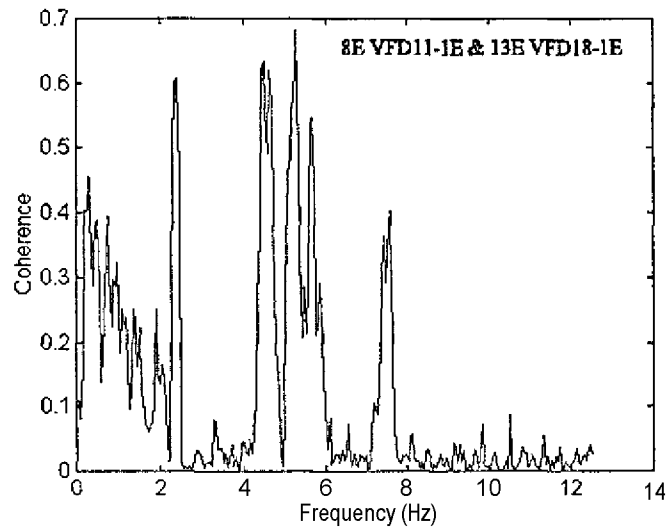

Figure 6.5. Coherence Between the In-Core Neutron Detectors

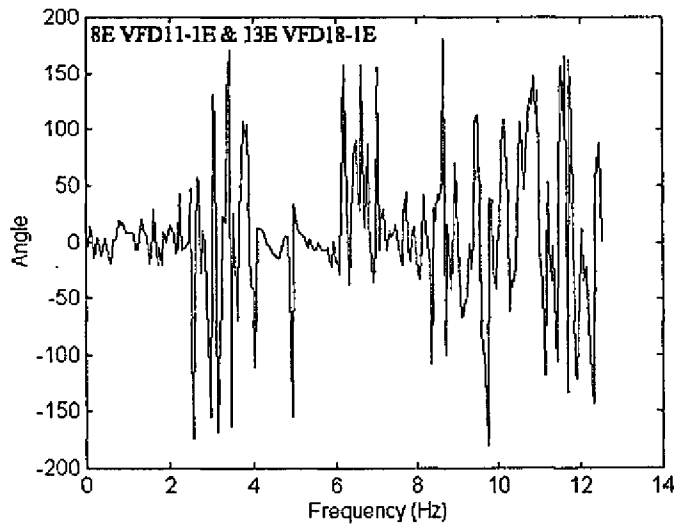

Figure 6.6. Phase Angle Between the In-Core Neutron Detectors

In Section 6.3.1, it was mentioned that during data analysis the detection and characterization of transients in the data would be investigated using the wavelet technique. The wavelet analysis requires, initially, the selection of the optimal wavelet to be used. Figure 6.7 shows the result of optimal wavelet selection for these signals using the minimum entropy energy selection method. The wavelet basis function Daubechies 10 was selected using this method (Program 4, Appendix B).

The multiresolution analysis (MRA) of two selected in-core sensors was performed and the discrete wavelet transform coefficients were obtained for each signal. The frequency sub-band levels are defined in Table 6.3. The reconstructed signals were obtained and their mean and RMS values were calculated. The idea of this computation is to check if there is any trend in the signal. The results for sensors ID #5 and ID #8 are shown in Figures 6.8-6.13 and Figures 6.14-6.19, respectively. The detail levels give an idea about the behavior of the signal at high frequency bands. The approximation signal at each sub-band level gives the behavior of the signal at low frequency ranges. The mean and RMS values obtained for each frequency sub-band level show that there are significant changes at low frequency bands. This behavior indicates some non-stationary characteristics in the signals at low frequencies.

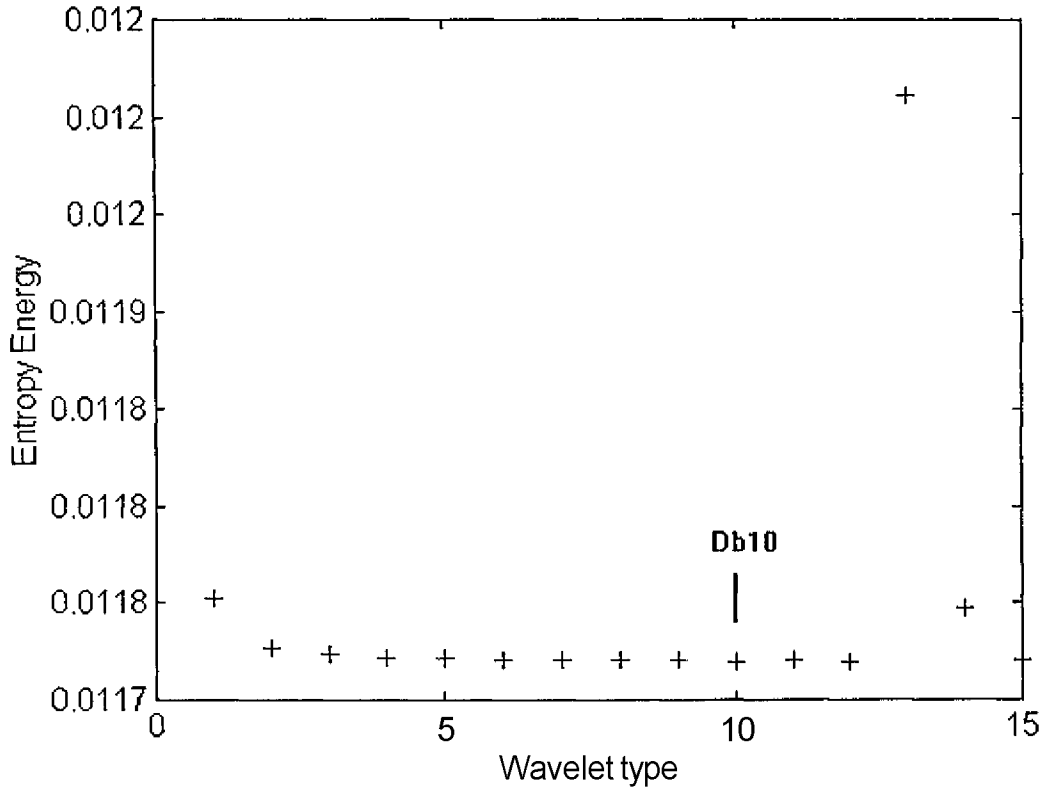

Figure 6.7 **Optimal Wavelet Selection for both ID** #5 **and ID** #8 **In-Core Neutron Detectors**

Table 6.3. Frequency Bands for Multiresolution Analysis (MRA) - Fuel Assembly Vibration Data (In Core-Neutron Detector) (Sampling rate = 25 Hz)

Sub-band Level	Details Frequency Range (Hz)	Approximations Frequency Range (Hz)
1	6.25 -12.5	0 - 6.25
2	3.12-6.25	0 - 3.25
3	1.56-3.125	0-1.56
4	0.78-1.56	0 - 0.78
5	0.39 - 0.78	0-0.39
6	0.195-0.39	0-0.195
7	0.0975 -0.195	0 - 0.0975
8	0.0488 - 0.0975	0 - 0.0488
9	0.0244 - 0.0488	0 - 0.0244
10	0.0122-0.0244	0 - 0.0122

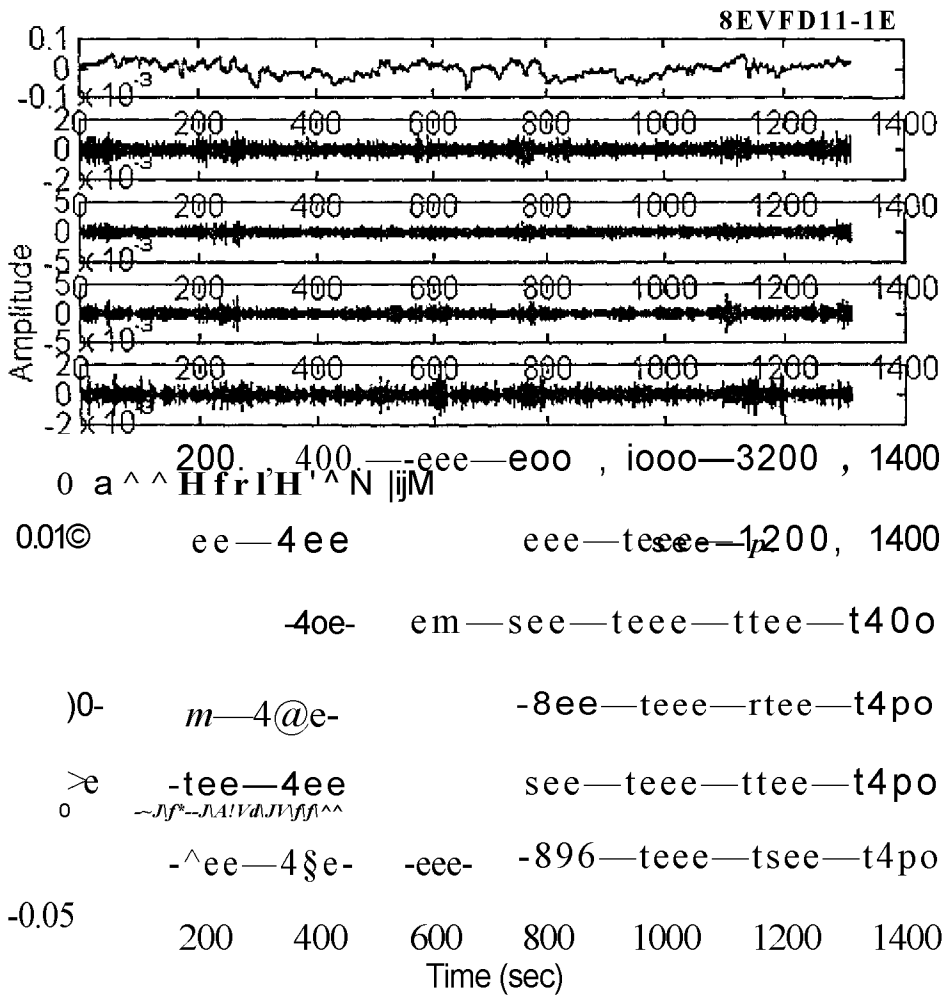

Figure 6.8. Multiresolution Analysis Results Showing the Detail Reconstruct Signals of In-Core Neutron Detector ID #5 (original signal at the top and 10th level at the bottom)

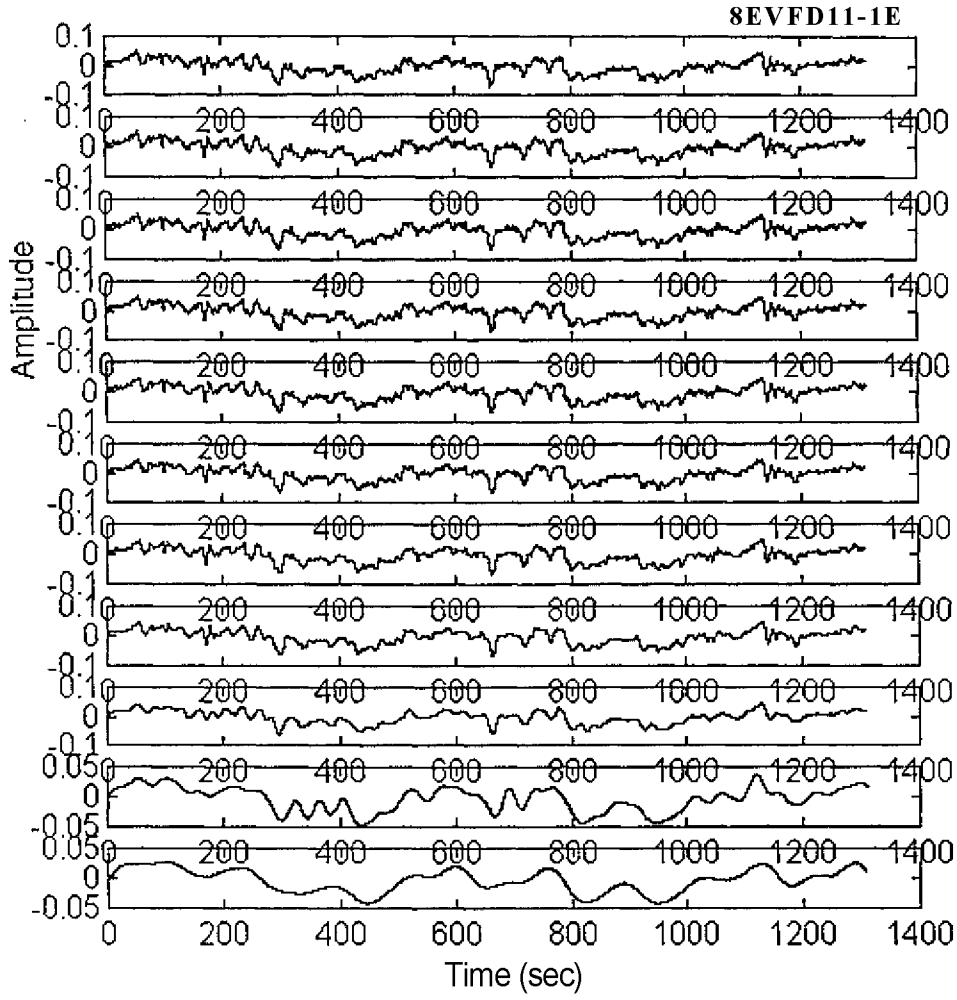

Figure 6.9. Multiresolution Analysis Results Showing the Approximation Reconstruct Signals of In-Core Neutron Detector ID #5 (original signal at the top and 10th level at the bottom)

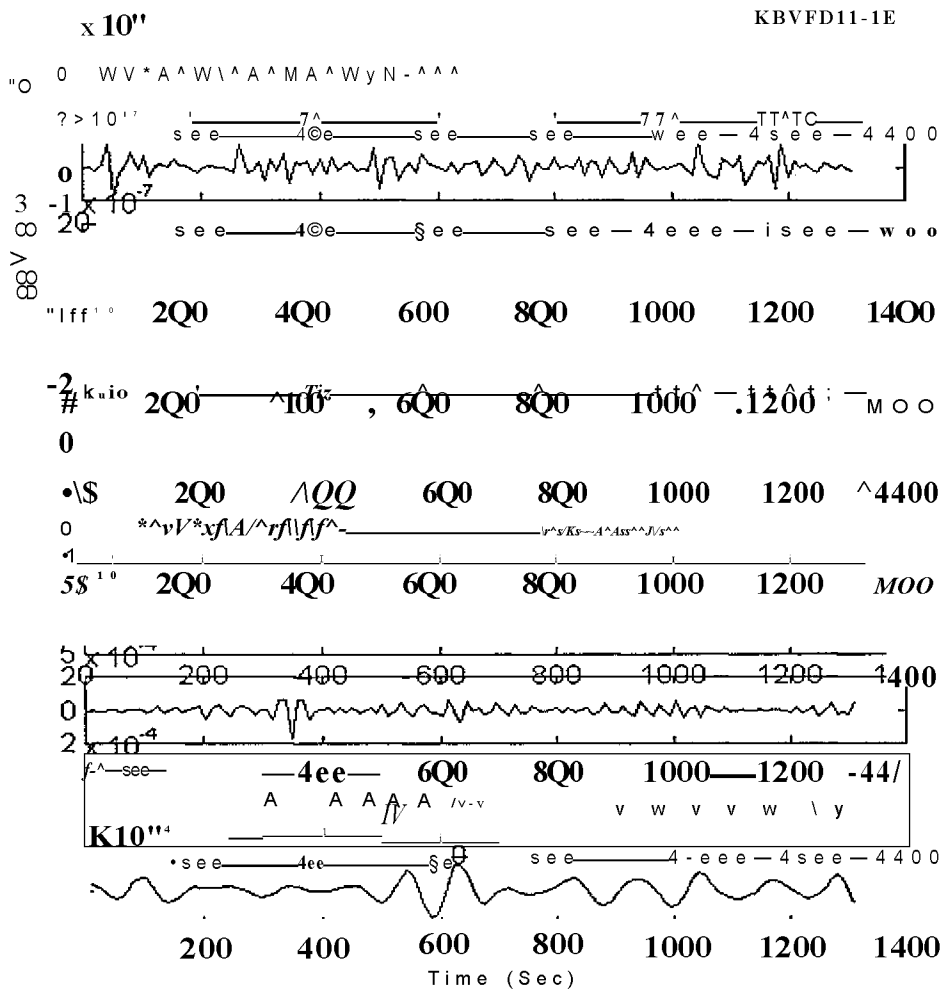

Figure 6.10. Multiresolution Analysis Results Showing the Mean Values of the Detail Reconstruct Signals of In-Core Neutron Detector ID #5 (1st level the top and 10th level at the bottom)

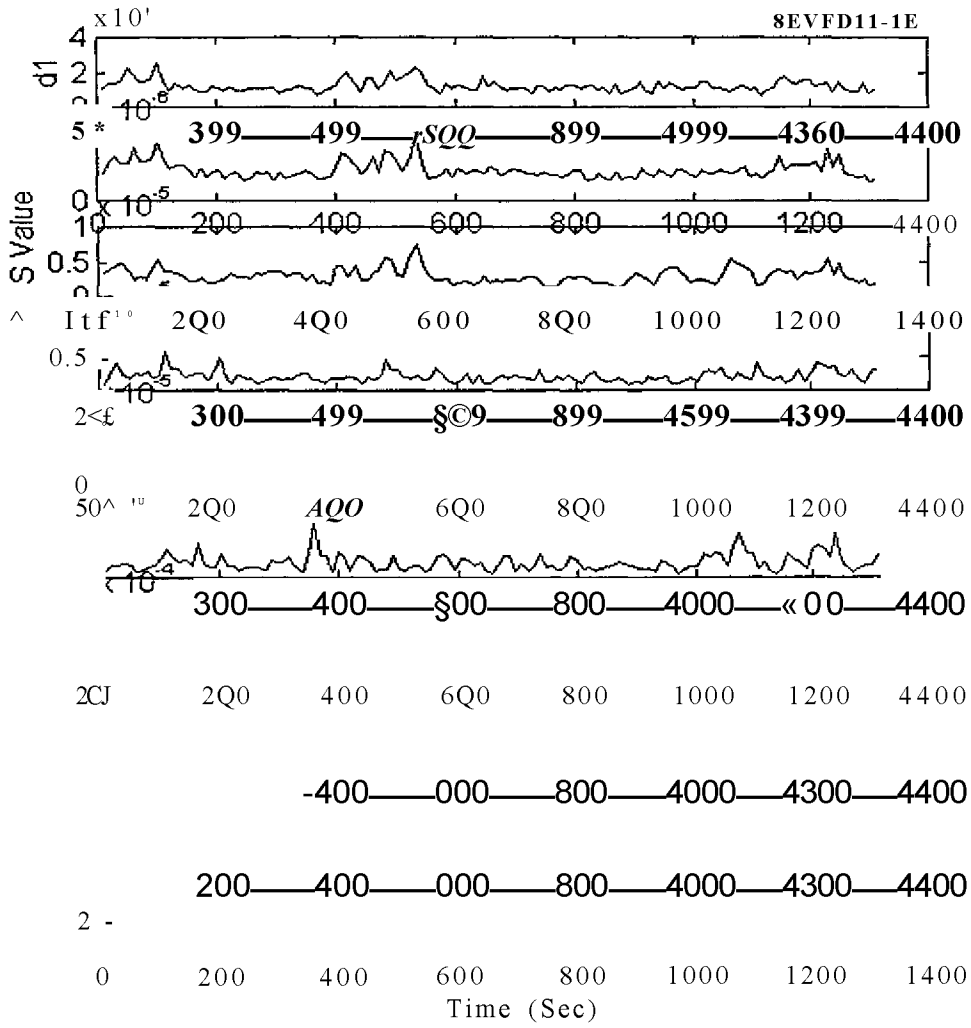

Figure 6.11. Multiresolution Analysis Results Showing the RMS Values of the Detail Reconstruct Signals of In-Core Neutron Detector ID #5 (1st level the top and 10th level at the bottom)

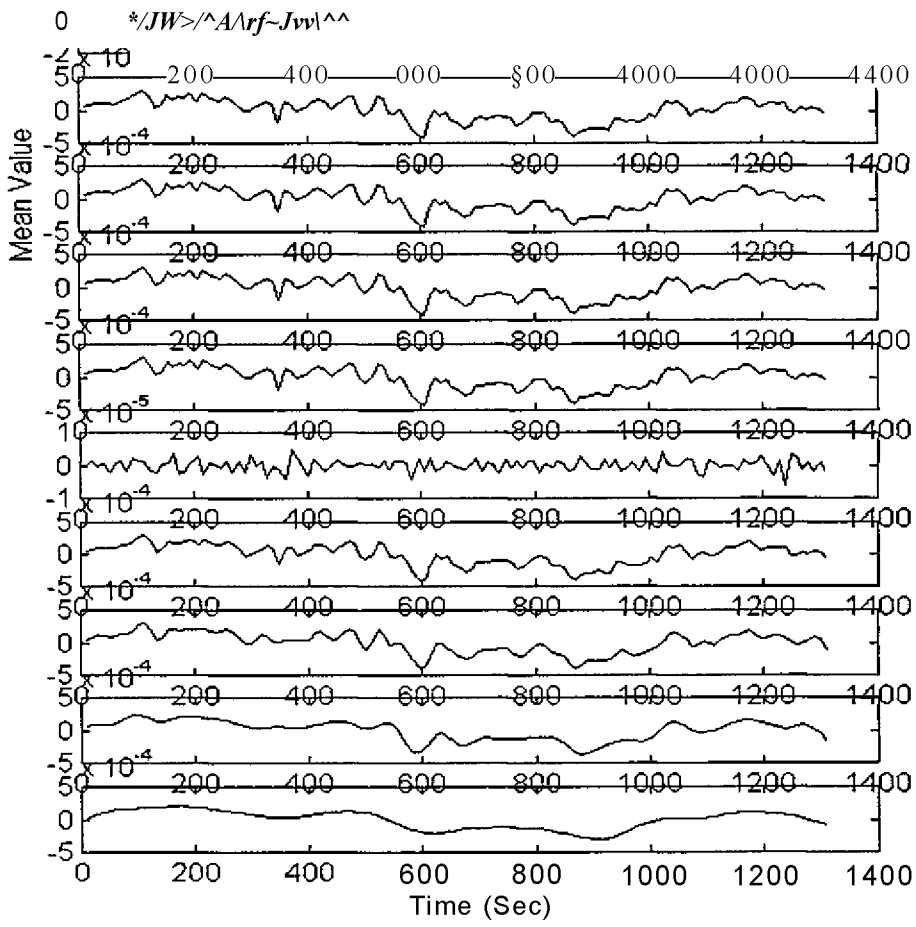

Figure 6.12. Multiresolution Analysis Results Showing the Mean Values of the Approximation Reconstruct Signals of In-Core Neutron Detector ID #5 (1st level the top and 10th level at the bottom)

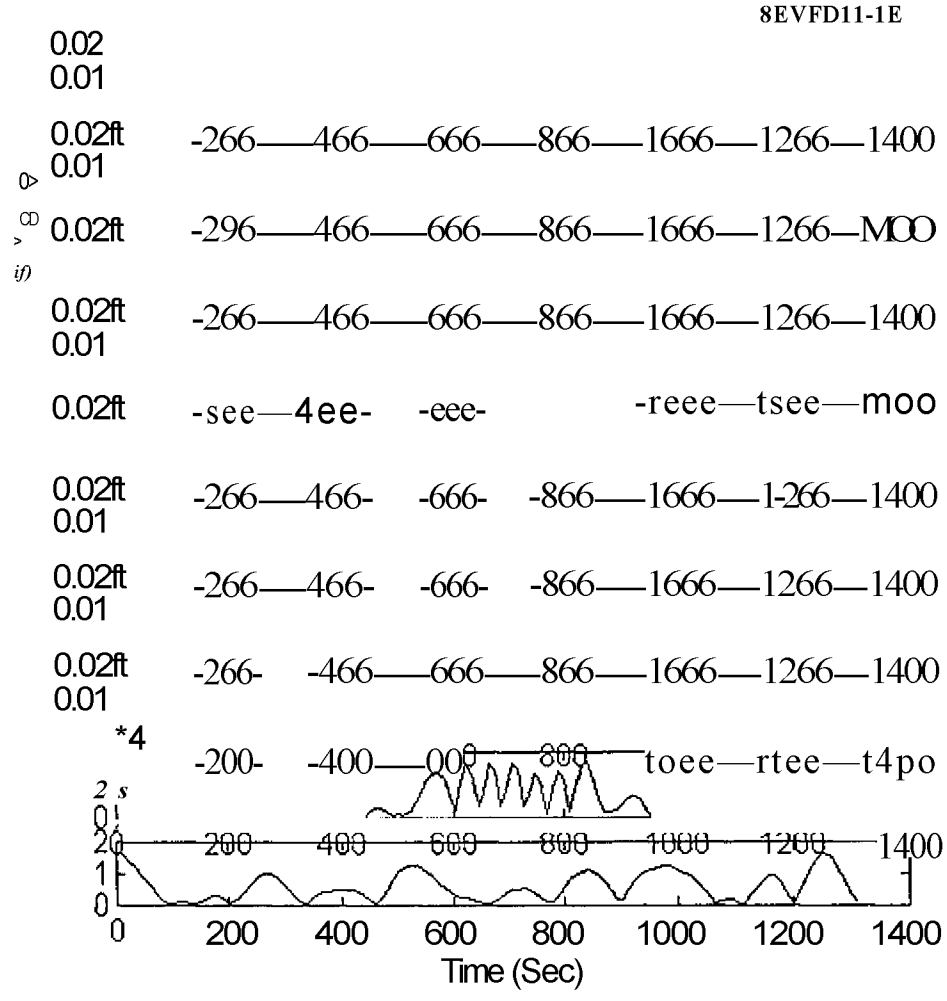

Figure 6.13. Multiresolution Analysis Results Showing the RMS Values of the Approximation Reconstruct Signals of In-Core Neutron Detector ID #5 (1st level the top and 10th level at the bottom)

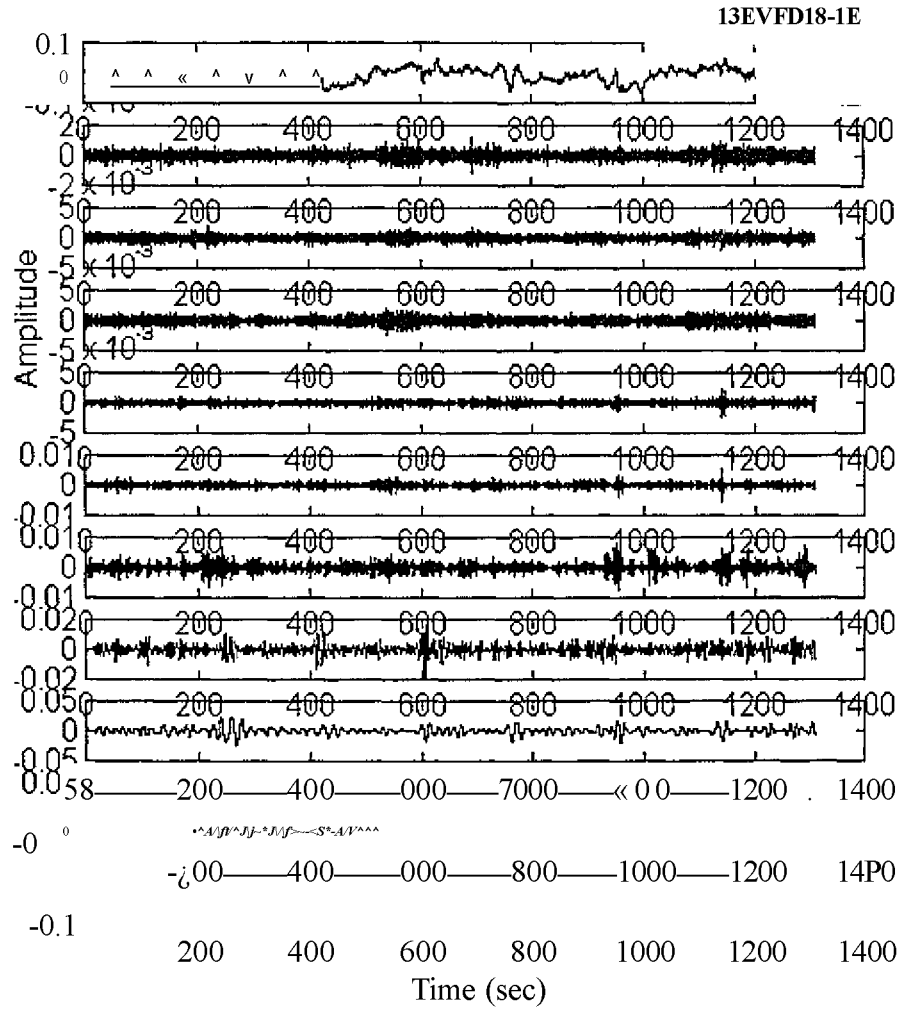

Figure 6.14. Multiresolution Analysis Results Showing the Detail Reconstruct Signals of In-Core Neutron Detector ID #8 (original signal at the top and 10th level at the bottom)

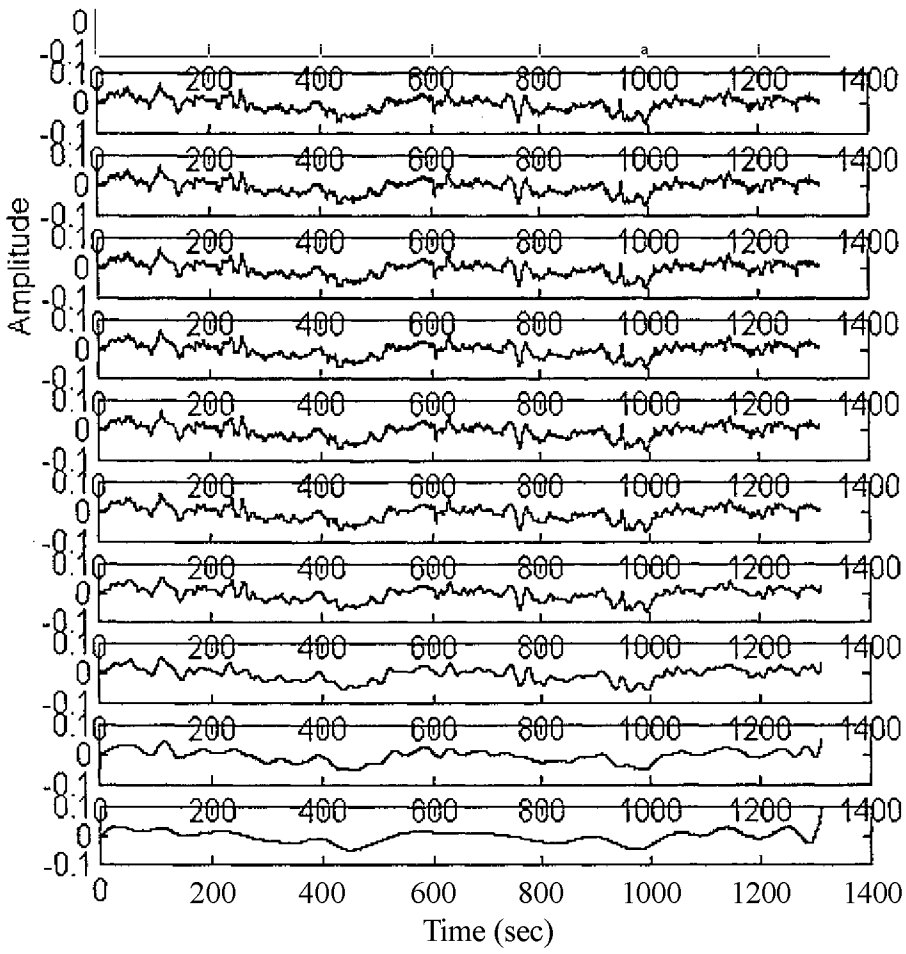

Figure 6.15. Multiresolution Analysis Results Showing the Approximation Reconstruct Signals of In-Core Neutron Detector ID #8 (original signal at the top and 10th level at the bottom)

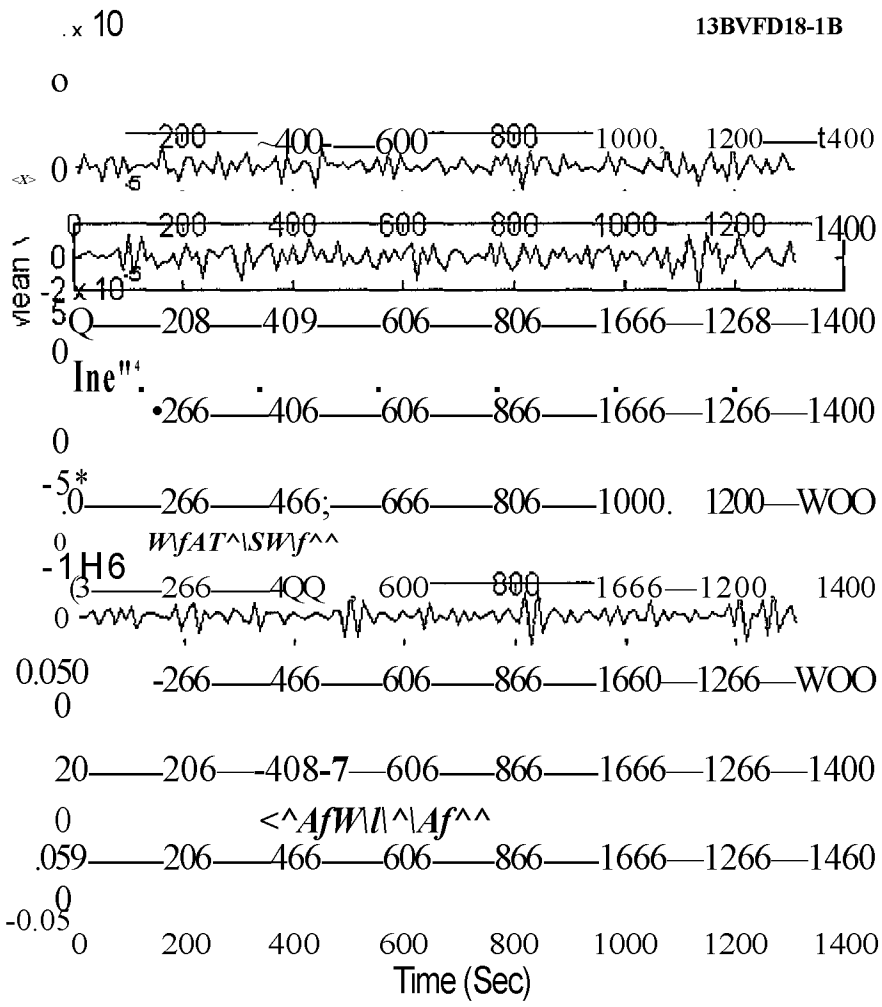

Figure 6.16. Multiresolution Analysis Results Showing the RMS Values of the Detail Reconstruct Signals of In-Core Neutron Detector ID #8 (1st level the top and 10th level at the bottom)

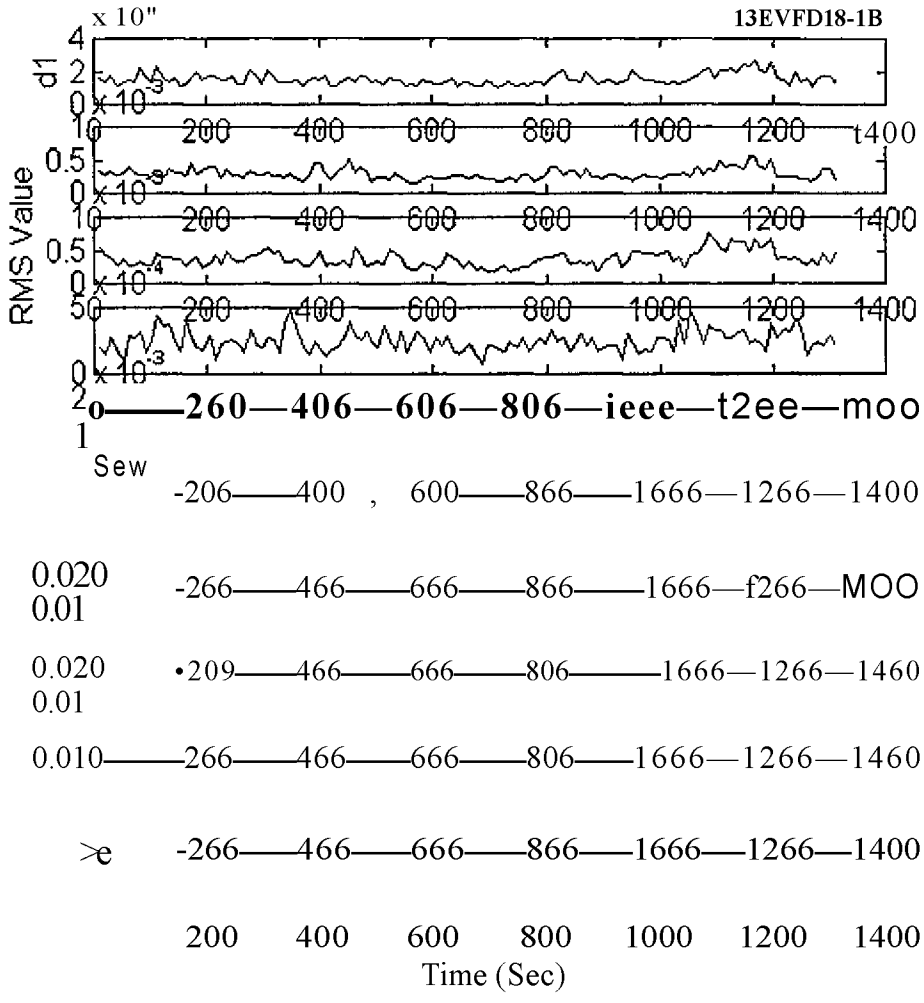

Figure 6.17. Multiresolution Analysis Results Showing the Mean Values of the Detail Reconstruct Signals of In-Core Neutron Detector ID #8 (1st level the top and 10th level at the bottom)

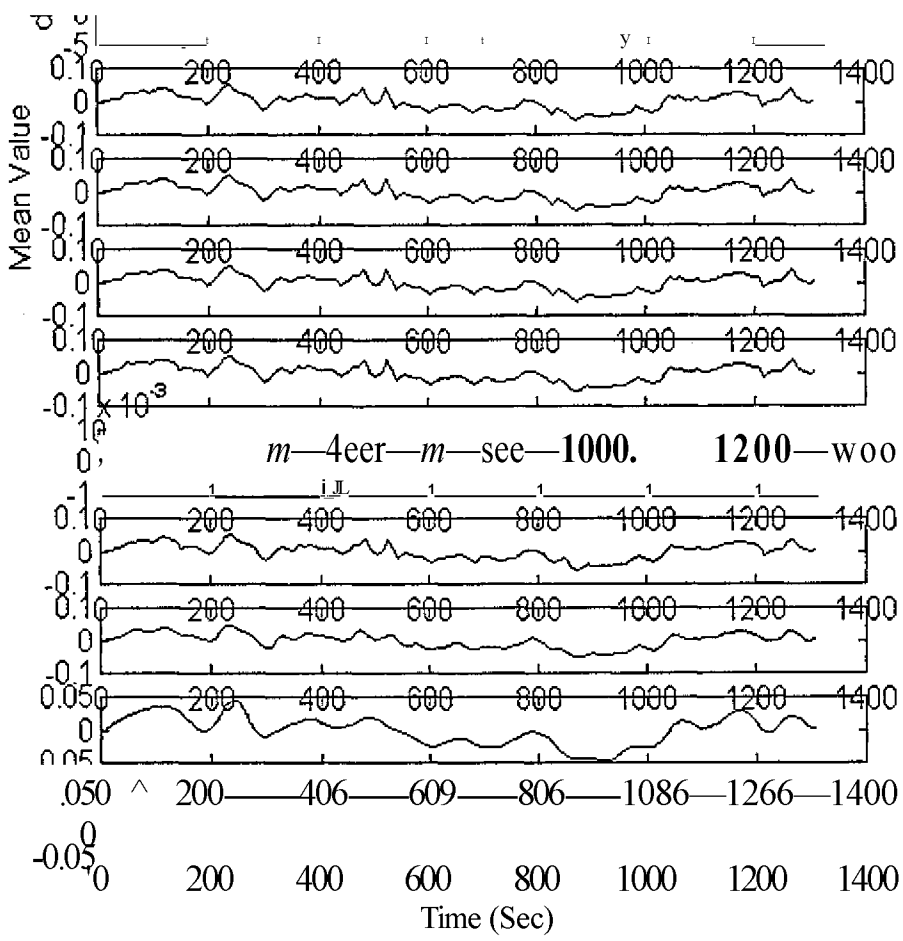

Figure 6.18. Multiresolution Analysis Results Showing the Mean Values of the Approximation Reconstruct Signals of In-Core Neutron Detector ID #8 (1st level the top and 10th level at the bottom)

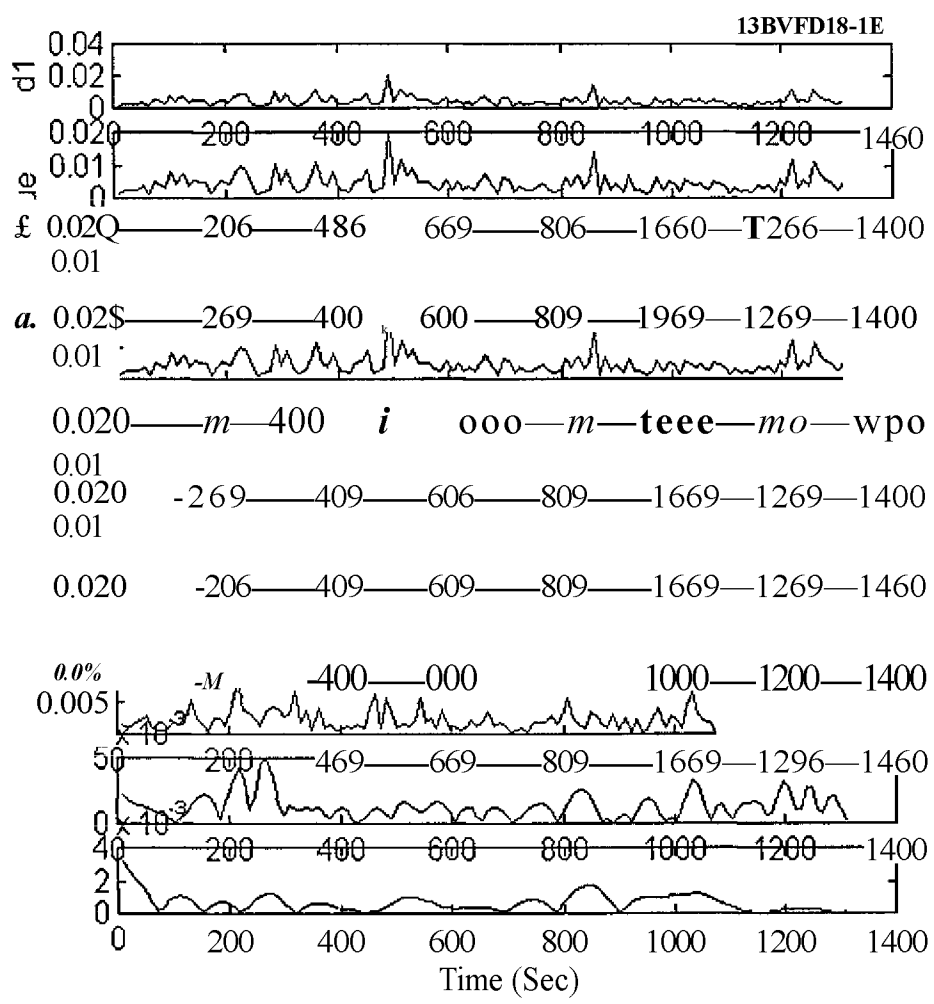

Figure 6.19. Multiresolution Analysis Results Showing the RMS Values of the Approximation Reconstruct Signals of In-Core Neutron Detector ID #8 (1st level the top and 10th level at the bottom)

The following steps will show the results obtained for the multichannel analysis using the MRA and FFT techniques. Some sub-band levels were selected and the auto-power spectral density (APSD), coherence and phase were computed and compared with the results using the original data. Figure 6.20 shows the auto-power spectral density of the reconstructed approximation signal at level 1. Figure 6.21 shows the APSD at detail level 3. Figures 6.22 and 6.23 show the coherence at the approximation and detail levels. Figure 6.24 shows the phase angle plot at the approximation level 1. All plots show the MRA results and the FFT analysis using the original signals. These results give a brief idea about the advantages of using MRA and FFT together. The analysis of signals that are contaminated by noise can be improved using the MRA technique. The advantage of using MRA technique is that one can zoom into the region of interest during signal analysis, avoiding the interference of undesirable frequencies.

The time-frequency and time-scale analysis, as stated before, help in identifying frequency bands that are most significant in showing time-varying signal behavior. The time-frequency analysis can be applied for monitoring the behavior of the fuel assembly vibration signals to detect any possible anomalies before, during and after their occurrences. During this analysis, the STFT, using the Gabor window, is combined with the MRA. Some results are shown using 2-D and 3-D plots.

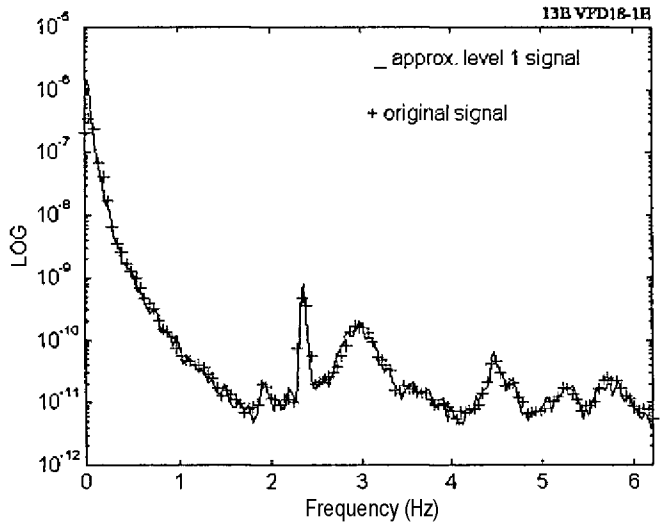

Figure 6.20. Auto Power Spectral Density for Approximation Level 1 and Original In-Core Fuel Assembly Vibration Signals (ID #8)

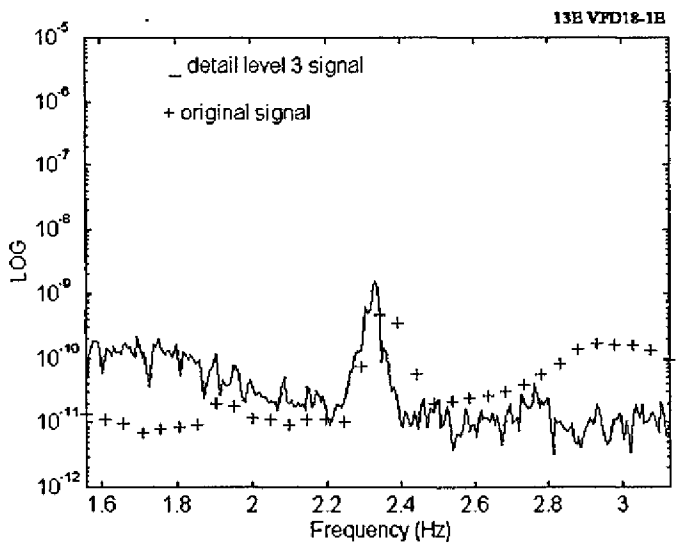

Figure 6.21. Auto Power Spectral Density for Detail Level 3 and Original In-Core Fuel Assembly Vibration Signals (ID #8)

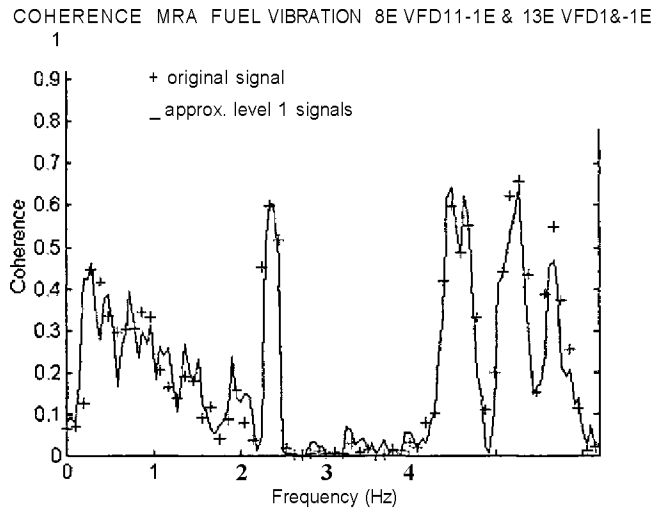

Figure 6.22. Coherence between Approximation Level 1 and Original In-Core Fuel Assembly Vibration Signals (ID #5 & ID #8)

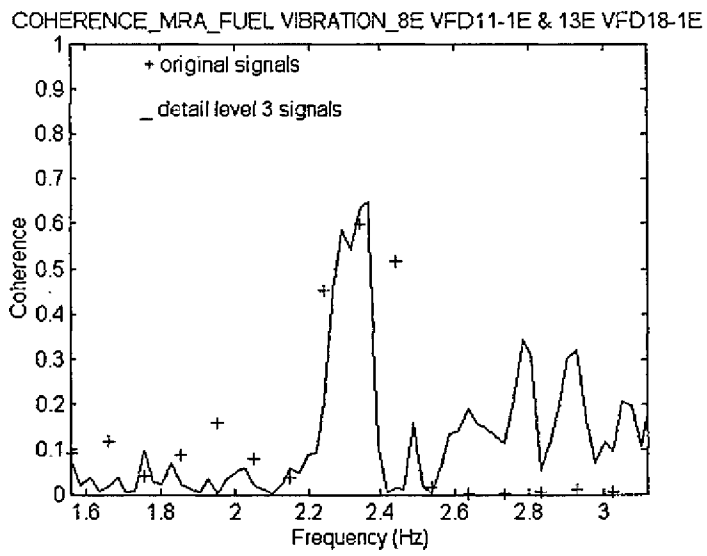

Figure 6.23. Coherence between Detail Level 3 and Original In-Core Fuel Assembly Vibration Signals (ID #5 & ID #8)

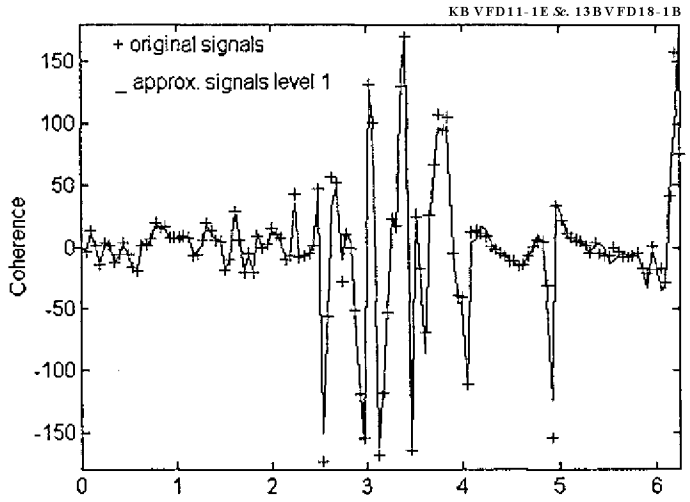

Figure 6.24. Phase between Detail Level 3 and Original In-Core Fuel Assembly Vibration Signals (ID #5 & ID #8)

Figures 6.25-6.28 show the STFT results of the neutron in-core signals (ID #5 and ID #8). The 2-D plots give a precise idea of the frequency and time localization of the peaks, while the 3-D plots provide an additional information about the magnitude of the STFT coefficients (power spectrum) in the time-frequency domain. Figures 6.29-6.32 describe the results using STFT and MRA techniques for the detail signals at level 3. The combination of these two signal analysis techniques provides a localized information about the sensor or process variable that is being monitored. Different fuel assembly vibration modes can be monitored individually using this type of technique. The 2.4 Hz peak was selected for analysis and it seems to be caused by mechanical vibration of the fuel element.

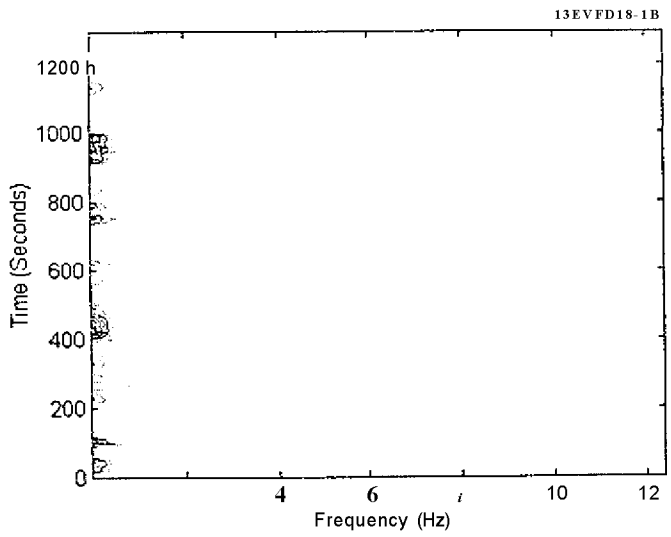

Figure 6.25. STFT Contour Plot for the In-Core Fuel Assembly Vibration Signal (ID #8)

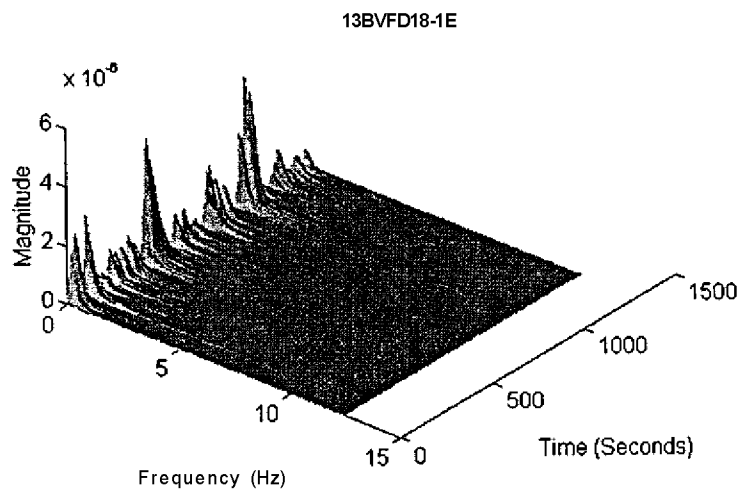

Figure 6.26. STFT 3-D Plot for the In-Core Fuel Assembly Vibration Signal (ID #8)

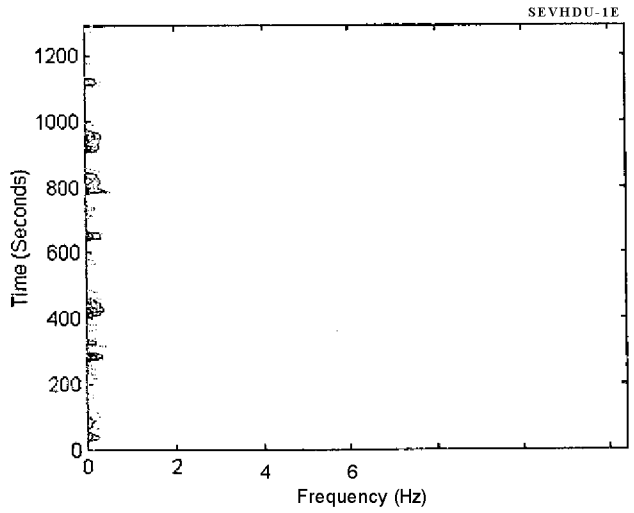

Figure 6.27. STFT Contour Plot for the In-Core Fuel Assembly Vibration Signal (ID #5)

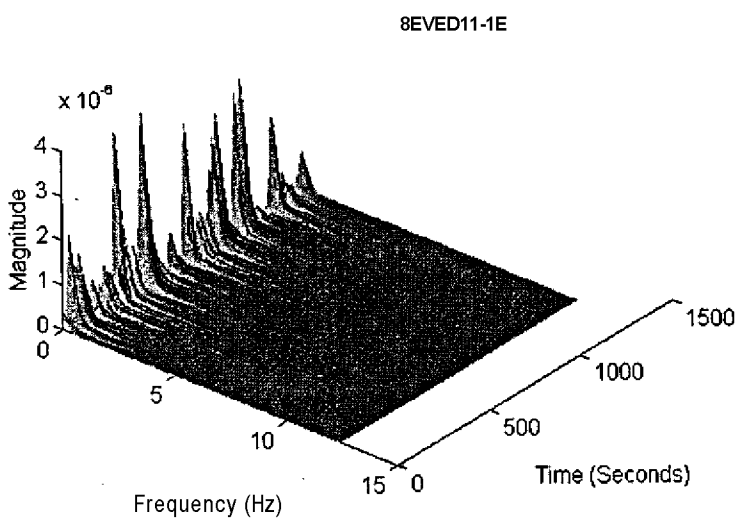

Figure 6.28. STFT 3-D Plot for the In-Core Fuel Assembly Vibration Signal (ID #5)

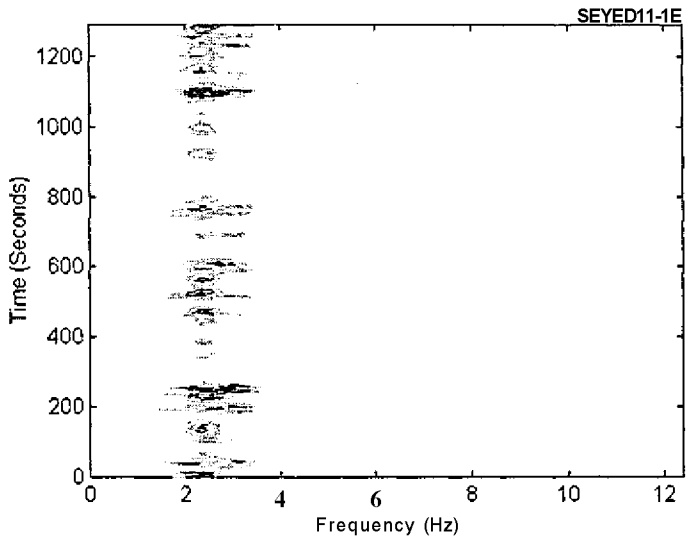

Figure 6.29. STFT and MRA Contour Plot for the Detail Level 3 In-Core Fuel Assembly Vibration Signal (ID #5)

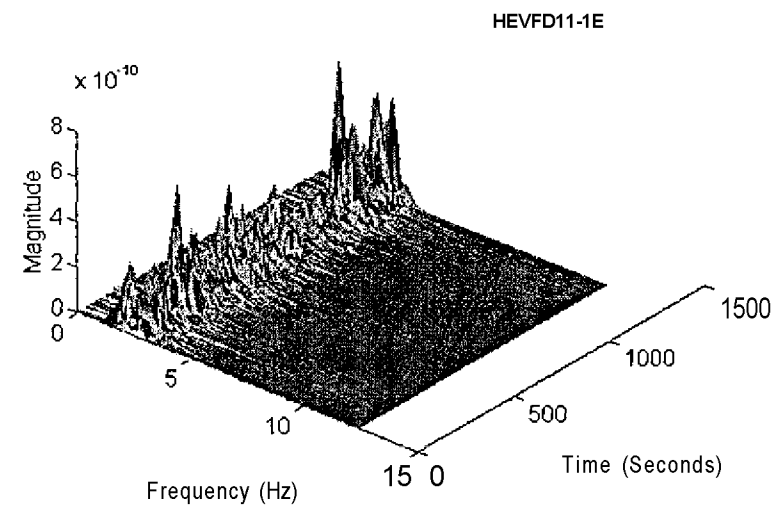

Figure 6.30. STFT and MRA 3-D Plot for the Detail Level 3 In-Core Fuel Assembly Vibration Signal (ID #5)

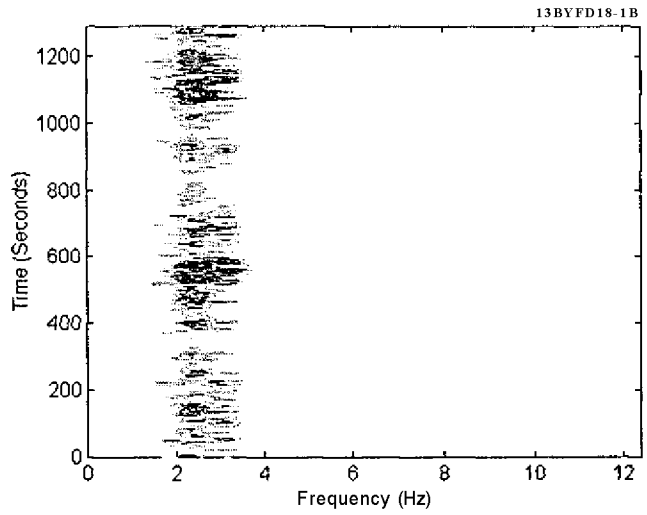

Figure 6.31. STFT and MRA Contour Plot for the Detail Level 3 In-Core Fuel Assembly Vibration Signal (ID #8)

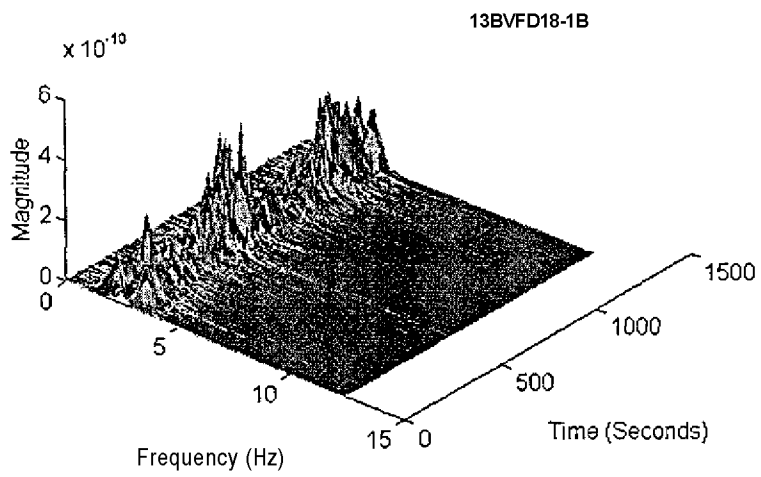

Figure 6.32. STFT and MRA 3-D Plot for the Detail Level 3 In-Core Fuel Assembly Vibration Signal (ID #8)

The non-stationary behavior of a signal can be detected more precisely using the wavelet transform. The discrete dilation wavelet transform has been chosen for signal evaluation because of its simplicity and the fast algorithm to compute the wavelet coefficients [12, 19, 20, 48].

In the next stage the fuel assembly vibration signal analysis is performed using the discrete wavelet transform with the Daubechies 10 wavelet basis function. For each selected signal, 2-D and 3-D plots were obtained. The frequency band in which the wavelet coefficients indicate significant changes, was then determined (Figures 6.33-6.36). This analysis shows that, at a low frequency band (<0.2 Hz), some anomalies were detected. The peaks portrayed in the 3-D plots represent possible abrupt changes in the signals during the time period. The relationship between the wavelet level number and the frequency center is defined in Table 6.4.

In Appendix A, two ex-core neutron detectors were analyzed. The results obtained using the short-time Fourier and discrete wavelet transforms are shown in Figures A1-A16. The STFT and MRA analysis provide the information, on a desired frequency band, about the behavior of the signal and/or process during the measurements. The DWT power spectrum plots show that most anomalies of the signals are in the high frequency band.

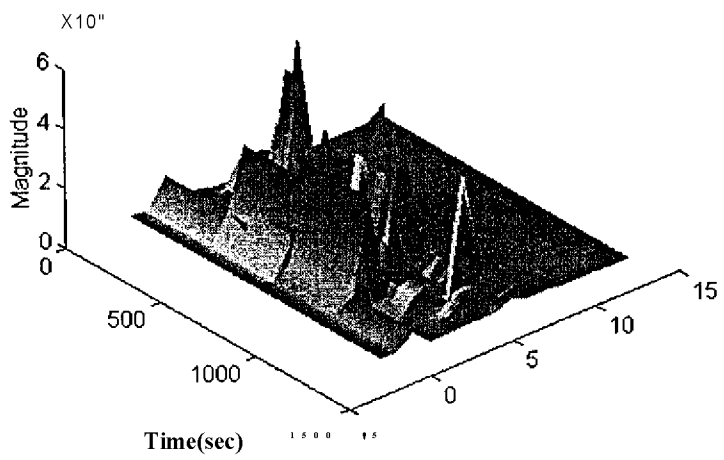

Figure 6.33. DWT 3-D Plot for the In-Core Fuel Assembly Vibration Signal (ID #5)

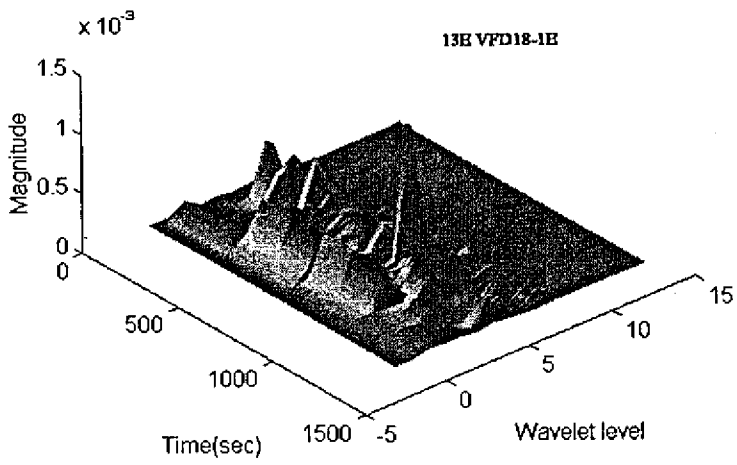

Figure 6.34. DWT 3-D Plot for the In-Core Fuel Assembly Vibration Signal (ID #8)

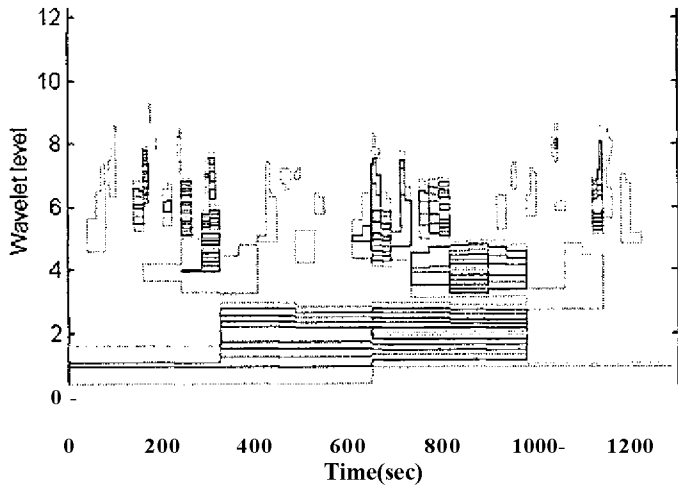

Figure 6.35. DWT Contour Plot for the In-Core Fuel Assembly Vibration Signal

(ID #5)

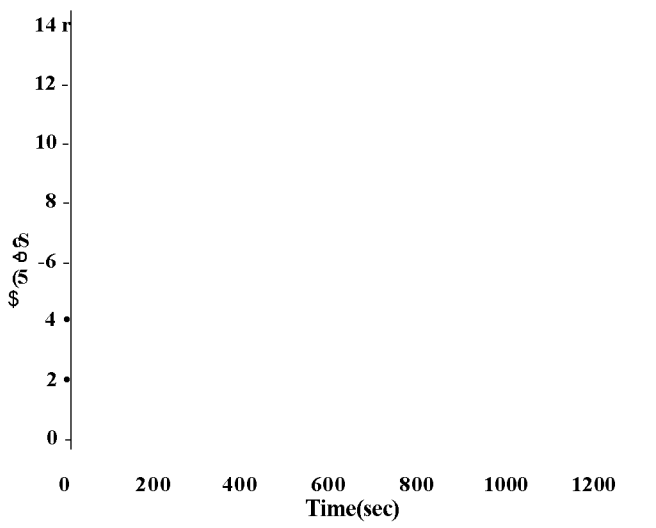

Figure 6.36. DWT Contour Plot for the In-Core Fuel Assembly Vibration Signal

(ID #8)

TABLE 6.4. Frequency Bands for Discrete Wavelet Transform Plots

Wavelet Level	Frequency Center (Hz)
6	0.0122
8	0.0488
10	0.195
11	0.781
12	3.125
13	12.5
14	25.0

6.4.2 Analysis of Flow and Pressure Signals

This section includes all data analysis performed for a select number of flow and pressure sensors from a PWR, as described in Table 6.2. Figures 6.37 and 6.38 show the time-amplitude plots of the flow and pressure sensor signals. The sensors reveal the appearance of several dips in the signal. Figures 6.39 and 6.40 show the auto-power spectral densities (APSD) for these sensors using the FFT technique.

The data analysis procedure followed in this dissertation requires initially the definition of the optimal wavelet, which was used during the analysis. The results of using the optimal wavelet selection method are shown in Figures 6.41 and 6.42. The Daubechies wavelets are the most appropriate basis functions to perform the analysis of these signals.

The MRA provides five sub-band frequency levels for each selected signal and their respective frequencies, which are given in Table 6.5. The frequency range selected, which is defined by the five sub-band levels, covers the region of interest for the sensors. Figures 6.43-6.46 show the approximation and detail signals obtained using the MRA technique. Each sub-band level represents the reconstructed signal at a low or at a high frequency band.

The reconstructed signals at each sub-band level, approximation and details may be analyzed using the STFT in order to get a better idea about their time-frequency behavior. Figures 6.47-6.50 show the STFT analysis for some selected sensors (raw data),

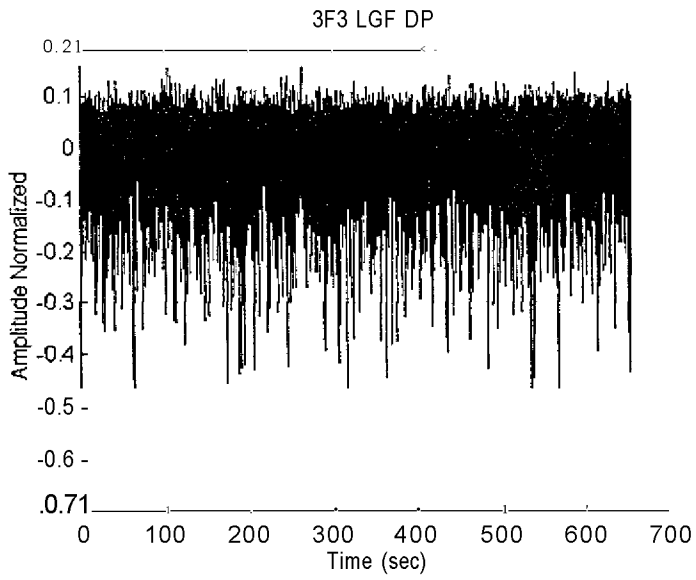

Figure 6.37. Time-Amplitude Plot of the Flow Sensor (ID #01)

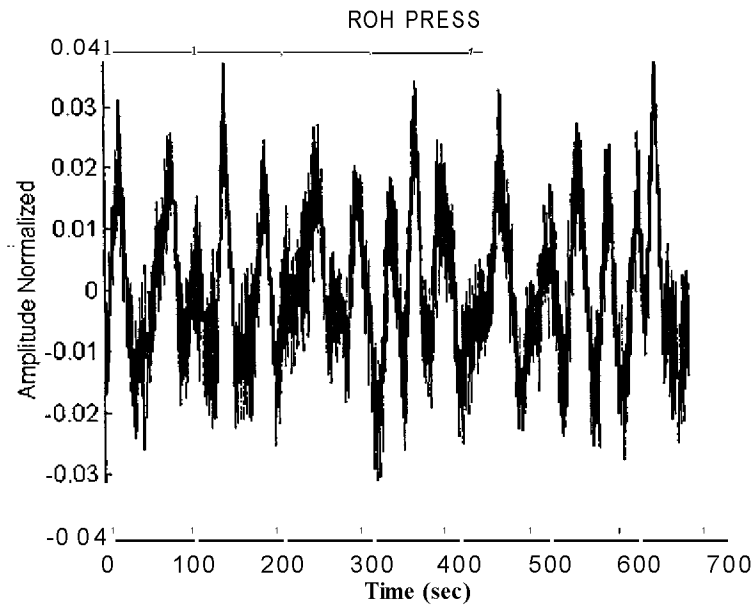

Figure 6.38 Time-Amplitude Plot of the Pressure Sensor (ID #07)

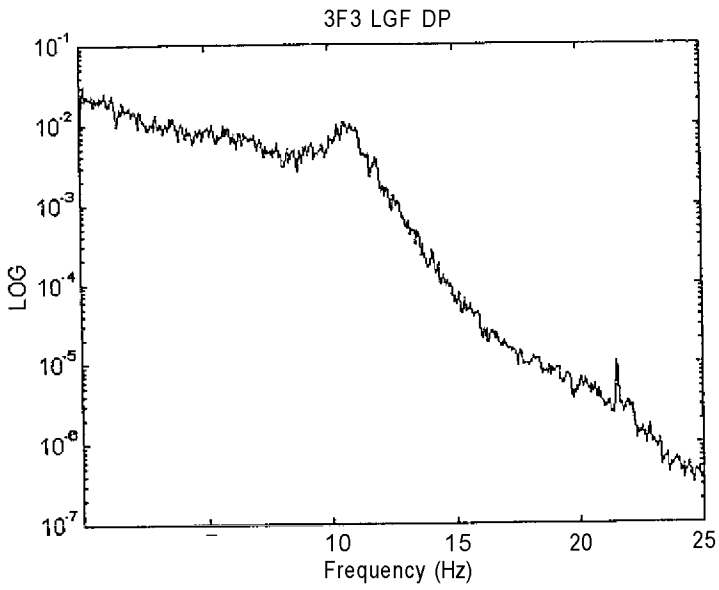

Figure 6.39. Auto Power Spectrum from the Flow Sensor (ID #01)

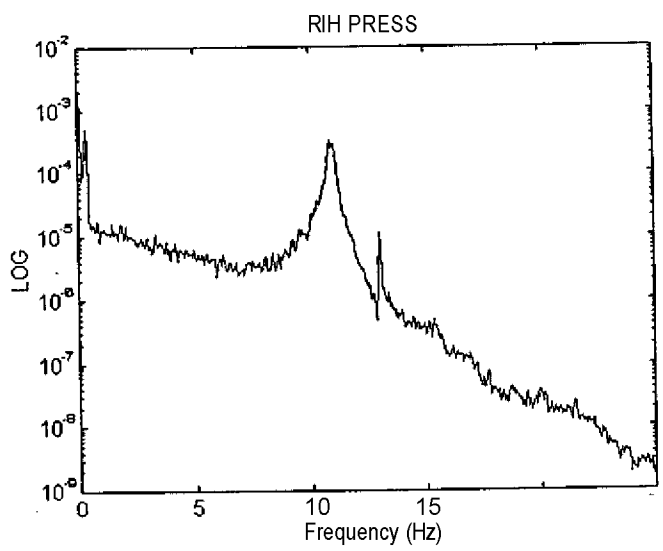

Figure 6.40. Auto Power Spectrum from the Pressure Sensor (ID #07)

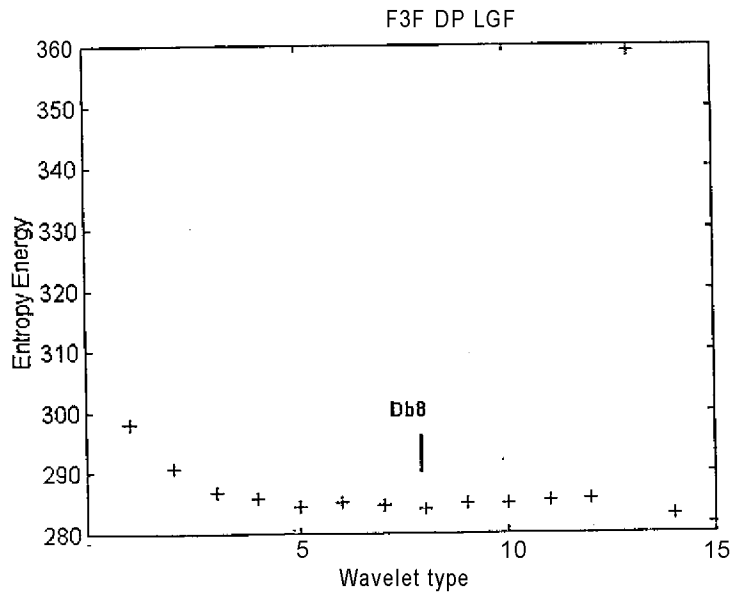

Figure 6.41. Optimal Wavelet Selection for the Flow Sensor (ID #01)

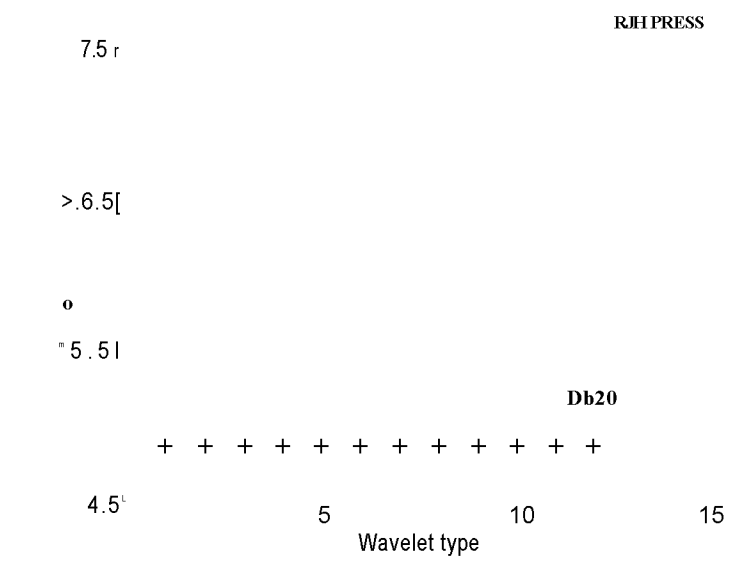

Figure 6.42. Optimal Wavelet Selection for the Pressure Sensor (ID #07)

Table 6.5. Frequency Bands for Multiresolution Analysis (MRA) - Flow and Pressure Data
(sampling rate = 50 Hz)

Wavelet Level	Details Frequency Range (Hz)	Approximations Frequency Range (Hz)
1	12.5-25	0-12.5
2	6.25 - 12.5	0 - 6.25
3	3.125-6.25	0 - 3.25
4	1.56-3.125	0-1.56
5	0.78-1.56	0 - 0.78

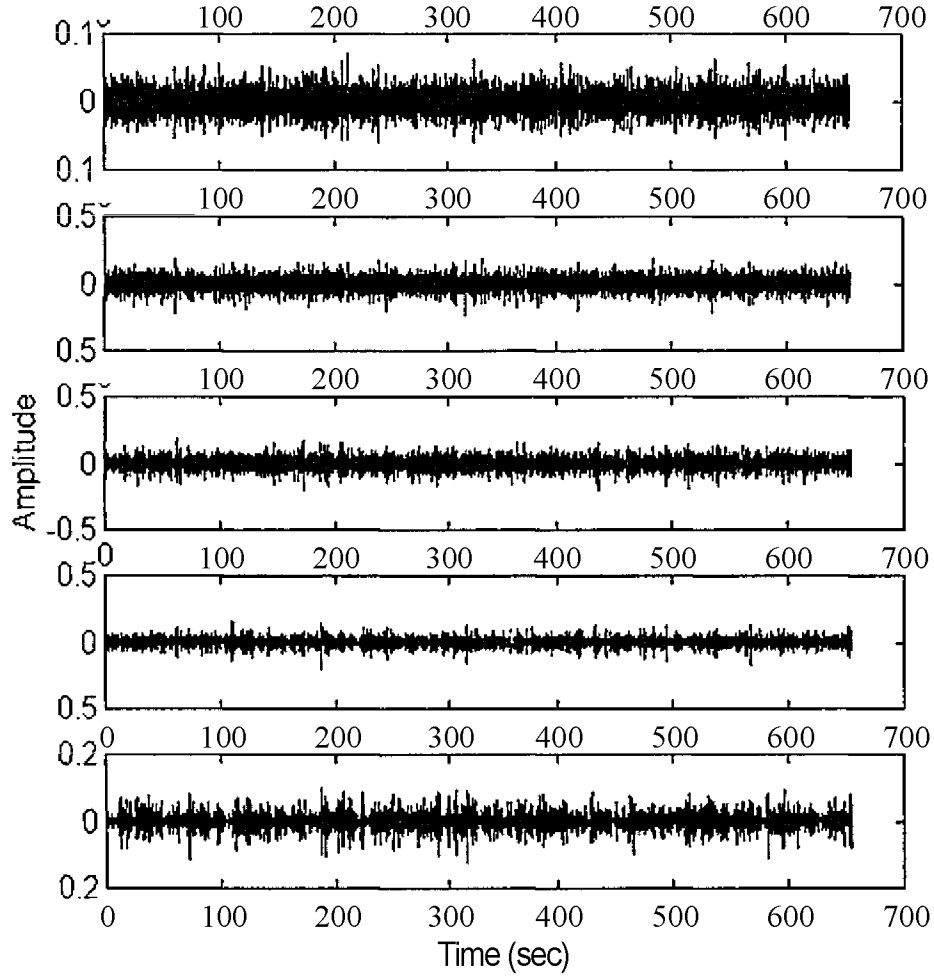

Figure 6.43. Multiresolution Analysis Results Showing the Detail Reconstruct Signals of Flow Sensor ID #01 (original signal at the top and 5th level at the bottom)

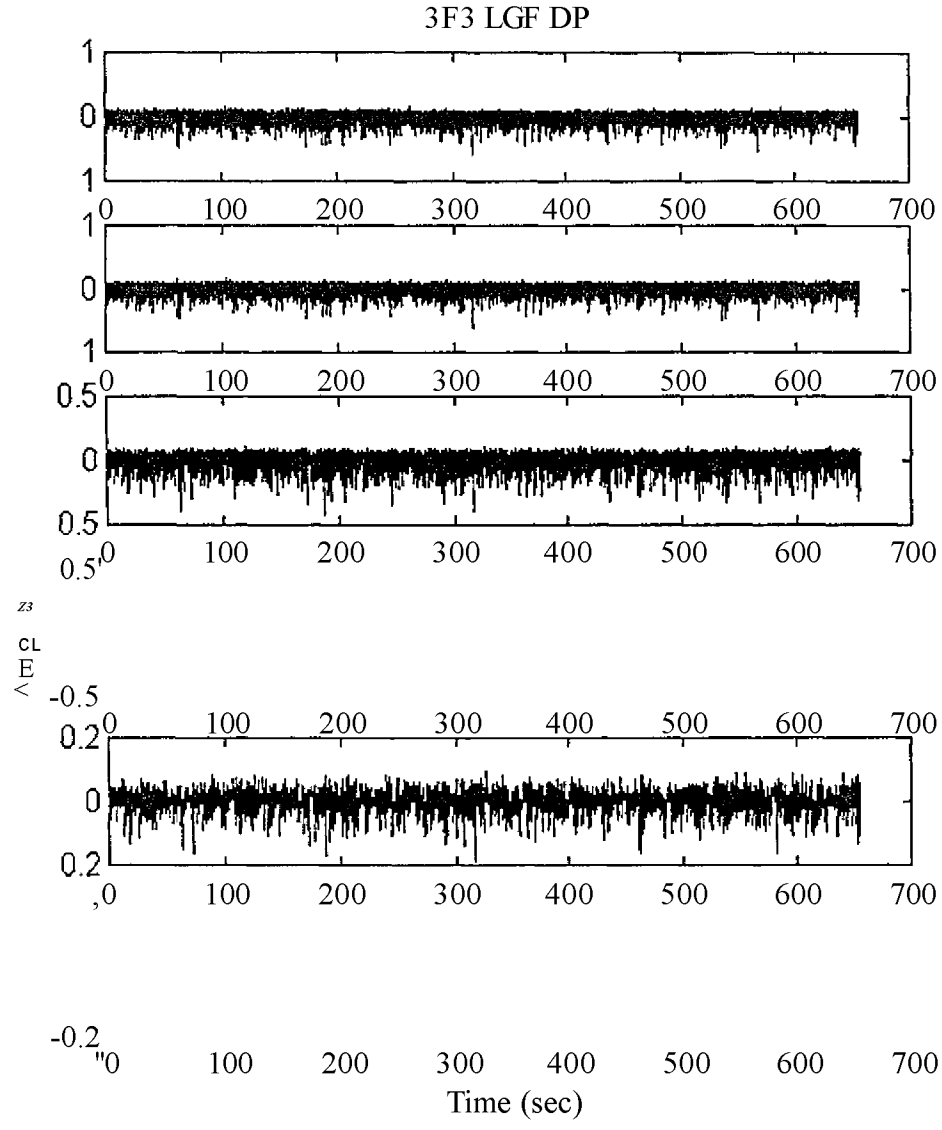

Figure 6.44. Multiresolution Analysis Results Showing the Approximation Reconstruct Signals of Flow Sensor ID #01 (original signal at the top and 5th level at the bottom)

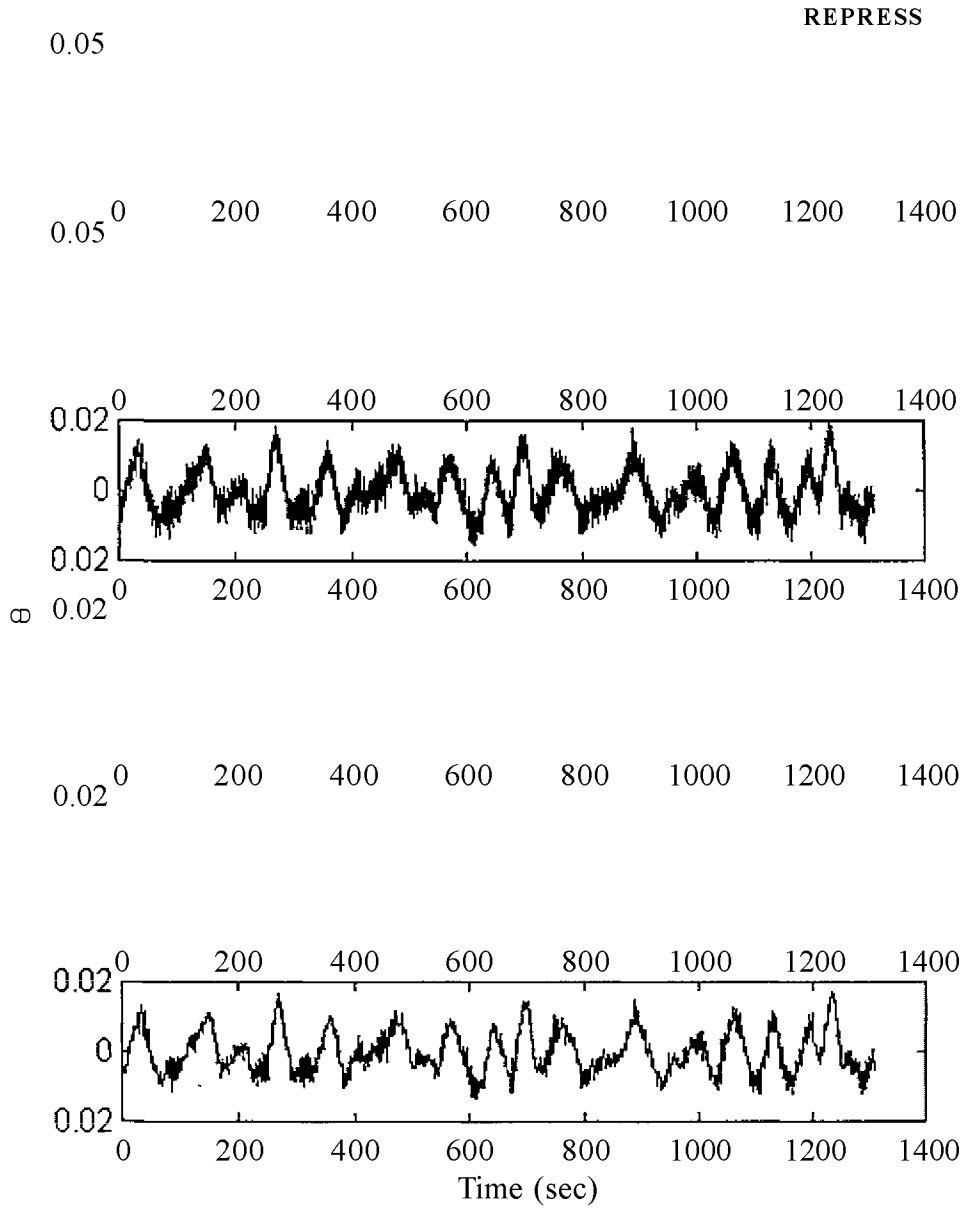

Figure 6.45. Multiresolution Analysis Results Showing the Approximation Reconstruct Signals of Pressure Sensor ID #07 (original signal at the top and 5th level at the bottom)

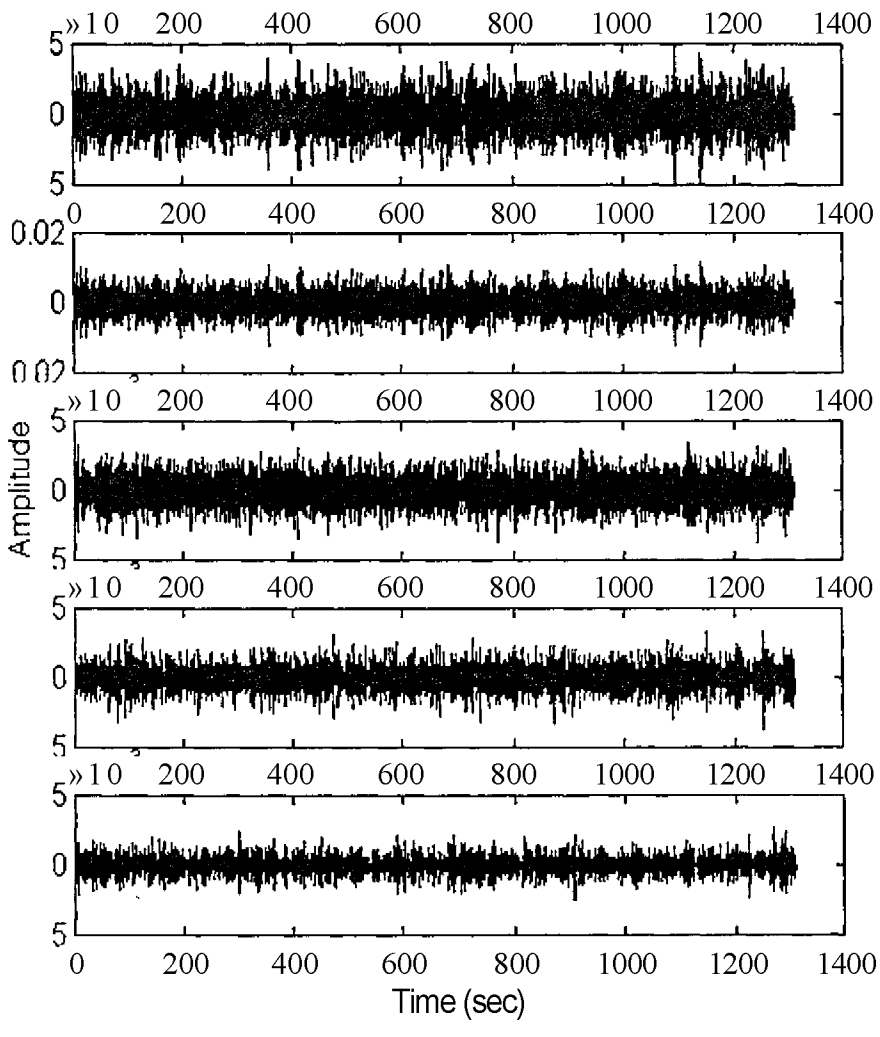

Figure 6.46. Multiresolution Analysis Results Showing the Detail Reconstruct Signals of Pressure Sensor ID #07 (original signal at the top and 5th level at the bottom)

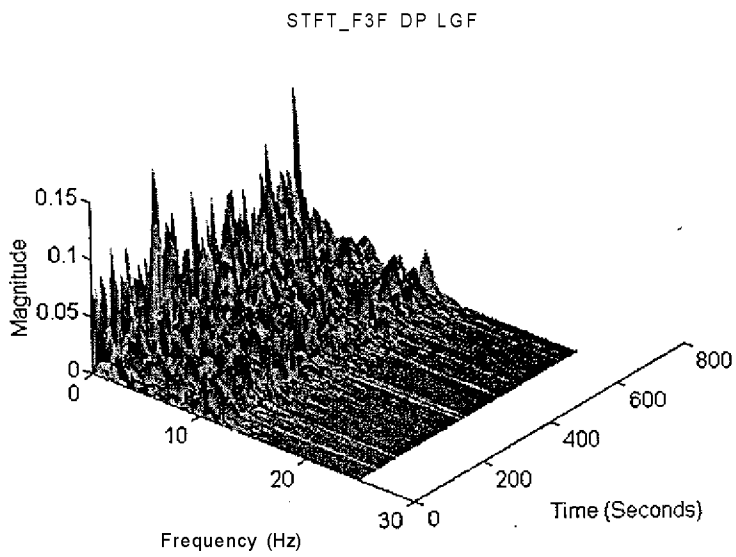

Figure 6.47. STFT 3-D Plot for the Flow Sensor Signal (ID #01)

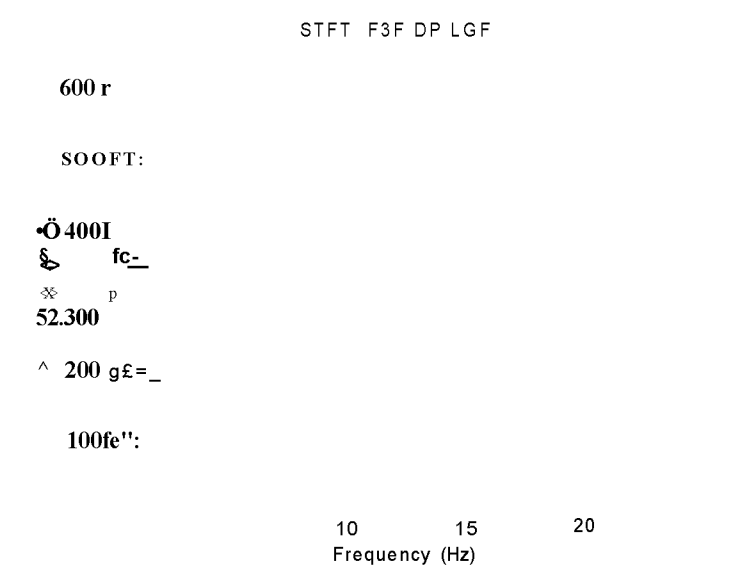

Figure 6.48. STFT Contour Plot for the Flow Sensor Signal (ID #01)

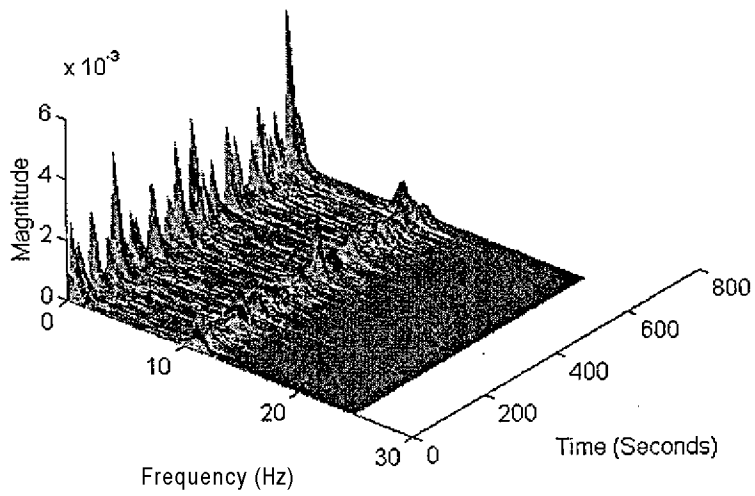

Figure 6.49. STFT 3-D Plot for the Pressure Sensor Signal (ID #07)

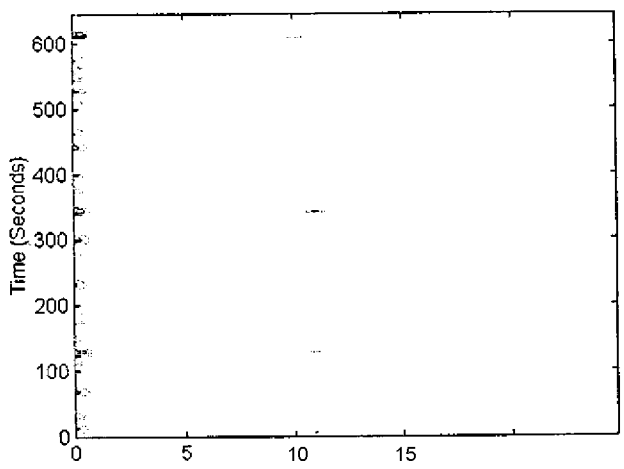

Figure 6.50. STFT Contour Plot for the Pressure Sensor Signal (ID #07)

and Figures 6.51-6.52 show the results for the pressure sensor at the sub-band level 2 (6.25 Hz -12.5 Hz). The main peak of the sensor response, which is around 10 Hz, is enhanced with this analysis method.

The primary goal of the present analysis is to define the frequencies at which most of the spikes and dips occur. In order to accomplish this objective, the discrete dilation wavelet transform was used to analyze the signals. The wavelet coefficients, which represent the abrupt changes in the signal during a period of time, can be visualized through 3-D and 2-D plots. The wavelet levels have a direct relationship with the frequency center of the spectrum at each sub-band level. These are defined in Table 6.5. Figures 6.53-6.56 show the 3-D and 2-D plots obtained using the DWT of the two selected sensors. Sensor ID #01 contains several abrupt changes (dips) in its signal, as shown in Figure 6.37. The wavelet power spectrum shows this behavior through the magnitude of peaks. The discrete wavelet transform spectrum reveals that most of the signal dips occur in the frequency range 3 -12 Hz , with the highest intensity peaks located close to 10 Hz. Sensor ID #07 (pressure) shows small changes in the wavelet coefficient magnitudes at a high frequency band (frequency range 10-12 Hz). The sensor plots give additional information in the low frequency band (<0.2 Hz) where some anomaly was identified.

The frequency information at a specific wavelet level is obtained for each signal. The 2-D plot localizes the time-frequency information, while the 3-D plot gives a better idea about the sensor response behavior before, during and after the occurrences of the events (spikes or dips in the signal).

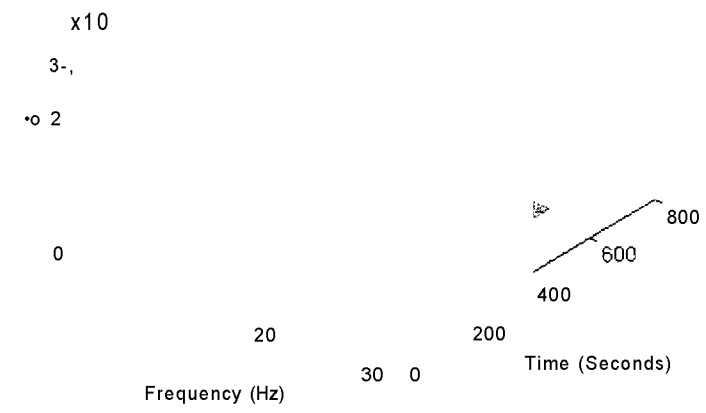

Figure 6.51. STFT and MRA 3-D Plot for the Pressure Sensor Signal (ID #07)

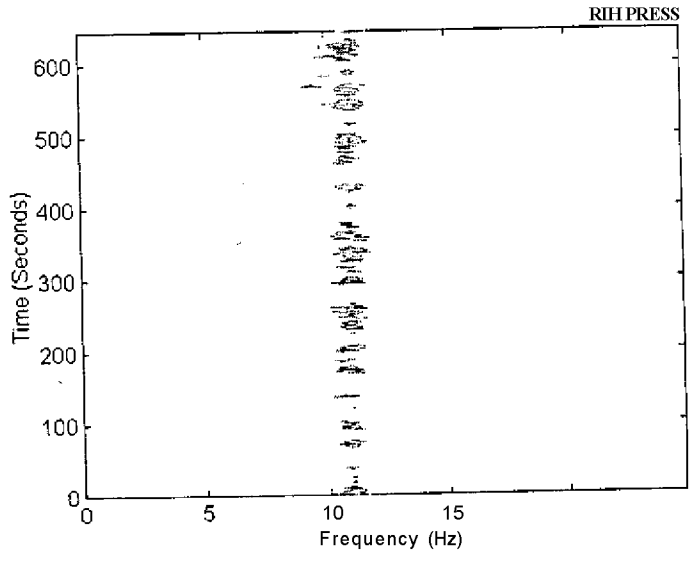

Figure 6.52. STFT and MRA Contour Plot for the Pressure Sensor Signal (ID #07)

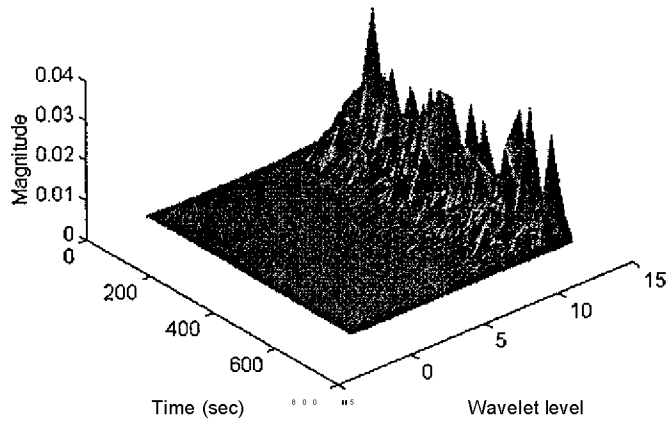

Figure 6.53. 3-D DWT Power Spectrum for the Flow Sensor Signal (ID #01) Using Daubechies 20 Wavelet

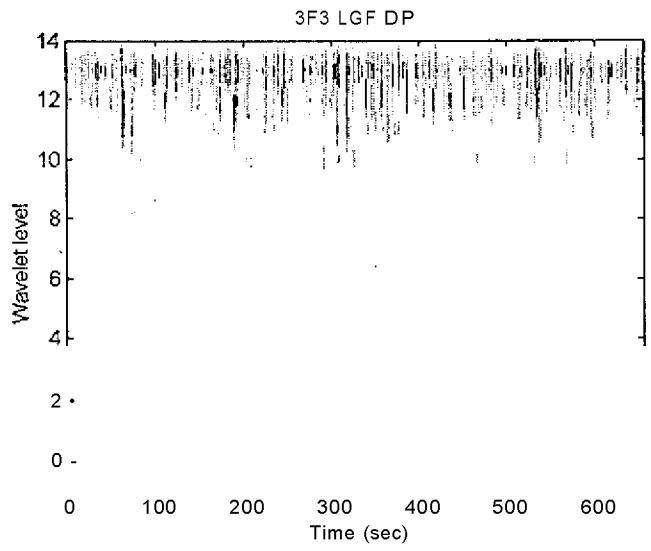

Figure 6.54.2-D DWT Power Spectrum for the Pressure Sensor Signal (ID #01) Using Daubechies 20 Wavelet

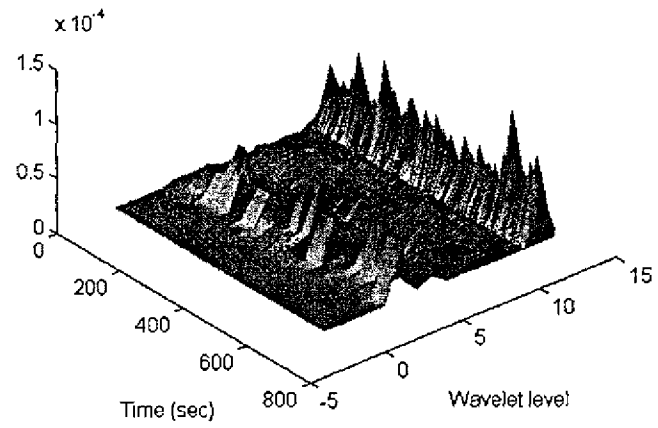

Figure 6.55. 3-D DWT Power Spectrum for the Pressure Sensor Signal (ID #07)

Using Daubechies 20 Wavelet

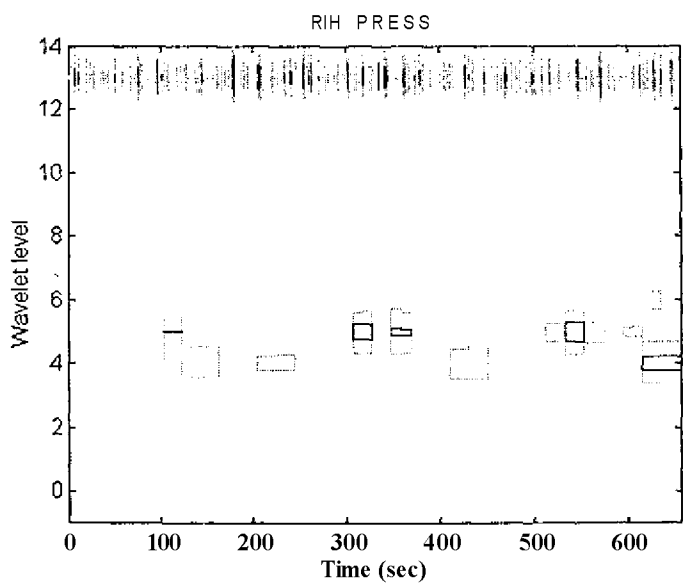

Figure 6.56. 2-D DWT Power Spectrum for the Pressure Sensor Signal (ID #07)

Using Daubechies 20 Wavelet

Appendix A presents the analysis performed for two others sensors. The STFT and DWT results are shown in Figures A17-A24 in Appendix A. Only the STFT and DWT power spectral plots are shown. The flow sensor shows that the highest intensities are located close to the main frequency peak of 12.5 Hz (Figures A19 and A20). There are also some spikes or dips of very low intensity in the low frequency band. The results obtained for the pressure sensor, Figures A23 and A24, reveal that most of the anomalies are located in the very low frequency band (<0.01 Hz). At this frequency band the intensity of the wavelet coefficients changes significantly during the measurement time period. The high frequency region also shows some low intensity peaks.

6.5 Conclusions

This chapter describes the signal analysis method using the discrete wavelet transform (DWT) and the short-time Fourier transform (STFT) applied to reactor coolant flow and pressure signals. The multiresolution analysis (MRA) was applied to obtain the reconstructed signal at different frequency sub-band levels for each selected sensor. The reconstructed signals were then used for different purposes. The statistical analysis (mean and RMS values) was performed in order to verify the existence of any trends in the signals. The combination of MRA and STFT provided a better insight into the non-stationary nature of the signals. The integration of these two techniques provides a more powerful information than the standard FFT technique. The DWT power spectrum (wavelet coefficients) offered additional information about the signal behavior in the

time-scale (or frequency) domain. This analysis was used to provide better information about the time evolution of the anomalies occurring during the monitoring process.

The data analysis performed in this chapter was divided into two parts. One described the fuel assembly vibration data, where only four sensors (two in-core detectors and two ex-core detectors) were used for the analysis. The other described the analysis of four selected sensor (flow and pressure) measurements.

The fuel assembly vibration analysis was performed using DWT and STFT. The results showed the potential of combining these techniques for monitoring and diagnosis of possible anomalies in the time-frequency domain. The MRA technique reconstructed the signal at different frequency sub-band levels. These signals were used for different purposes. The multichannel analysis at each sub-band level was very useful in getting better-localized correlation information between different signals. It also avoided any interference of undesired frequencies during the analysis (high frequency noise contamination, for example). The preliminary analysis of these fuel assembly vibration data showed that some anomalies were found at very low frequency bands.

The selected channels from Table 6.2 contain flow and pressure sensor measurements from a commercial PWR and they showed significant non-stationary characteristics. The analysis performed using DWT and STFT techniques was able to give a preliminary idea about the frequencies related to these anomalies in the signals. Better identification of anomalies was given by the wavelet power spectrum obtained by

the DWT coefficient plots. The time-scale (or frequency) domain provided an excellent visualization of the characteristics of the signals using 2-D and 3-D plots. Each peak in the wavelet power spectrum represented an abrupt change in the signal (dips or spikes). Through the wavelet level, one can identify the corresponding frequency center.

Excellent localized information was obtained using the MRA technique and the wavelet power spectrum. Reconstructed signals at different levels were analyzed using the DWT, and their coefficients were plotted (power spectrum) to show the behavior of the signals at the desired frequency sub-band.

CHAPTER 7

Summary, Conclusions and Recommendations for Future Work

7.1 Summary

The purpose of this dissertation is to develop a new approach for fault monitoring and diagnosis of nuclear power plant systems and rotating machinery. This approach integrates the short-time Fourier transform and the discrete wavelet transform techniques.

Chapters 2 and 3 describe the results of the literature review on time-scale and time-frequency data analysis methods. The discussion includes the basic theory of wavelet transform and short-time Fourier transform, multiresolution analysis and filter banks. Various advantages and disadvantages of applications of these methods to signal analysis are also discussed.

Implementation of the theory is discussed in Chapter 4. The data analysis system components are described in this chapter. A novel method is introduced using the wavelet multiresolution analysis (MRA), Fast Fourier Transform (FFT) and Short-time Fourier transform (STFT) to perform stationary and transient data analysis, in order to detect possible incipient faults. The MATLAB programs developed are also discussed. The improvements using the proposed ideas are highlighted.

Chapter 5 describes the rotating machinery experiment and the data analysis method. The stationary and non-stationary signals, measured in the rotor rig system at different load conditions, are analyzed using the wavelet transform and STFT. The results are discussed showing the advantages and disadvantages of using this method for condition monitoring activities.

Chapter 6 contains the description of the nuclear power plant experiment and the method used for processing several signals from in-core neutron detectors, pressure and flow sensors. The main concern of this research was to define whether the in-core signals presented non-stationary behavior, and to determine the frequency contents of the dips or spikes that appear in the flow and pressure sensor signals. Various in-core and ex-core neutron detectors, flow and pressure sensors were selected for the analysis. A discussion of the results follows, indicating the main advantages of using this novel method.

7.2 Conclusions

The major contribution of the dissertation is the development and implementation of an integrated approach for fault monitoring and diagnosis for a PWR and a rotating machinery system. The neutron detector and process signals were analyzed using the STFT and discrete wavelet transform (DWT) techniques, during stationary as well as transient conditions. The developed method combines the STFT and MRA techniques, which was applied to stationary data analysis from rotating machinery. The effectiveness of machinery condition monitoring was clearly demonstrated.

The methodology for processing the nonstationary data allows one to visually track the frequencies of interest. It provides efficient and localized information of the system behavior in time-scale or time-frequency domain. The use of MRA for signal decomposition and the STFT for subsequent spectral analysis is a novel approach for handling both stationary and transient signals. It also brings new insight into signal analysis. The data analysis results showed that a significant improvement in signal-to-noise ratio was obtained. A multi-channel wavelet analysis was introduced to obtain the most useful correlation functions in monitoring activities. It combines the features of the multiresolution analysis with the robustness of the FFT technique.

The application of the wavelet transform in signal analysis required a prior knowledge of the best basis wavelet function for the given application. This was necessary in order to guarantee the best match during the signal reconstruction process. This dissertation introduced a procedure to perform the optimal wavelet selection for each desired application based on the minimum entropy energy method.

The signals from the rotor test rig were analyzed using the techniques mentioned above, and the frequencies obtained through the analysis are presented in 2-D and 3-D plots. The discrete wavelet power spectrum was able to detect the time instants at which the rotor speed was changed and the STFT was able to track the non-stationary data to identify the time-dependent changes in the frequency components.

The combined STFT and MRA techniques were applied to the rotor signal analysis and incipient changes were detected during steady-state motor operations at different load conditions. These changes were indicative of possible anomalies in the system or in the sensors.

The results obtained from the analysis of the rotor rig experiment showed that the combination of STFT and MRA techniques gave a better performance than the standard FFT technique. Also, it was demonstrated that the STFT and DWT (2-D and 3-D power spectra) techniques were the best tools to be applied for non-stationary motor data analysis.

The application of wavelet and STFT transforms in nuclear power plant sensor signal analysis brought about a new insight to the sensor signal signature characterization when the system is under steady-state or transient operation. The method developed in this dissertation also pursued the detection and characterization of transients in a 515 MWe commercial PWR. The estimation of the frequency contents of the flow and pressure signals was made before, during and after the transients. The definition of time dependency and stationary characteristics of the fuel channel vibration and the estimation of the coherence and correlation functions between monitored sensor signals, were performed to reveal the dominant frequencies triggering the dips and spikes at the transmitter's output.

The fuel assembly vibration analysis was performed using the discrete wavelet and the STFT transforms, and the combined results from these techniques showed their potential for monitoring and diagnosis of possible sensor signal anomalies in the time-frequency domain.

The results obtained using MRA technique were also combined with the standard FFT tools and a multi-channel data analysis was performed. The results indicated that the MRA provided better results than the standard FFT analysis. The MRA allows the separation of the desired frequencies, avoiding the interference from high frequency components. The DWT power spectrum obtained during the fuel assembly vibration data analysis showed that some anomalies were found at very low frequency ranges (< 0.2 Hz).

The primary goal of the analysis of the flow and pressure sensor signals, as we mentioned before, was to define the frequencies where most of the spikes and dips that occur in the signals. To accomplish this objective, the discrete wavelet transform was used. The wavelet coefficients, that represent the transients, were visually portrayed in 2-D and 3-D plots. The peaks in the wavelet power spectrum were associated with the time-scale or time-frequency domains.

The results obtained from the flow sensor analysis lead one to conclude that most transient features are localized in the frequency range 3-12 Hz. The pressure sensor showed small anomalies at a frequency range 10-12 Hz and at low frequencies (<0.2 Hz).

The multiresolution analysis technique was also used in conjunction with the multi-channel data analysis to obtain the power spectrum, cross-power spectrum, coherence and phase of the signals. The advantage of using this method lies on the fact that the signals were analyzed in different frequency bands and the interference of some undesired frequencies were avoided.

In conclusion, the method introduced and developed in this dissertation brought a new insight into the stationary and non-stationary data analysis activities for monitoring the machinery and nuclear power plant systems.

7.3 Recommendations for Future Work

The research developed in this dissertation is a first step in establishing the implementation of a method for stationary and non-stationary signal analysis. Improvements are necessary in order to obtain better information from the process and sensors monitored. The following are a few suggestions for future research.

- The wavelet and STFT window (or basis) functions are still an open research topic. It is possible to use different basis functions to perform the computation in the transform coefficients and to obtain an improvement in the data analysis results. An example consists of extending the data analysis

by using the Wavelet Packet basis functions to verify the feasibility of any improvements in the results.

Reactor experiments and data analysis is crucial in order the evaluation of the effectiveness of the method developed in this dissertation. Transient experiments should be conducted using a reactor experimental facility, where several scenarios may be created during the experiments.

The signal correlation analysis in time-frequency or time-scale domain should provide valuable information about the system behavior. Cross-spectral and coherence analysis of non-stationary data are easily obtained numerically [45,74]. Further research should be done in order to extend this idea similar to those problems investigated in this dissertation where the signals have predominantly random in nature.

Development of a MRA fault monitoring system with the time-amplitude of the reconstructed signals and their statistical information as monitored variable [98].

Development of a hybrid system using Artificial Neural Network (ANN) and MRA techniques to perform pattern analysis of the reconstructed signal at each sub-band level. This method should be able to characterize the signatures of the system at a variety of conditions, detecting possible anomalies and identifying the pattern changes of the time-scale maps [75-79]. The main purpose of this hybrid system would be to identify the transients in early stages of evolution.

- The diagnosis of incipient process variations is still a challenge. The MRA technique could be associated with artificial intelligence techniques (ANN and fuzzy logic) to perform pattern classification and to predict the transition from stationary to non-stationary state, if it occurs, during the process monitoring [32, 93].

LIST OF REFERENCES

LIST OF REFERENCES

[1] Proceedings of a Symposium on Nuclear Reactor Surveillance and Diagnostics, SMORN VI, Gatlinburg, TN, May 19-24,1991.

[2] Symposium on Nuclear Reactor Surveillance and Diagnostics, SMORN VII, Avingnon, France, June 19-23,1995.

[3] G. L. Swaggerty and B. R. Upadhyaya "Surveillance and Analysis of Multivariate Processing Using Digital Signal Processing," Final Report, The University of Tennessee, MCEC/UTNE/93-01, December 1993.

[4] D. Gabor, "Theory of Communication," J. IEE, Vol. 93, No. Ill, pp. 429-457, London, November 1946.

[5] S. Qian and D. Chen, "The Joint Time-Frequency Analysis - Methods and Applications," Prentice-Hall, Englewood Cliffs, NJ, 1996.

[6] J. K. Mattingly, "Time-Frequency Analysis of Nonstationary Signals," M. S. Thesis, The University of Tennessee, May 1995.

[7] C. L. Bentley, M. E. Dunn, J. K. Mattingly and D. Casada, "Time-Frequency Analysis of Electric Motors," Proceedings ANS Trans., Vol. 73, pp. 310-311, ANS Winter Meeting, San Francisco, CA, Oct. 29-Nov. 02,1995.

[8] B. Saminy and G. Rizzoni, "Mechanical Signature Analysis Using Time-Frequency: Application to Internal Combustion Engine Knock Detection," Proceedings of the IEEE, Vol. 84, No. 9, pp. 1330-1343, September 1996.

[9] L. Cohen, "Time-Frequency Analysis," Prentice-Hall, Englewood Cliffs, NJ, 1995.

[10] R. O. Wells Jr., "Recent Advances in Wavelet Technology," Computational Mathematics Laboratory, Department of Mathematics, Rice University, 1994.

[11] I. Daubechies, "Ten Lectures on Wavelets," Philadelphia, PA: Society for Industrial and Applied Mathematics, 1992.

[12] D. E. Newland, "An Introduction to Random Vibrations, Spectral & Wavelet Analysis," Third Edition, Scientific and Technical, 1993.

[13] G. Kaiser, "A Friendly Guide to Wavelets," Birkhauser, Boston, MA, 1994.

[14] C. K. Chui, "An Introduction to Wavelets," Academic Press, Boston, 1992.

[15] C. K. Chui, L. Monteforco and L. Puccio, "Wavelet Theory, Algorithms and Applications," Vol. 5, Academic Press, Boston, 1994.

[16] G. Strang and T. Nguyen, "Wavelet and Filter Banks," Wellesley-Cambridge Press, Wellesley, MA, 1996.

[17] T. F. Tibhals, "On the Use of Wavelets as an Alternative to Fourier Analysis for Transient Dynamic Data," M. S. Thesis, The University of Tennessee, August 1994.

[18] B. B. Hubbard, "The World According to Wavelets," A. K. Peters Ltd., 1996.

[19] D. E. Newland, "Wavelet Analysis of Vibration, Part I: Theory," Journal of Vibration and Acoustics, 116 (4), pp. 409-415, October 1994.

D. E. Newland, "Wavelet Analysis of Vibration Part II: Wavelet Maps," Journal of Vibration and Acoustics, 116 (4), pp. 417-425, October 1994.

O. Rioul and M. Vetterli, "Wavelets and Signal Processing," IEEE Signal Processing Magazine, 8 (4), pp. 14-38, October 1991.

L. G. Weiss, "Wavelets and Wideband Correlation Processing," IEEE Signal Processing Magazine, pp. 13-32, January 1994.

K. Hayashi; Y. Shinohura and E. Türkcan, "A Method of Nonstationary Noise Analysis Using Instantaneous AR Spectrum and its Application to Borssele Reactor Noise Analysis," Progress in Nuclear Energy, Vol.21, pp.707-716, 1988.

M. Kitamura and E. Türkcan, "Analysis of Time-Varying Characteristics of Signals from Borssele Reactor," Progress in Nuclear Energy, Vol. 15, pp. 853-861, 1985.

Ö. Ciftcioglu and E. Türkcan, "Transient Detection by Wavelet Transform in Plant Monitoring," Symposium on Nuclear Reactor Surveillance and Diagnostic Proceedings, SMORN VII, Avingnon, France, June 19-23, 1995.

E. Türkcan and Ö. Ciftcioglu, "Multiresolution Pattern Analysis for Neural Network Training," Symposium on Nuclear Reactor Surveillance and Diagnostic Proceedings, SMORN VII, Avingnon, France, June 19-23,1995.

Ö. Ciftcioglu and E. Türkcan," "Wavelets" Understand Neural Networks," ECN-RX-94-031, May 1994.

R. Polikar, "The Wavelet Tutorial,"
http://www.public.iastate.edu/~rpolikar/WAVELETS, June 1996.

F. Hlawatscch and G. F. Bourdreaux-Bartels, "Linear and Quadratic Time-Frequency Signal Representations," IEEE Signal Processing Magazine, pp. 21-67, April 1992.

R. Burnett; J. F., Watson and S. Elder, "The Application ofModern Signal Processing Techniques to Rotor Fault Detection and Location Within Three Phase Induction Motors," IEEE Instrumentation and Measurement Technology Conference, Waltham, MA, April 23-36, 1995.

S. Mallat, "A Theory for Multi-resolution Signal Decomposition: The Wavelet Representation," IEEE Transaction on Pattern Analysis and Machine Intelligence, Vol. 11, No. 7, 674-693, July 1989.

M. Marseguerra, S. Minoggio, A. Rossi and E. Zio, "Neural Networks Prediction and Fault Diagnosis Applied to Stationary and Nonstationary ARMA Modeled Time Series," Progress in Nuclear Energy, Vol. 27, No. 1, pp. 25-36, 1992.

M. Marseguerra et al. "Artificial Neural Networks Applied to Multiple Signals in Nuclear Power Plants," Progress in Nuclear Energy, Vol. 27, No. 4, pp. 297-304, 1992.

R. E. Uhrig, "Research Projects," http://www.engr.edu/dept/nuclear/projreu.html

D. R. Baughman and Y. A. Liu, "Neural Networks in Bioprocessing and Chemical Engineering," Academic Press, 1995.

O. Glockler, Personal Communication Nov. 1995.

W. Sweldens and R. Piessens, "Wavelet Sampling Techniques," Joint Statistical Meeting, San Francisco, CA, August 1993.

L. Hudgins, C.A. Friehe and M.E. Mayer, "Wavelet Transform and Atmospheric Turbulence," Physical Review Letter, Vol. 71, No. 20, Nov. 1993.

M. Novaes, "Multiresolution Signal Cross-Correlation," Ph.D. Dissertation, The University of Texas, Denton, Texas, Dec. 1994.

J.F.G. Freitas, H.L. Stevens, A.P. Gaylard, J.N Ridley and C.F. Landy, "Identification of Vibrating Structures and Fault Detection Using Neural Networks," Proceeding of the International Conference of Neural Networks, Washington D.C., June 3-6, 1996.

C.H. Chen and G.G. Lee, "Multiresolution Wavelet Analysis Based Feature Extraction for Neural Network Classification," Proceeding of the International Conference on Neural Networks, Washington D.C., June 3-6, 1996.

T.Brotherton, T. Pollard and D. Jones, "Application of Time-Frequency and Time-Scale Representations to Fault Detection and Classification," Proceedings of IEEE-SP International Symposium on Time-Frequency and Time-Scale Analysis, Victoria, B.C., Canada, Oct. 4-6, 1992.

S. Haykin, "Neural Networks Expand SP's Horizons," IEEE Signal Processing Magazine, Vol. 13, No.2, March 1996.

H. Zengjia, Z. Jiyuan, M. Qingfeng and N. Yiming, "Wavelet Transform in Tandem with Autoregressive Technique for Monitoring and Diagnosis of Machinery," 6th International Conference on Condition Monitoring and Diagnostic Engineering Management, New Delhi, September, 1994.

S. Santoso and E. J. Powers, "Development of a Linear Time-Scale Coherence Spectrum," in Wavelet Applications in Signal and Image Processing IV, M. A. Unser, A. Aldroubi, A. F. Laine (Editors), Proc. SPIE 2825, pp. 992-1002, 1996.

J. H. Karspersen and L. Hudgins, "Wavelet Quadrature Methods for Detecting Coherent Structures in Fluid Turbulence," in Wavelet Applications in Signal and Image Processing IV, Michael A. Unser, Akram Aldroubi, Andrew F. Laine, Editors, Proc. SPIE 2825, pp.540-550,1996.

R. E. Unrig, "Random Noise Techniques in Nuclear Reactor System", The Ronald Press Company, N.Y., 1970.

M. Misiti, Y. Misiti, G. Oppenheim and J. M. Poggi, "Wavelet Toolbox User's Guide," The MathWorks, Inc., March 1996

O. Glockler and M. V. Tullet, "Reactor Noise Measurements at Pickering-B Nuclear Generating Station of Ontario Hydro," Proceedings of the 9th. Power Plant dynamics, Control & Testing Symposium, Knoxville, Tennessee, May 24-25,1995.

O. Glockler, D. Cooker, G. Czuppon and K. Kapoor, "Reactor Noise Applications in Ontario Hydro: A Statistical Technique Used for Systems Surveillance and Condition Assessment," in Proceedings of the Maintenance and Reliability Conference - MARCON 97, Knoxville, Tennessee, Vol.1, pp. 13.01-13.17, May, 1997.

M. A. Kohls, "A Fuzzy-Wavelet Approach to Medical Image Fusion," M. S. Thesis, The University of Tennessee, August 1997.

L. N. Graham, "Coincidence Image Fusion Using the Discrete Wavelet Transform," M. S. Thesis, The University of Alabama at Huntsville, 1994.

[53] E. V. Hoeskstra, "Multiscale Analysis of Seismic Data by Wavelet Transform," M. S. Thesis, Delft University of Technology, July 1996.

[54] J. P. Chang and N. Z. Cho, "Wavelet Transform Decomposition and Denoising for Reactor Monitoring," Proceedings ANS Trans., Vol. 76, pp. 345-346, ANS Winter Meeting, Florida, June 1-5,1997.

[55] M. Akay, "Wavelet Applications in Medicine," IEEE Spectrum 50-56, May 1997.

[56] H. Li, B. S. Manjunath and S. K. Mitra, "Multi-Sensor Image Fusion Using the Wavelet Transform," Proc. IEEE, pp. 51-55, 1994.

[57] B. Vidakovic and P. Miiller, "Wavelets for Kids," ftp://ftp.isds.duke.edu/pubAJser/brani/papers/.

[58] A. Graps, "An Introduction to Wavelets," http://www.best.com/~agraps/agraps.html.

[59] S. Mallat, "A Theory for Multiresolution Signal Decomposition: The Wavelet Representations" IEEE Transactions on Pattern Analysis and Machine Intelligence, Vol. 11, No. 7, pp. 674-693, July 1989.

[60] L. H. Tsoukalas and R. E. Uhrig, "Fuzzy and Neural Approaches in Engineering," John Wiley & Sons, Inc., New York, NY, 1997.

[61] N. Gulley and J. -S. R. Jang, "Fuzzy Logic Toolbox," The MathWorks, Inc., Natick, MA, 1995.

D. N. S. Permann," Wavelet Fast Fourier Transform (WFFT) Analysis of a Milivolt Signal for a Transient Oscillating Chemical Reaction," J. Phys. Chem., Vol. 97, pp. 12670-12673,1993

C. Chiann and P. Morettin, "A Wavelet Analysis for Stationary Processes," http://www.ime.usp.br/~pam/.

A. Lucifredi and M. Rossi, "Advanced Signal Processing Techniques For Plant Monitoring, Diagnosis and Maintenance," in Proceedings of the Maintenance and Reliability Conference - MARCON 97, Knoxville, Tennessee, pp. 17.01-17.06, May, 1997.

A. A. Da Silva and B. R. Upadhyaya, "Rotating Machinery Monitoring and Diagnosis Using Short-time Fourier transform and Wavelet Techniques," in Proceedings of the Maintenance and Reliability Conference - MARCON 97, Knoxville, Tennessee, Vol. 1,pp. 14.01-14.015, May, 1997.

J. Reifman, "Survey of Artificial Intelligence Methods for Detection and Identification of Component Faults in Nuclear Power Plants," Nuclear Technology, Vol. 119, pp. 76-97, July 1997.

C. T. Nguyen and K. F. Gong, "Performance Analysis of a Wavelet-based Hybrid Neurosystem for Signal Classification," in Wavelet Applications in Signal and Image Processing IV, Michael A. Unser, Akram Aldroubi, Andrew F. Laine, Editors, Proc. SPIE 2825, pp. 982-991,1996.

M. Farge, "Wavelet Transforms and Their Applications to Turbulence," Annual Rev. Fluid Mech., Vol. 24, pp. 395-457,1992.

[69] W. J. Wang, and P. D. McFadden, "Application of Wavelet to gearbox Vibration Signals for Fault Detection," J. Sound Vibration. Vol. 192(5), pp. 927-939, May 23, 1996.

[70] H. Zhengjia, H., Z. Jiyuan, M. Qingfen, N. Yiming, "Wavelet Transform in Tandem with Autoregressive Technique for Monitoring and Diagnosis of Machinery," Proceedings of Condition Monitoring and Diagnosis Engineering Management-COMADEN 94, pp. 458-465, September 26-29, 1994.

[71] M. A. Cody, "The Fast Wavelet Transform- Beyond Fourier Transforms," Dr. Dobb's Journal, pp. 16-26, April 1992.

[72] J. Altmann and J. Mathew," Wavelets: An Emerging Force in Condition Monitoring," MCM Research Bulletin, Vol. 7, pp. 9.1-9.6, 1995.

[73] J. Driesen, T. Van Craenenbroeck, R. Reekmans and D. Van Dommelen, "Analyzing Time-Varying Power System Harmonics Using Wavelet Transform," in Proceedings of IEEE Instrumentation and Measurement Technology Conference, Brussels, Belgium, pp. 474-479, June 4-6, 1996.

[74] L. B. White and B. Boashash, "Time-Frequency Coherence - A Theoretical Basis for Cross Spectral Analysis of Non-Stationary Signals," in Proceeding of IASTED International Symposium on Signal Processing and Its Applications, ISSPA 87, Brisbane, Australia, pp. 18-23, August 24-28, 1987.

[75] H. Krim, K. Drouichet, and J. C. Posquet," Multiscale Detection of Nonstationary Signal," Proceeding of the IEEE-SP International Symposium on Time-Frequency and Time-Scale Analysis, Victoria, BC, Canada, October 4-6, 1992.

[76] M. A. Cody, " A Wavelet Analyzer," Dr. Dobb's Journal, pp.44-54, 1993.

[77] C. H. Chen and G. G. Lee, "Multiresolution Wavelet Analysis Based Feature Extraction for Neural Network Classification," Proceedings of the International Conference on Neural Networks ICNN, Washington, DC, pp.1416-1421, June 3-6,1996.

[78] D. J. Chen and W. J. Wang, "Pattern Changes of Time-Shifted Vibration Signals on Wavelet Time-Scale Maps," Proceedings of the Design Engineering Technical Conference, The 15th Biennial Conference on Mechanical Vibration Noise, Boston, MA, September 17-20,1995.

[79] K. R. Castlemay, "Digital Image Processing," Prentice-Hall, Englewood Cliffs, NJ, 1996.

[80] K. Farry, "MatLab Functions for Spectral Analysis." http://tommy.jsc.nasa.gov/~farry/ml_sum.html.

[81] J. Lewalle, "Tutorial on Wavelet analysis of Experimental Data," http://www.mame.syr.edu/faculty/lewalle/tutor/tutor.html.

[82] AES Papers, http://cnmat.cnmat.berkeley, edu/~alan/MS-html/MSv2.html.

[83] R. R. Coifman and O. V. Wickerhauser, "Entropy-Based Algorithms for Best Basis Selection," IEEE Transactions on Information Theory, Vol.38 (2), pp. 713-718, 1992.

[84] B. Jawerth and W. Sweldens, "An Overview of Wavelet Multiresolution Analysis," Technical Report, University of South Carolina, 1993.

[85] C. A. Lerch and R. H. Lyon, "A Harmonic Tracking Technique for Recovery of Gear Motion from Non-Stationary Vibration Signals," Proceedings of the Design

Engineering Technical Conference, The 15th Biennial Conference on Mechanical Vibration and Noise, Boston, MA, September 17-20, 1995.

S. Seilbold, "Fault Detection and Isolation Procedures Contribute to Damage of Rotating Machinery," Proceedings of the Design Engineering Technical Conference, The 15th Biennial Conference on Mechanical Vibration and Noise, Boston, MA, September 17-20, 1995.

A. Soom and D. E. Newland," Transients Signal Processing and Wavelets in Vibrations and Acoustics," Proceedings of the Design Engineering Technical Conference, The 15th Biennial Conference on Mechanical Vibration and Noise, Boston, MA, September 17-20, 1995.

D. E. Newland, "Progress in the Application of Wavelet Theory to Vibration Analysis," Proceedings of the Design Engineering Technical Conference, The 15th Biennial Conference on Mechanical Vibration and Noise, Boston, MA, September 17-20, 1995.

M. Perry, "A Correlation Approach to Time-Frequency Representations," Proceedings of the IEEE-SP International Symposium on Time-Frequency and Time-Scale Analysis. Victoria, BC, Canada, October 4-6, 1992.

K. R. Castleman, "Image Processing - Digital Techniques," Prentice-Hall, Englewood Cliffs. New Jersey, 1996.

S. Mallat and W. L. Hwang, "Singularity Detection and Processing with Wavelet," Technical Report, Courant Institute of Mathematical Sciences, New York University, New York, May 1991.

[92] E. P. Serrano and M. A. Fabio, "Application of the Wavelet Transform to Acoustic Emission Signals Processing," IEEE Transactions on Signal Processing, Vol. 44, No. 5, pp. 1270-1275, May 1995.

[93] B. Tak, "A New Method for Forecasting Stock Prices Using Artificial Neural Network and Wavelet Theory," Ph.D. Dissertation, University of Pennsylvania, 1995.

[94] M. Holschneider, "Wavelets - An Analysis Tool," Clarendon Press, Oxford, 1995.

[95] M. A. Cody, "The Wavelet Packet Transform - Extending the Wavelet Transform," Dr. Dobb's Journal, pp. 44-54, April 1994.

[96] G. Andria et al., "Application of Wigner-Ville Distribution to Measurements of Transient Signals," Proceeding of the IEEE Instrumentation and Measurement Technology Conference, 1993.

[97] G. Strang, "Wavelets," American Scientist, Vol.82, pp. 250-255, May-June, 1994.

[98] J. L. Schmaltez and J. F. Johnson, "Pattern Recognition Based on Fuzzy Logic," Proceedings of the IEEE Instruments and Measurements Technology Conference, Irvine, Orange County, May 18-20, 1993.

[99] L. Cai et al. "Separation Between Vibratory Modes in Internal Structure Monitoring Domain," Symposium on Nuclear Reactor Surveillance and Diagnostic Proceedings, SMORN VII, Avingnon, France, June 19-23, 1995.

[100] D. Belluzzo, M. Marseguerra and S. Tarantola, "Wavelet Analysis of Fast, Short Lived Transients with Noise," Symposium on Nuclear Reactor Surveillance and Diagnostic Proceedings, SMORN VII, Avingnon, France, June 19-23,1995.

[101] S. D. Steams and R. A. David, "Signal Algorithms in MATLAB," Prentice-Hall, Englewood Cliffs., NJ, 1996.

[102] M. Glumac, "Automated Diagnosis of Motor-Operated Valves Using Motor Power Signature Analysis," M. S. Thesis, The University of Tennessee, Knoxville, TN, May 1996.

[103] B. R. Upadhyaya, W. Hooper, W. Yan, M. M. Behravesh and G. Henry, "Advances in Information Processing in Eddy Current Diagnosis of Steam Generator Tubing," in Proceedings of the Maintenance and Reliability Conference - MARCON 97, Knoxville, Tennessee, Vol. 2, pp. 85.01-85.13, May, 1997.

[104] V. Wowk, "Machinery Vibration,"Mc Graw-Hill, New York,1991.

[105] C. J. Pank and N. Z. Chao, "Wavelet Transform Decomposition and Denoising for Reactor Monitoring," ANS Transactions, Vol.76, pp. 345-347, Orlando, June, 1997.

[106] N. Z. Chao and C. J. Pank, "Wavelet Theory for Solution of Neutron Diffusion Equation," Nucl. Sci. Eng.,Vol. 124, p. 417,1996.

APPENDICES

APPENDIX A

Additional Results of Reactor Data Analysis

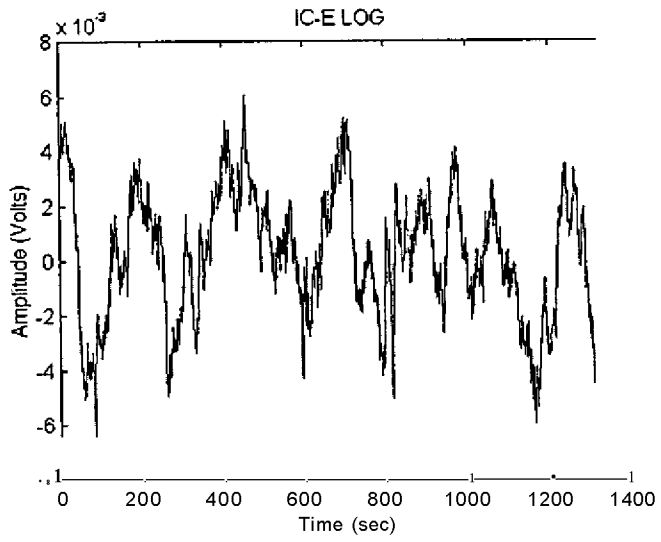

Figure A1. Time-Amplitude Plot for the Ex-Core Neutron Detector Signal (ID #14)

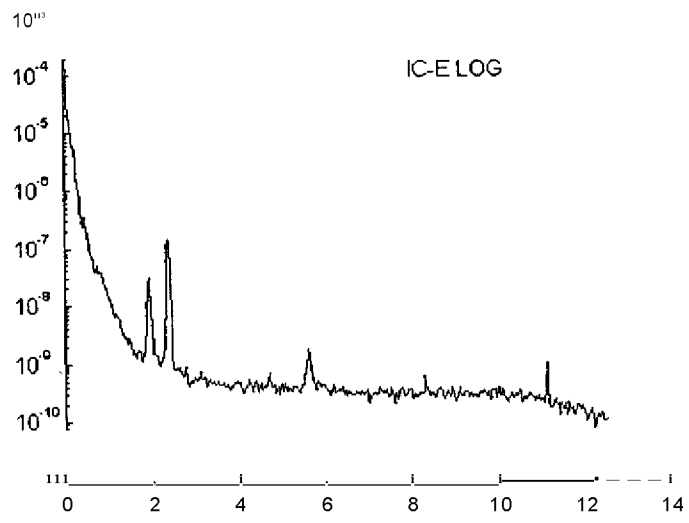

Figure A2, Power Spectrum Density Plot for the Ex-Core Neutron Detector Signal (ID #14)

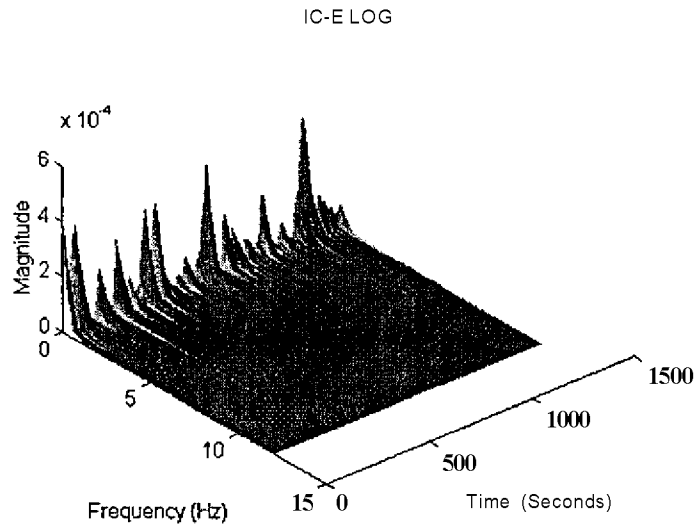

Figure A3. STFT 3-D Power Spectrum Density Plot for the Ex-Core Neutron Detector Signal (ID #14)

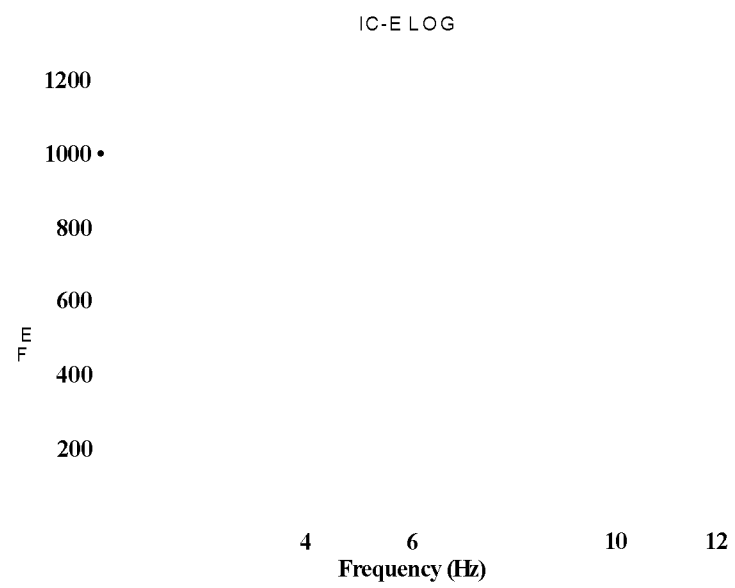

Figure A4. STFT 2-D Power Spectrum Density Plot for the Ex-Core Neutron Detector Signal (ID #14)

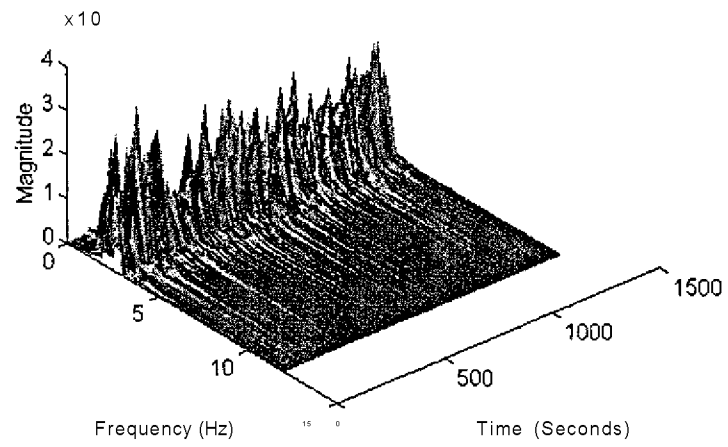

Figure A5. STFT & MRA 3 D Power Spectrum Density Plot for Detail Level 3 Ex-Core Neutron Detector Signal (ID #14)

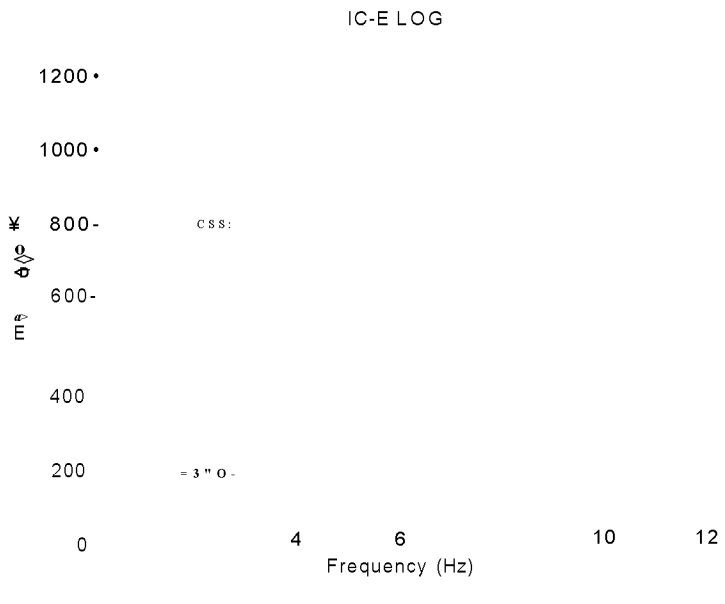

Figure A6. STFT & MRA 2-D Power Spectrum Density Plot for Detail Level 3 Ex-Core Neutron Detector Signal (ID #14)

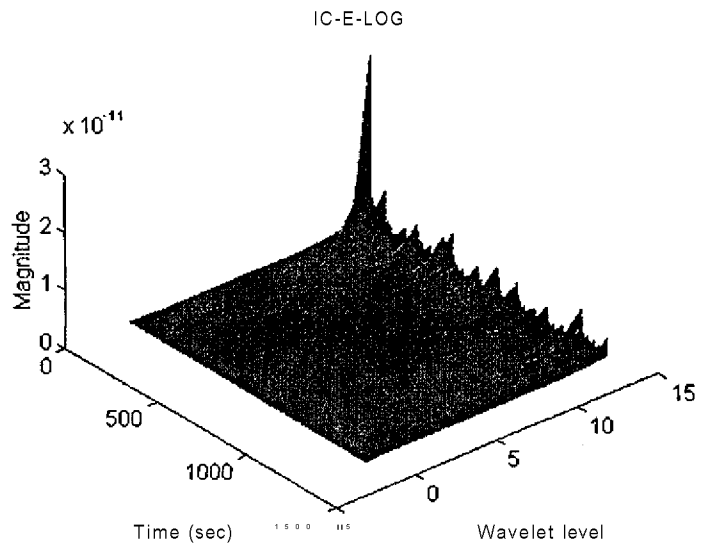

Figure A7. DWT 3-D Power Spectrum Density Plot for Detail Level 3 Ex-Core Neutron Detector Signal (ID #14)

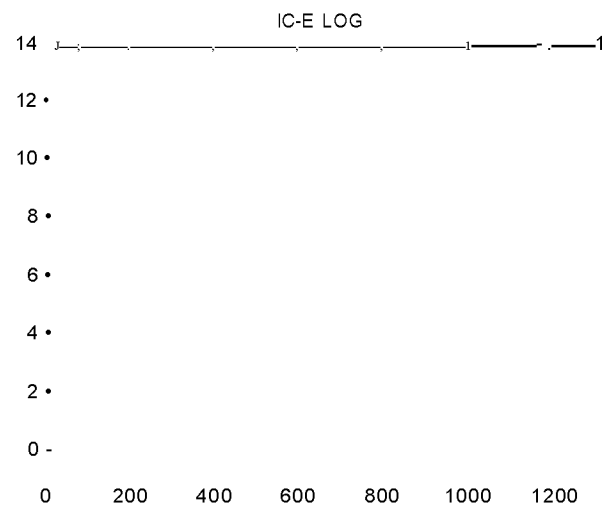

Figure A8. DWT 2-D Power Spectrum Density Plot for Detail Level 3 Ex-Core Neutron Detector Signal (ID #14)

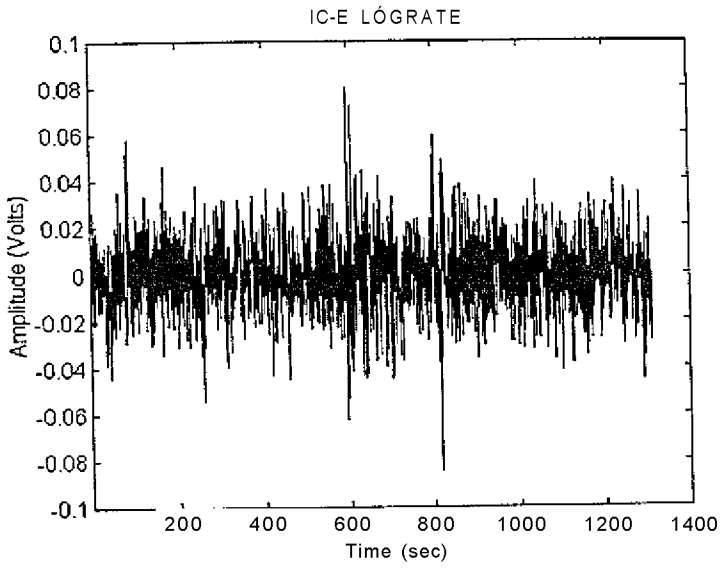

Figure A9. Time-Amplitude Plot for the Ex-Core Neutron Detector Signal (ID #15)

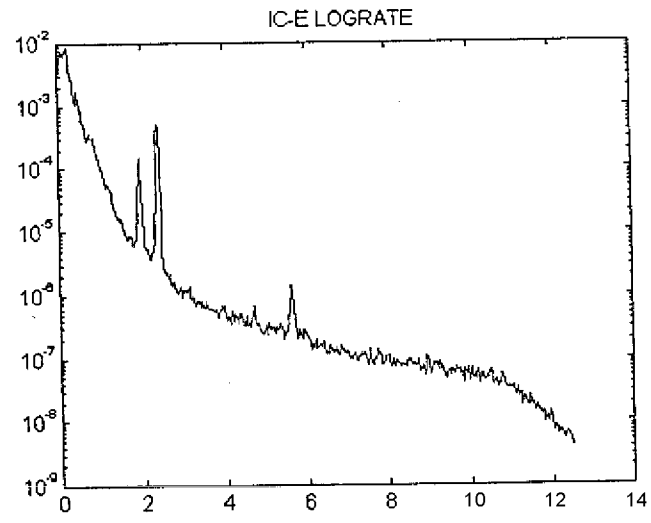

Figure A10. Power Spectrum Density Plot for the Ex-Core Neutron Detector Signal (ID #15)

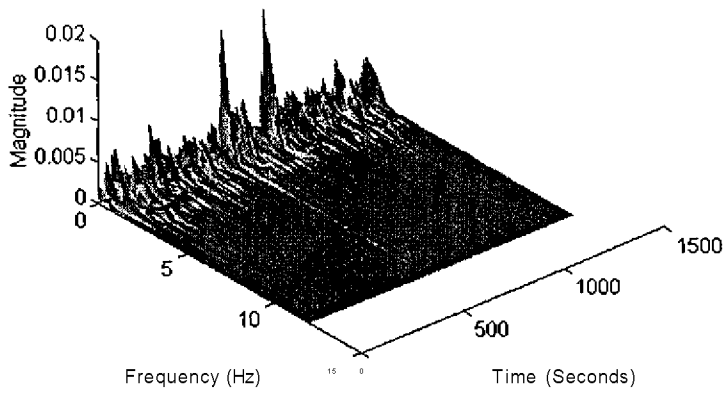

Figure A11. STFT 3-D Power Spectrum Density Plot for the Ex-Core Neutron Detector Signal (ID #15)

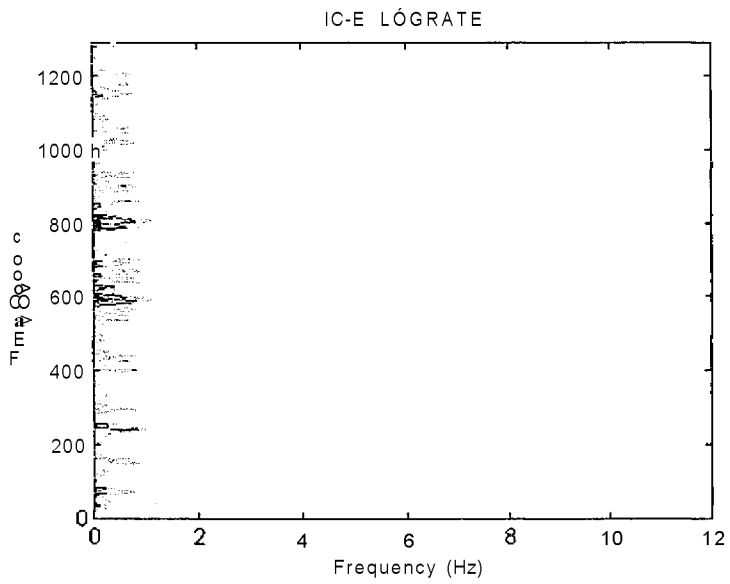

Figure A12. STFT 2-D Power Spectrum Density Plot for the Ex-Core Neutron Detector Signal (ID #15)

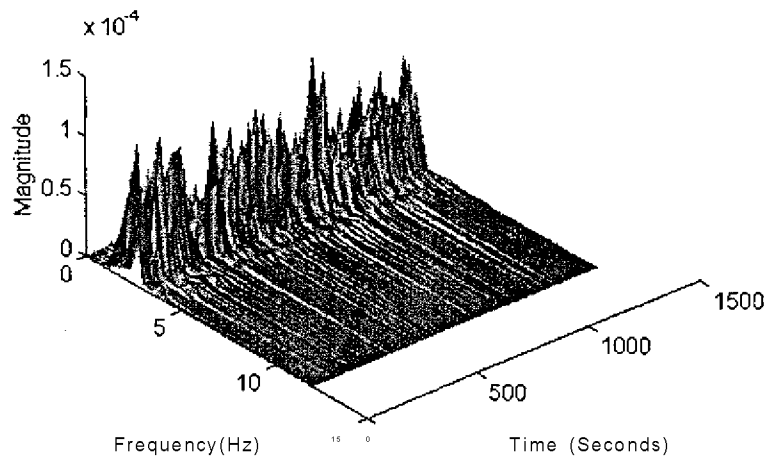

Figure A13. STFT & MRA 3 D Power Spectrum Density Plot for Detail Level 3 Ex-Core Neutron Detector Signal (ID #15)

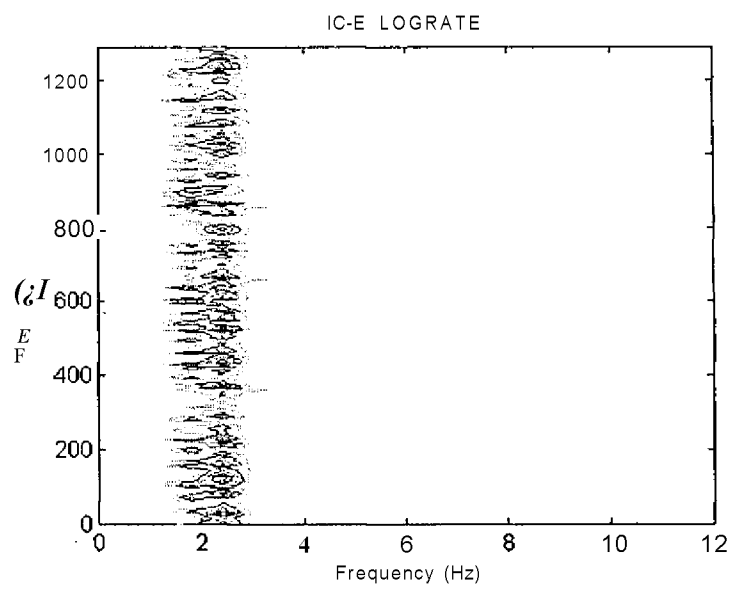

Figure A14. STFT & MRA 2-D Plot for Detail Level 3 Ex-Core Neutron Detector Signal (TD #15)

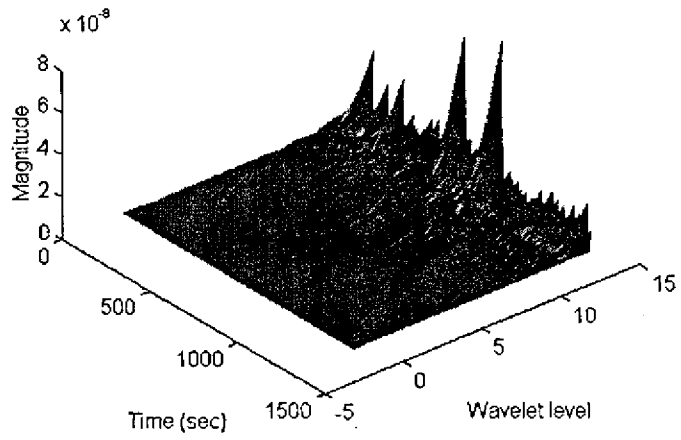

Figure A15. DWT 3-D Power Spectrum Density Plot for Ex-Core Neutron Detector Signal (ID #15)

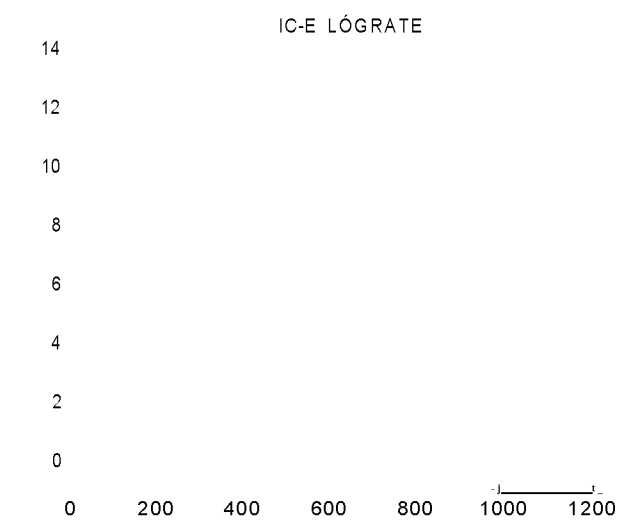

Figure A16. DWT 2-D Power Spectrum Density Plot for Ex-Core Neutron Detector Signal (ID #15)

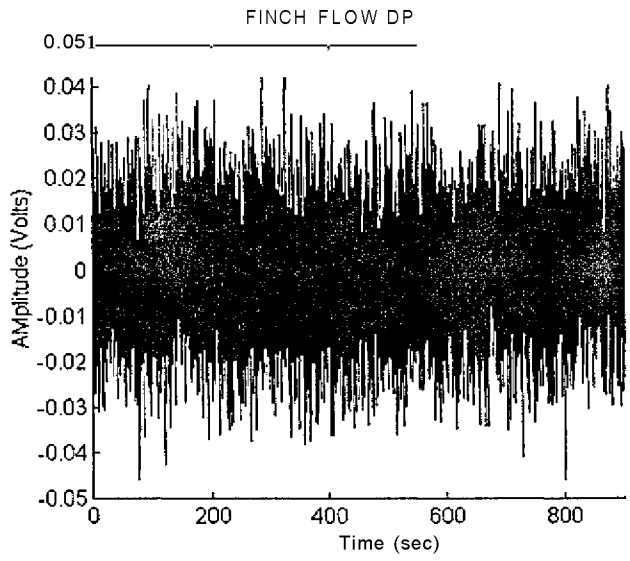

Figure A17. Time-Amplitude Plot for Flow Signal (ID #02)

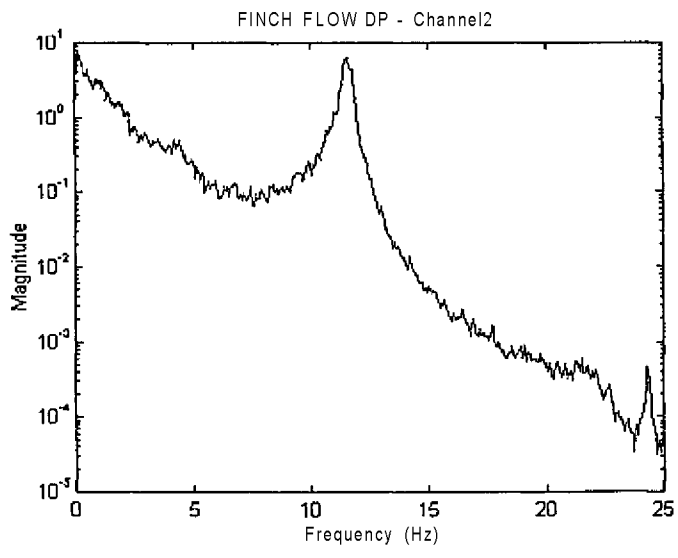

Figure A18. Power Spectrum Density Plot for Flow Signal (ID #02)

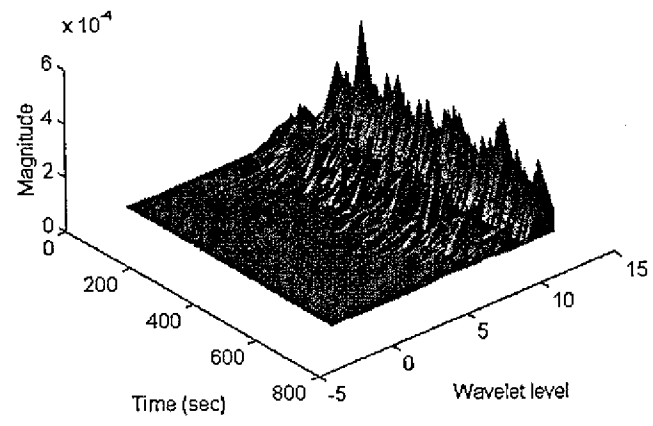

Figure A19. DWT 3-D Power Spectrum Density Plot for Flow Signal (ID #02)

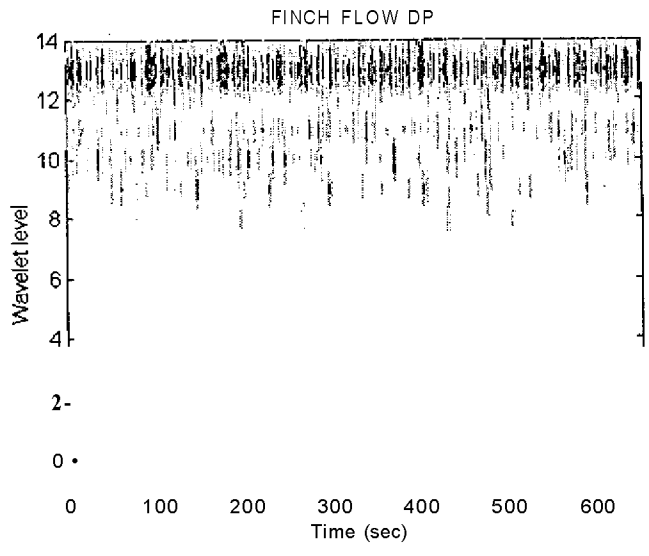

Figure A20. DWT 2-D Power Spectrum Density Plot for Flow Signal (ID#02)

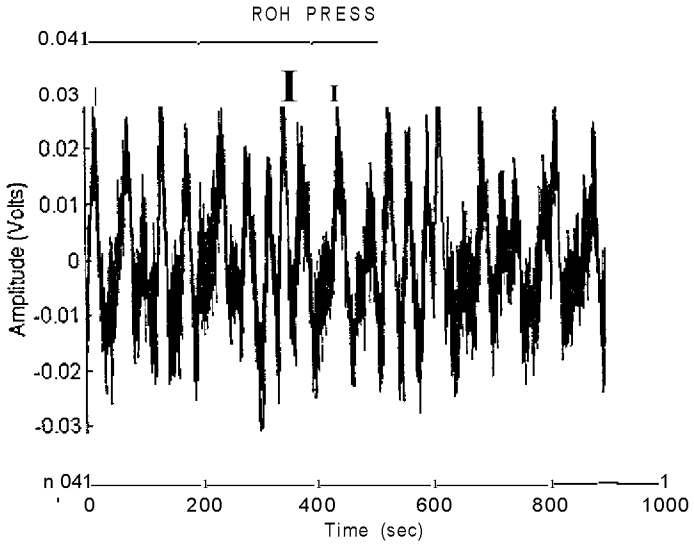

Figure A21. Time-Amplitude Plot for Pressure Signal (ID #08)

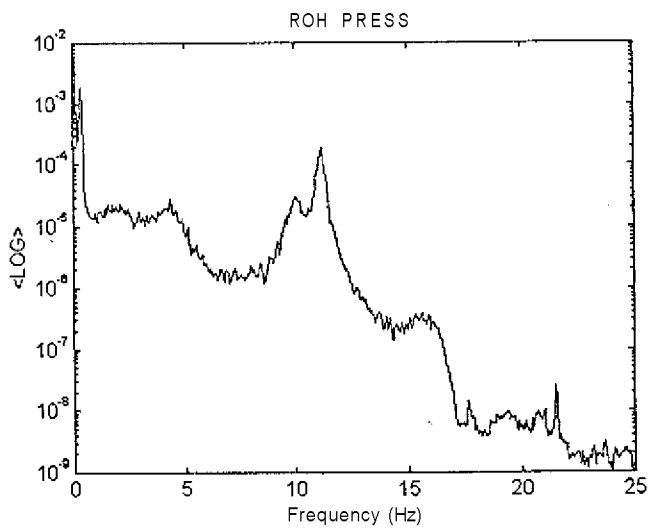

Figure A22. Power Spectrum Density Plot for Pressure Signal (ID #08)

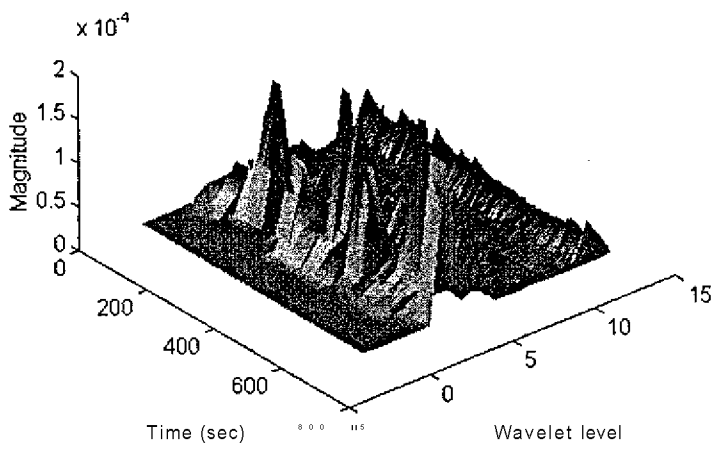

Figure A23. DWT 3-D Power Spectrum Density Plot for Pressure Signal (ID #08)

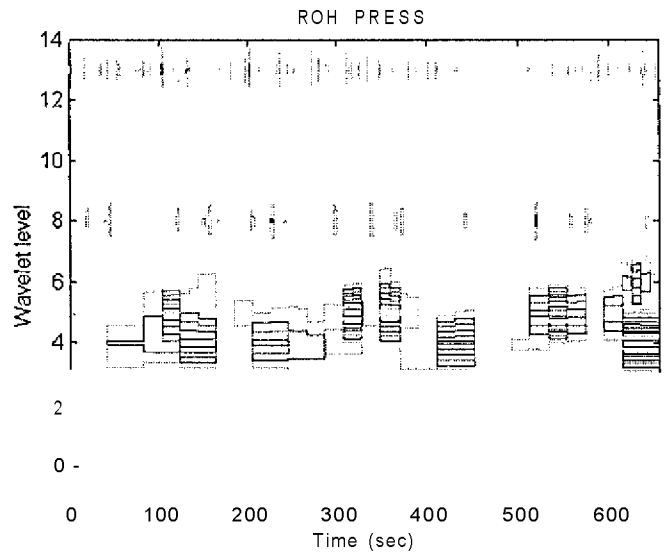

Figure A24. DWT 2-D Power Spectrum Density Plot for Pressure Signal (ID #08)

APPENDIX B

Computer Programs

Program 1

```
%-------------------------------------------------------------------
% This program computes the short-time Fourier transform (STFT) of the signals from
%motor experiment  and also computes the STFT of the selected detail level signals. A
%Hanning window was selected to perform the STFT analysis.
% The MATLAB Wavelet Toolbox functions are used to compute the MRA wavelet
%  coefficients.
%-------------------------------------------------------------------.


%    Multiresolution Analysis (MRA)


% load signal


load  c:\aucyone\data\radianl\rl

x=r1(1:2^12);
x=x(:);


% Define type of wavelet

wav='dblO';

% Number of sub-band levels

lev=5;

% Perform the MRA and obtain the wavelet coefficients

[pr1 coef prl longs]=wavedec(x,lev,wav);
prlcoef=prlcoef;


% Reconstruct the signal from the wavelet coefficients

for i=1:lev
eval(['det(',int2str(i),',:)=wrcoef("d",prlcoef,prllongs,wav,i);']);
eval(['app(',int2str(i),',:)=wrcoef("a",prlcoef,prllongs,wav,i);']);
end
```

```
% Short- Time Fourier Transform (STFT) using a Hanning window - Original Signal

d=x(:);
fs=2000; % Frequency sample
lw=512; % window length

[px  f t]=specgram(d,lw,fs,hanning(lw/2),lw/4);

 % Frequency magnitude, linear plot

figure

 mesh(t,f,abs(px)),colormap(jet),view(50,50)

 title('')
 ylabel(Trequency  (Hz)')
 xlabel('Time  (Seconds)')
 zlabel('Magnitude')

% Power spectral density, semilog plot


figure

 imagesc(t,f,abs(px)),axis  xy,colormap(jet)
 title('')
 ylabel('Frequency  (Hz)')
 xlabel('Time  (Seconds)')


% Short- Time Fourier Transform (STFT) using a Hanning window - Reconstructed
detail signal

 [px  f t]=specgram(det(5,:),lw,fs,hanning(lw/2),lw/4);

% Frequency magnitude, linear plot


figure

 mesh(t,f,abs(px)),colormap(jet),view(50,50)
 title('Detail  3')
 ylabel('Frequency  (Hz)')
```

```
xlabel(Time (Seconds)')
zlabel('Magnitude')

% Power spectral density, semilog plot

figure

imagesc(t,f,abs(px)),axis xy,colormap(jet)
title('Detail 3')
ylabel('Frequency (Hz)')
xlabel('Time (Seconds)')
```

Program 2

```
%-------------------------------------------------------------------
% This program computes the short-time Fourier transform (STFT) of the signals from
%reactor experiment and also computes the STFT of the selected detail level signals.
%A Hanning window was selected to perform the STFT analysis.
% The MATLAB Wavelet Toolbox functions are used to compute the MRA.
%-------------------------------------------------------------------

%  Multiresolution Analysis (MRA)


% load signal

load c:\aucyone\data\candu\fuel\rl37el5.dat

x=rl37el5(1:2^13);
x=x(:);

% Define type of wavelet

wav='dblO';

% Number of sub-band levels

lev=5;

% Perform the MRA and obtain the wavelet coefficients

[pr 1 coef prl longs]=wavedec(x,lev,wav);
```

```
prlcoef^rlcoef;


% Reconstruct the signal from the wavelet coefficients

for i=1:lev
eval(['det(',int2str(i),',:)=wrcoef("d",prlcoef,prllongs,wav,i);']);
evalCPappC^strC^/jO-wrcoefC'a^prlcoefjprllongs^av,!);']);
end


% Short- Time Fourier Transform (STFT) using a Gaussian window - Original Signal

fs=25;

lw=512;

dt=lw/4;

fig_num=1;

zpad=lw/12;

ffrac=0.5;

[fd,f,psdl] = stftgab(x,dt,lw,fs,zpad,fig_num,ffrac);
clear x

% Short- Time Fourier Transform (STFT) using a Gaussian window - Reconstructed
detail Signal

x=det(3,:);


[fd,f,psdl] = stftgab(x,dt,lw,fs,zpad,fig_num,ffrac);


function [fd,f,psdl] = stftgab(x,dt,lw,fs,zpad,fig_num,ffrac)

%-----------------------------------------------------------------
% This function computes Short Time Fourier Transforms using a Gabor
%  window
%
% Adapted from:
```

```
% Kristin Farry
% NASA/Johnson Space Center/ER, Houston, Texas 77058 USA
%
%_____

% Inputs:
%  x  = time series
%  dt = spacing of windows in time (in samples)
%  lw = length of window (in samples)
%  fs = sample rate (in samples per second)
%  zpad = zero padding for interpolation
%       (Optional:  if omitted, no zero padding used)
%  fig_num = plot flag and figure number
%       (Optional:  if omitted, no plotting)
%  ffrac = frequency fraction to be plotted
%       (Optional:  if omitted, 0 to 0.5*sr plotted)
%
% Outputs:
%  fd = Complex STFT matrix:  rows are each window's FFT; row variable
%       is time and column variable is frequency
%  psd = Power spectral density matrix corresponding to f
%       frequency vector (energy scaled)
%   f = x frequency vector from 0 to 0.5 * sr


sr=fs;
d=x(:);

% Fill in for missing arguments
if nargin  =  6
  zpad = lw;  % no zero padding
  fig_num = 0;  % no plotting
end
if nargin  =  7
  fig_num = 0;  % no plotting
  ffrac = 0.5;  % full frequency (0 to 0.5*sr) plotted
end
if nargin  =  8
  ffrac = 0.5;  % full frequency (0 to 0.5*sr) plotted
end

% Compute size of data vector
Id = length(d);
% Compute number of windows in data vector
ifld<lw,
```

```
 error('data stream too small')
else
 wc = 1 + floor((ld - lw)/dt);
end
% Compute Gaussian window

[gab] = gabfilt(lw);

% Orient data vector properly
if size(d,2) ~= 1
 d = d.';  % Transpose if necessary
end

% Compute STFT

for i=1 :wc,
 s(i) = ((i-1)*dt);
 fdw = d((s(i)+1):(s(i)+lw));
 energy = sum(fdw .* fdw);  % signal energy for scaling
 fdw = fdw .* gab;  % apply Gaussian window
 ffd(i,:) = fft(fdw,zpad)'./ sqrt(zpad);
 psd(i,:) = (ffd(i,1:(zpad/2)) .* conj(ffd(i,1:(zpad/2)))./ zpad;
 en_psd = (sum(psd(i,:)) * 2) * (lw/zpad);  % psd energy for scaling
 if en_psd ~= 0
  psd(i,:) = psd(i,:) * (energy/en_psd);  % energy scaling
 end
 fdl(i,:) = ffd(i,1:(zpad/2));
 psdl(i,:)=psd(i,:);
end


f=  [0:(sr/(zpad-1)):(0.5*sr)];



% Plot short time fourier power spectra

 ff=[0:(sr/(zpad-1)):(ffrac*sr)];
 fpl  =psdl(:,1:length(ff));

 % Frequency magnitude, linear plot

figure

 surfl(ff,(s./sr),fpl),shading   interp,colormap('gray'),view(50,50)
 title('Powerx - STFT')
```

```
 xlabel('Frequency (Hz)')
 ylabel('Time (Seconds)')
 zlabel('Magnitude')

figure

 contour(ff,(s./sr),fpl)
 title('Powerx - STFT')
 xlabel('Frequency (Hz)')
 ylabel('Time (Seconds)')

end


% Gaussian window

function [gab]=gabfilt(lw)

gab=(pi^(-1/4))*exp(-0.5*(1:lw)'.^2/(lw+1));
```

Program 3

```
%-------------------------------------------------------------------------
% Multiresolution Analysis (MRA)
%
%This program computes the wavelet MRA coefficients and reconstructs the
%approximation and detail level signals using a selected optimal wavelet basis
%function. The MATLAB Wavelet Toolbox functions are used to compute the wavelet
%coefficients
%-------------------------------------------------------------------------


% Load the signal
load  c:\data\fuel\rl37el5.dat

x=rl37el5(1:16384);
x=x(:);

% Define type of wavelet basis function to be used (from optimal wavelet
% selection program)
```

```
wav='db12';

% Number of sub-band levels
lev=10;

% Perform the MRA and obtain the wavelet coefficients


%Board distortion corretion using smooth method

dwtmode('spd');
dwtmode('spd');

% Compute wavelet coefficients

[pr l coef prl longs]=wavedec(x, 10,wav);

prlcoef=prlcoef;


% Reconstruct the signal from the wavelet coefficients using 10 levels

for i=l:lev
eval(['det(',int2str(i),',:)-wrcoef("d",prlcoef,prllongs,wav,i);']);
eval(['app(',int2str(i),',:)=wrcoef("a",prlcoef,prllongs,wav,i);']);
end


% Plot results

% Time interval

t=0: l/fs:(length(x)* l/fs)-l/fs;


% Plots

figure
subplot(l 1,l,l),plot(t,x,'b')

title('MRA_ Fuel_Chl - Original signal & Details 1-10')

end
for i=l:lev, subplot(ll,l,i+l);plot(t,det(i,:),'b');
if i==3
ylabelCAmplitude')
end
```

```
end

xlabel(Time (sec)')

figure
subplot( 11,1,1 ),plot(t,x,"b')
title('MRA_ Fuel_Chl - Original signal & Approximations 1-10')
for i=l:lev, subplot(l l,l,i+l);plot(t,app(i,:),*b');
if i = 3
ylabelCAmplitude')
end
end
xlabel('Time (sec)')
```

Program 4

```
%  This program performs the optimal wavelet selection using the minimum entropy
%  Energy criterion. The MATLAB Wavelet Toolbox functions are used to compute the
%  wavelet coefficients.
%-----------------------------------------------------------------------

% Load data

load  c:\data\fuel\rl37el5.dat

x=rl37el5(1:16384);
x=x(:);

% Define the type of wavelet

wl='dbl'; % Daubechies 1 wavelet
w2-db2'; % Daubechies 2 wavelet
w3-db3'; % Daubechies 3 wavelet
w4='db4'; % Daubechies 4 wavelet
w5-db5'; % Daubechies 5 wavelet
```

```
w6-db6'; % Daubechies 6 wavelet
w7-db7'; % Daubechies 7 wavelet
w8='db8'; % Daubechies 8 wavelet
w9='db9'; % Daubechies 9 wavelet
wlO-'dblO'; % Daubechies 10 wavelet
w12='db12'; % Daubechies 12 wavelet
w20='db20'; % Daubechies 20 wavelet
wbl-bior3.7'; % Biorthogonal 3.7 wavelet
wb2-bior6.8';% Biorthogonal 6.8 wavelet
wcol-coif4'; % Coiflet 4 wavelet
wsy-sym5';% Symmlet 5 wavelet


for i=l:15

if i=1
wav=wl;
end
if i=2
wav=w2;
end
if i=3
wav=w3;
end
if i—4
wav=w4;
end
if i=5
wav=w5;
end
ifi==6
wav=w6;
end
if i=7
wav=w7;
end
if i=8
wav=w8;
end
if i=9
wav=w9;
end
if i=10
wav=w10;
end
if i=11
```

```
wav=w12;
end
if i=12
wav=w20;
end
ifi=13
wav=wb1;
end
if i=14
\vav=wb2;
end
if i—15
wav=wco1;
end
if i=16
wav=wsy;
end

% Compute wavelet coefficients using Wavelet Packet basis functions and Shannon
% entropy

[t d]=wpdec(x,5,wav,'shannon');

elO=wpcoef(t,d,[1 0]);
ell-wpcoef(t,d,[1 1]);
e20=wpcoef(t,d,[2 0]);
e21=wpcoef(t,d,[2 1]);
e30=wpcoef(t,d,[3 0]);
e31=wpcoef(t,d,[3 1]);
e40=wpcoef(t,d,[4 0]);
e41=wpcoef(t,d,[4 1]);
e50=wpcoef(t,d,[5 0]);
e51=wpcoef(t,d,[5 1]);


% Compute the entropy values

e00=wentropy(x,'shannon');
e 10=wentropy(e 10,'shannon');
el 1=wentropy(el 1,'shannon');
e20=wentropy(e20,'shannon');
e21=wentropy(e21,'shannon');
e3 0=wentropy(e3 0,'shannon');
e3 1=wentropy(e31,'shannon');
e40=wentropy(e40,'shannon');
e41=wentropy(e41,'shannon');
```

```
e50=wentropy(e50,'shannon');
e51 =wentropy(e51 ,'shannon');

e11=e1O+e11;
e12=e20+e21;
e13=e30+e31;
e14=e40+e41;
e15=e50+e51;

ifell>eOO
fprintf('minimum entropy level -  1')
ee(i)=e1O+e11;
        elseif e12>e10
        fprintf('minimurn entropy level - 2')
        ee(i)=e20+e21+e11;
                elseif e13>e20
                fprintf('minimum entropy level - 3')
                ee(i)=e30+e31+e21+e11;


                        elseif e14>e30
                        fprintf('minimum entropy level- 4')
                        ee(i)=e40+e41+e31+e21+e11;


                                elseif e15>e40 | e15<e40
                                fprintf('minimum entropy level - 5')
                                ee(i)=e50+e51+e41+e31+e21+e11;

end
end


% Plot results

figure

plot(ee/b+')
xlabel('Wavelet type')
ylabel('Entropy  Energy')
title('Optimal wavelet selection -IE VFD2-3E*)


% Print results

fprintf('Minimuni entropy energy =  ')
```

min(ee)
ee

Program 5

Program 5.1

```
%-------------------------------------------------------------------
% This program performs the discrete wavelet transform (DWT) analysis using the
% Daubechies and Harmonic wavelets. The original algorithms are described
% in the reference [12].
%-------------------------------------------------------------------

% Load data

load  c:\data\fuel\rl37el5.dat

x=r 137el 5(1:2^15)./(3.45*40);

x=x(:);


% Compute the wavelet power spectrum (WPSD) using the Daubechies  and Harmonic
% wavelets


% Define the number of Daubechies wavelet

wav=20;


% Compute the WPSD - Dilation Wavelet Transform Algorithm (Daubechies wavelet)

wpsd = mapdn(x,20);


% Compute the WPSD - Discrete Harmonic  Wavelet Algorithm

hwpsd=hmapdn(x);
```

```
% Plot results


figure

surfl(wpsd),shading  interp,colormap(gray),view(50,50)

figure

surfl(hwpsd),shading  interp,colormap(gray),view(50,50)
```

Program 5.2

```
%-------------------------------------------------------------------------
%  This program computes the discrete wavelet transform (DWT) coefficients using the
%   MATLAB Wavelet Toolbox functions and it computes the Wavelet Power
%Spectrum.
%-------------------------------------------------------------------------

% Load data - Fuel Assembly Vibration Data

load  c:\data\flow1.dat
load  c:\data\pressl.dat

x=flow1(1:2^16)';
y=pressl(1:2^16)';

fs=25; % frequency sample

t=0:1/fs:(1/fs)*length(x)-1/fs; % time interval
1=1:10; % wavelet level

x=x;
y=y;


%-------------------------------------------------------
%  Perform Discrete wavelet transform at level 10
%-------------------------------------------------------


% Define the wavelet basis function

wav='db20';
```

```
[cx lx]=wavedec(x,10,wav);
[cy ly]=wavedec(y,10,wav);

%————————————————————
% Extract the Detail Coefficients
%————————————————————

lex = length(x);
cfdx=zeros(10,lex);
fork=1:10
        dx=detcoef(cx,lx,k);
        dx=dx(ones(1,2^k),:);
        cfdx(k,:) = wkeep(dx(:)',lex);
end

cfdx=cfdx(:);
I=find(abs(cfdx)<sqrt(eps));
cfdx(I)=zeros(size(I));
cfdx=reshape(cfdx, 10,lex);



ley = length(y);
cfdy=zeros(1 0,ley);
fork=1:10
        dy=detcoef(cy,ly,k);
        dy=dy(ones(1,2^k),:);
        cfdy(k,:)=wkeep(dy(:)',ley);
end

cfdy=cfdy(:);
I=fmd(abs(cfdy)<sqrt(eps));
cfdy(I)=zeros(size(I));
cfdy=reshape(cfdy, 10,ley);

%————————————————————
% Discrete Wavelet Power Spectrum
%————————————————————

wpsx=cfdx .* conj(cfdx);
wpsy=cfdy .* conj(cfdy);
```

```
% Plot results

figure

surfl(t,l,wpsx),shading  interp,colormap(gray),view(50,50)

figure

surfl(t,l,wpsy),shading  interp,colormap(gray),view(50,50)
```

Program 6

```
%-------------------------------------------------------------------------
% This program performs the MAP analysis using the discrete wavelet transform (DWT)
% (Daubechies and Harmonic wavelets). The original algorithms are described
% in the reference [12].
%-------------------------------------------------------------------------


% Load data

load  c:\data\fuel\rl37el5.dat

x=rl37el5(l:2^15)./(3.45*40);

x=x(:);

% Time interval of the measurement

fs=50 % sampling frequency

t=0:(l/fs):(length(x)*l/fs)-l/fs;

% Compute the wavelet power spectrum (WPSD) using the Daubechies  and Harmonic
% wavelets

% Define the number of Daubechies wavelet

wav=20;

% Compute the WPSD - Dilation Wavelet Transform Algorithm (Daubechies wavelet)
```

```
wpsd = mapdn(x,20);


% Compute the WPSD - Discrete Harmonic  Wavelet Algorithm

hwpsd=hmapdn(x);


% Plot results

% 1 is the number of wavelet levels obtained by the algorithm,
figure

contour(t,l,wpsd)

figure

contour(t,l,hwpsd)
```

Program 7

```
%-------------------------------------------------------------------------
% This program performs the multi-channel analysis using multiresolution analysis
%  technique (MRA). The MATLAB Wavelet Toolbox functions are used to compute the
%  wavelet coefficients.
%-------------------------------------------------------------------------


% Read  original signals and compute auto-power spectrum density (APSD) and
%Coherence

load  c:\data\fuel\rl37el5.dat
load c:\data\candu\rl 37el 8.dat

x=rl37el5(l:16384)./(40*3.45);
y=rl37el8(l:16384)./(40*3.48);

[px ff]=psd(x,256,25);% APSD
[py ffj=psd(y,256,25);          % APSD
[cohxy fco]=cohere(x,y,256/2,25);% Coherence
```

```
% Results

figure
semilogy(ff,px)
figure
semilogy(ffpy)
figure
plot(fco,cohxy)


% Compute the wavelet coefficients using a selected  wavelet basis function

wav-'db20';% Wavelet basis function

lev=5; % Number of sub-band levels

[cx lx]=wavedec(x,lev,wav);
[cy ly]=wavedec(y,lev,wav);


% Extracting approximation and detail coefficients for each level


% Approximations Coefficients

cay 1 =appcoef(cy,ly,wav,1 );
cax1 =appcoef(cx,lx,wav,1 );
cay2=appcoef(cy,ly,wav,2);
cax2=appcoef(cx,lx,wav,2);
cay3=appcoef(cy,ly,wav,3);
cax3=appcoef(cx,lx,wav,3);
cay4=appcoef(cy,ly,wav,4);
cax4=appcoef(cx,lx,wav,4);
cay5=appcoef(cy,ly,wav,5);
cax5=appcoef(cx,lx,wav,5);

% Detail Coefficients

cdy 1 =detcoef(cy,ly, 1 );
cdx1=detcoef(cx,lx, 1 );
cdy2=detcoef(cy,ly,2);
cdx2=detcoef(cx,lx,2);
cdy3=detcoef(cy,ly,3);
```

```
cdx3=detcoef(cx,lx,3);
cdy4=detcoef(cy,ly,4);
cdx4=detcoef(cx,lx,4):
cdy5=detcoef(cy,ly,5);
cdx5=detcoef(cx,lx,5):


% APSD spectrum at each approximation level

[pxa1  f1]=psd(cax1,256,12.5);
[pya1  f1]=psd(cay1,256,12.5);
[pxa2  f2]=psd(cax2,256,6.25);
[pya2  f2]=psd(cay2,256,6.25);
[pxa3  ß]=psd(cax3,256,3.125);
[pya3  ß]=psd(cay3,256,3.125);
[pxa4  f4]=psd(cax4,256,1.5625);
[pya4  f4]=psd(cay4,256,1.5625);
[pxa5  f5]=psd(cax5,256,0.782);
[pya5  f5]=psd(cay5,256,0.782);


% Coherence at each  approximation level

[coha1  fa1]=cohere(cax1,cay1,256,12.5);
[coha2  fa2]=cohere(cax2,cay2,256,6.25);
[coha3  fa3]=cohere(cax3,cay3,256,3.125);
[coha4  fa4]=cohere(cax4,cay4,256,1.5625);
[coha5,fa5]=cohere(cax5,cay5,256,0.7812);


% APSD spectrum at each detail level

[pxd1  f1]=psd(cdx1,256,12.5);
[pyd1  f1]=psd(cdy1,256,12.5);
[pxd2  f2]=psd(cdx2,256,6.25);
[pyd2  f2]=psd(cdy2,256,6.25);
[pxd3  D]=psd(cdx3,256,3.125);
[pyd3  f3]=psd(cdy3,256,3.125);
[pxd4  f4]=psd(cdx4,256,1.5625);
[pyd4  f4]=psd(cdy4,256,1.5625);
[pxd5  f5]=psd(cdx5,256,0.7812);
[pyd5  f5]=psd(cdy5,256,0.7812);


% Coherence at each  detail level
```

```
[cohd1  fal]-cohere(cdx1,cdy1,256,12.5);
[cohd2fa2]=cohere(cdx2,cdy2,256,6.25);
[cohd3  fa3]=cohere(cdx3,cdy3,256,3.125);
[cohd4  fa4]=cohere(cdx4,cdy4,256,1.5625);
[cohd5,fa5]=cohere(cdx5,cdy5,256,0.7812);


% Plot results
figure

semilogy(f3+3.125/2,pxd3;rf0»no;semilogy(ff,px,'b')
axis([3.125/2 6.25/2 1e-15 1e-9])
title('')
xlabel('Frequency (Hz)')
ylabel('LOG')

figure

semilogy(f3+3.125/2,pyd3,'r+'),hold;semilogy(ff,py,'b')
axis([3.125/2 6.25/2 1e-15 1e-9])
title('')
xlabel('Frequency (Hz)')
ylabel('LOG')

figure
plot(fa3+3.125/2,cohd3,'r'),hold;plot(fco,cohxy,'b+')
axis([3.125/2 6.25/2 0 1])
title('')
xlabel('Frequency (Hz)')
ylabel('Coherence Estimate')
```

Program 8

```
%-------------------------------------------------------------------
% This program divides the data in n block sizes n is a integer number power of 2 and
%perform the statistics analysis ( mean and variance) using the multiresolution
%analysis (MRA) results. The MATLAB Wavelet Toolbox functions are used to
%compute the %  wavelet coefficients.
%-------------------------------------------------------------------

%   Compute the wavelet coefficient using MRA
```

```
% Load data

load  c:\data\fuel\rl37el5.dat

x=rl37el5(1:16384);
x=x(:);

% Define type of wavelet

wav='db20';
lev=5; % wavelet level

% Perform the MRA and obtain the wavelet coeficients


[pr l coef pr l longs]=wavedec(x,lev,wav);
prlcoef^prlcoef ;


% Reconstruct the approximation and detail signals from the wavelet coefficients

for i=1:5
eval(['det(',int2str(i),',:)=wrcoef("d",prlcoef,prllongs,wav,i);']);
eval(['app(',int2str(i),',:)-wrcoef("a",prlcoef,prllongs,wav,i);']);
end


% Plot approximation results

fs=25; % frequency sample

t=0:l/fs:(l/fs)*length(x)-l/fs;

figure
subplot(6,1,1 ),plot(t,x,'b')
title('Tachometer_ Original signal & Approximations 1-5')


for i=1:lev, subplot(6,1,i+l);plot(t,app(i,:),'b');
if i = 3
ylabelCAmplitude')
end
end
```

```
xlabel(Time (sec)')
end


% Plot detail results

figure

subplot(6,1,1),plot(t(1 :4096),x(1 :4096),'b')
title('')

fori=1:1ev,  subplot(6,1,i+1);plot(t(1:4096),det(i,1:4096),'b');
if  i = 3
ylabel('Amplitude')
end
end
xlabel(Time (sec)')
title('Tachometer_ Original signal & Details 1-5')
clear t


% Dividing data in blocks

xd1=det(1,:)';
xd2=det(2,:)';
xd3=det(3,:)*;
xd4=det(4,:)';
xd5=det(5,:)';


xad1=app(1,:)';
xad2=app(2,:)';
xad3=app(3,:)';
xad4=app(4,:)';
xad5=app(5,:)';


number=128; % number of blocks


block_size=length(xd5)/number;

time=0;
n=1;
for j=1:number
time=time+( 1/fs)* block_size;
```

```
t(j)=time;
z=n;
k=z:(j/block_size)*length(xd1);


% Compute Mean value

mean_value1(j)=mean(xd1(k));
mean_value2(j)=mean(xd2(k));
mean_value3(j)=mean(xd3(k));
mean_value4(j)=mean(xd4(k));
mean_value5(j)=mean(xd5(k));


amean_value1(j)=mean(xad1(k)):
amean_value2(j)=mean(xad2(k));
amean_value3(j)=mean(xad3(k)):
amean_value4(j)=mean(xad4(k)):
amean_value5(j)=mean(xad5(k))


% Compute Variance

stand_value1(j)=sqrt(var(xd1(k)));
stand_value2(j)=sqrt(var(xd2(k)));
stand_value3(j)=sqrt(var(xd3(k)));
stand_value4(j)-sqrt(var(xd4(k)));
stand_value5(j)=sqrt(var(xd5(k)));

astand_value1(j)=sqrt(var(xad1(k))):
astand_value2(j)=sqrt(var(xad2(k))):
astand_value3(j)=sqrt(var(xad3(k))):
astand_value4(j)=sqrt(var(xad4(k))):
astand_value5G)=sqrt(var(xad5(k)));


n=(j/block_size)*length(xd5)+1;
end

% Plot results

figure

subplot(6,1,1), plot(t,mean_valuel,'b')
ylabelCdl")
```

```
titleC Mean Value Trend_Tachometer_Detail levels ')
subplot(6,1,2),plot(t,mean_value2,'b')
subplot(6,1,3),plot(t,mean_value3,'b')
ylabelC Mean Value')
subplot(6,1,4),plot(t,mean_value4,'b')
subplot(6,1,5),plot(t,mean_value5,'b')
xlabel('Time (Sec)')
figure

subplot(6,1,1), plot(t,stand_valuel,'b');
ylabel('dl')
title(' RMS Trend_Tachometer_Detail levels ')
subplot(6,1,2),plot(t,stand_value2,'b')
subplot(6,1,3),plot(t,stand_value3 ,'b')
ylabelC RMS Value')
subplot(6,1,4),plot(t,stand_value4,'b')
subplot(6,1,5),plot(t,stand_value5,'b')
xlabel('Time (Sec)')

figure
subplot(6,1,1), plot(t,mean_value1,'b');
ylabel('dl')
title(' Mean Value Trend_Tachometer_Approximations levels ')
subplot(6,1,2),plot(t,amean_value2,'b')
subplot(6,1,3),plot(t,amean_value3,'b')
ylabelC Mean Value')
subplot(6,1,4),plot(t,amean_value4,'b')
subplot(6,1,5),plot(t,amean_value5,'b')
xlabel('Time (Sec)')

figure

subplot(6,1,1), plot(t,astand_value1,'b');
ylabel('dl')
title(' RMS Trend_Tachometer_ Approximations levels')
subplot(6,1,2),plot(t,astand_value2,'b')
subplot(6,1,3),plot(t,astand_value3,'b')
ylabelC RMS Value')
subplot(6,1,4),plot(t,astand_value4,'b')
subplot(6,1,5),plot(t,astand_value5,'b')
xlabel('Time (Sec)')
```

VITA

Aucyone A. da Silva was born in S. Benedito, CE, Brazil on June 12, 1953. He attended the Physics Department at the Federal University of Rio de Janeiro, RJ, Brazil and received his B.S. degree in Physics in December 1976. From 1977 until 1980 he was a graduate student at the COPPE / Department of Nuclear Engineering at the Federal University of Rio de Janeiro, where he received his Master of Science degree in 1980. From 1979 until 1986, he worked at the Nuclear Engineering Institute-IEN/CNEN, Rio de Janeiro, Brazil, as a research physicist. From 1987 until 1993 he worked at the Energy and Nuclear Research Institute, IPEN/CNEN, Sao Paulo, Brazil, where he developed several research activities in the nuclear engineering field. During this period he was also developing numerous research activities for the Brazilian Navy and Angra I Nuclear Power Plant. In 1993 he was granted a scholarship from Brazilian Research Council, CNPq. He then started working as a graduate student, in the Department of Nuclear Engineering at The University of Tennessee, Knoxville, TN, where he received his Ph.D. degree in December 1997. He is currently employed as a senior researcher at IPEN/CNEN, Sao Paulo, Brazil.